YEAST MODEL FOR SEEDING AND CROSS-SEEDING OF PROTEIN AGGREGATION IN PROTEOPATHIES

A Dissertation
Presented to
The Academic Faculty

by

Zachery Deckner

In Partial Fulfillment
of the Requirements for the Degree
Doctor of Philosophy in the
School of Biological Sciences

Georgia Institute of Technology
August 2021

YEAST MODEL FOR SEEDING AND CROSS-SEEDING OF PROTEIN AGGREGATION IN PROTEOPATHIES

Approved by:

Dr. Yury Chernoff, Advisor
School of Biological Sciences
Georgia Institute of Technology

Dr. Nicholas Seyfried
Department of Biochemistry
Emory University

Dr. Kirill Lobachev
School of Biological Sciences
Georgia Institute of Technology

Dr. Matthew Torres
School of Biological Sciences
Georgia Institute of Technology

Dr. Francesca Storici
School of Biological Sciences
Georgia Institute of Technology

Date Approved: July 08, 2021

ACKNOWLEDGEMENTS

I would like to thank all of the many people who have assisted in this work, including my advisor Dr. Yury Chernoff for guidance, Gary Newman for all of his advice and assistance through the years, and my mentors Drs. Denis Kiktev and Pavithra Chandramowlishwaran, who helped me begin my scientific journey in the lab. I would like to thank my family and friends for all of the support through the years through all of the ups and downs, especially my parents, for without their love and support this would not have been possible. I would also like to thank my colleagues Dr. Sathya Balachander, Dr. Katy Bruce, Dr. Rebecca Howie, Dr. Rakhee Ganti, Lina Garcia, and Aspen Hirsch for their continued support for helping me get through all of the stressful situations.

TABLE OF CONTENTS

LIST OF TABLES

LIST OF FIGURES

LIST OF SYMBOLS AND ABBREVIATIONS

aa	amino acid
AD	Alzheimer's disease
Aβ	Amyloid beta
Ade1-14	Allele containing a premature UGA sop codon
$CuSO_4$	Copper sulfate
GuHCl	Guanidine hydrochloride
MAPT	Microtubule binding protein tau
Prion	Proteinaceous infectious particle
PrD	Prion domain
PrP	Prion protein
QN or Q/N	AN-rich stretch
SDD-AGE	Semi-denaturing detergent agarose gel electrophoresis
YPD	Yeast extract peptone dextrose media
TauRD	Tau microtubule repeat domain
5-FOA	5-Flouroorotic acid
LB	Luria Bertani broth
Amp	Ampicillin
SDS-PAGE	Sodium dodecyl sulfate
SD	Standard deviation
SE	Standard error

SUMMARY

A variety of human diseases, including Alzheimer's disease (AD) and tauopathies, are associated with the accumulation of misfolded protein aggregates. These protein aggregates are composed of amyloids, protein aggregates that contain highly ordered β-sheet structures that are very stable and quite insoluble. Yeast are also plagued by amyloids. In yeast, amyloids manifest themselves as infectious proteins, termed yeast "prions" that are heritable via the cytoplasm. While not necessarily considered a disease in yeast, our understanding in how and why yeast prions form and propagate have led to insights that have translated to our understanding of proteins associated with human diseases. My thesis work has employed yeast as a model system to understand the specific sequence elements as well as other cellular factors that contribute to protein misfolding of proteins associated with disease in humans, including $A\beta_{42}$, MAPT, and U1-70k, all of which are associated with AD. Firstly, I have shown that the Aβ-based prion in yeast is controlled by the $A\beta_{42}$ peptide. I also used this prion system to study $A\beta_{42}$ isolated from patients suffering from AD to demonstrate that $A\beta_{42}$ is capable of forming prion variants. Secondly, using high expression plasmids I have shown that MAPT, the repeat domain of MAPT, and the C-terminal domain of U1-70k are capable of forming detergent-resistant aggregates in yeast, a characteristic of amyloids. Lastly, I have used a novel yeast assay to study the nucleation capabilities of protein peptides that have recently been associated with diseases, as well as use it as a high-throughput screening platform to test newly

synthesized compounds to determine if they can prevent the initial nucleation of Aβ, the triggering event in AD. Overall, this work provides new information on the molecular mechanisms that drive protein aggregation.

CHAPTER 1. INTRODUCTION AND BACKGROUND: STUDYING MAMMALIAN AMYLOIDOGENIC PROTEINS IN YEAST

Proteins can incorrectly fold and accumulate to form insoluble cross-beta fibril structures called amyloids. Amyloids are associated with more than 50 human diseases categorized as amyloidosis many of which are fatal and incurable, and the list of these diseases is continuously growing [1]. This list includes many neurodegenerative disorders including Alzheimer's disease (AD), Parkinson's disease, and Huntington's disease, but also some systemic diseases like type II diabetes (T2D) [2].

The common feature in this group of diseases is the emergence of proteins folded into insoluble aggregates but the processes leading to cell death remains to be elucidated. While there is consensus in the field that these diseases are caused by the protein misfolding event, the mechanisms of how and when these events occur still remain poorly understood.

Yeast have emerged as a powerful tool for understanding protein misfolding diseases as they are also plagued by amyloids, termed yeast prions. While most of the prions in yeast are not necessarily associated with disease, the underlying features that drive protein misfolding are the same as in humans. Also, another hallmark in many of these neurodegenerative diseases in that they are all mostly late onset disease with long incubation periods, which has made their study in traditional models arduous. In the last several years, there have been many

successful yeast models established to study many of the proteins associated with these amyloid diseases. These models have been effective in studying different features of amyloid biology, both protein aggregation and cellular toxicity associated with them, however none of these models to date are capable of demonstrating the switch between the normal monomeric form and the amyloidogenic form of the protein, and that the amyloidogenic form is capable of propagating in yeast. Here we will demonstrate such a model for the protein peptide Aβ, one protein associated AD. We will also demonstrate other models aimed at studying the protein aggregation of other AD associated proteins: microtubule-associated protein tau (MAPT) and U1 small nuclear ribonucleoprotein 70k (U1-70k). Previous models for MAPT have only recapitulated the feature of protein aggregation, but have not demonstrated that they are amyloid in nature. Lastly, we will demonstrate another yeast model for studying amyloid nucleation, the first step in amyloid formation, and its use as a high throughput drug screening assay.

1.1 Prions and amyloids

Prions are misfolded proteins that are transmissible (heritable or infectious). The term prion (proteinaceous infectious particle) was first coined by Stanley Prusiner in his work studying the “scrapie” agent (the PrP protein) as a protein only pathogen capable of causing disease in mammals [3]. From this work, we now know that prions confer changes to protein confirmation but does not alter their genetic or amino acid sequence. Rather this change in confirmation is driven solely by protein interactions leading them to be incorporated into fibrous aggregates like

amyloids. Amyloids are protein aggregates composed of cross-β sheets that have been associated with many human diseases. The distinguishing characteristics between a prion and an amyloid is that a prion can self-propagate and is transmissible between organisms [4]. Their key unifying feature is that many of these proteins identified as having amyloid properties often have unstructured domains, that are often glutamine and asparagine rich, which are important for achieving these altered non-soluble confirmations [5, 6]. Amyloid-based prion formation occurs via a two-step process (Figure 1.1). First is nucleation, in which a normal soluble protein is converted into an aggregate or “nuclei” of the prion isoform. This nucleation event can be driven by mutations, but most often this is a sporadic phenomenon [7]. The second is ‘propagation” in which the established seed during the nucleation step continues to grow via incorporating monomers, but these longer fibers can then be sheared creating more, smaller infectious units or “propagons” [8].

Mammalian amyloidosis and disease related proteins

More than 50 diseases in humans can be associated with protein misfolding, many of which are fatal and incurable (see examples in Table1.1). These diseases are associated with at least one protein or peptide that is capable of adopting an amyloid conformation, a protein fold associated with ordered cross- β aggregates. While we most often think of these proteins as associated with disease, it is important to note that there are examples of functional amyloids in nature. In humans amyloids play a role in melanin formation [9], hormone storage [10], and the formation of memories [11].

Table 1.1 Examples of human amyloid diseases.

Amyloid Disease	Disease Associated Protein
Alzheimer's Disease (AD)	Aβ and MAPT
Parkinson's disease	α-synuclein
Prion disease	Prion protein (PrP)
Type II diabetes	Amylin
Huntington's disease (one type of Polygluatine disease)	Huntingtin

1.1.1.1 Alzheimer's Disease (AD)

Alzheimer's Disease (AD) is the leading cause of dementia and is hallmarked by the features of beta-amyloid (Aβ) plaques and neurofibrillary tangles (NFT's) developing within brain tissues(Figure 1.2) [12]. AD symptoms can vary between individuals, but they usually consist of the loss of ability to learn new information and as the disease progresses, more neurons are deteriorating, it can cause individuals to experience confusion, impaired thinking, and disorientation, thus requiring long-term health care. Currently, AD is the 6th leading cause of death [12]. However, AD has been routinely underdiagnosed in the past, thus estimates evaluating it as the 3rd leading cause of death are likely to be more realistic [13]. Also, with medical advances increasing the life expectancy of individuals into their 80's or 90's, and the highest risk factor of dementia related illness being age, the number of individuals affected by these neurodegenerative diseases is only going to increase. Currently, there are only therapeutics that help to minimize the

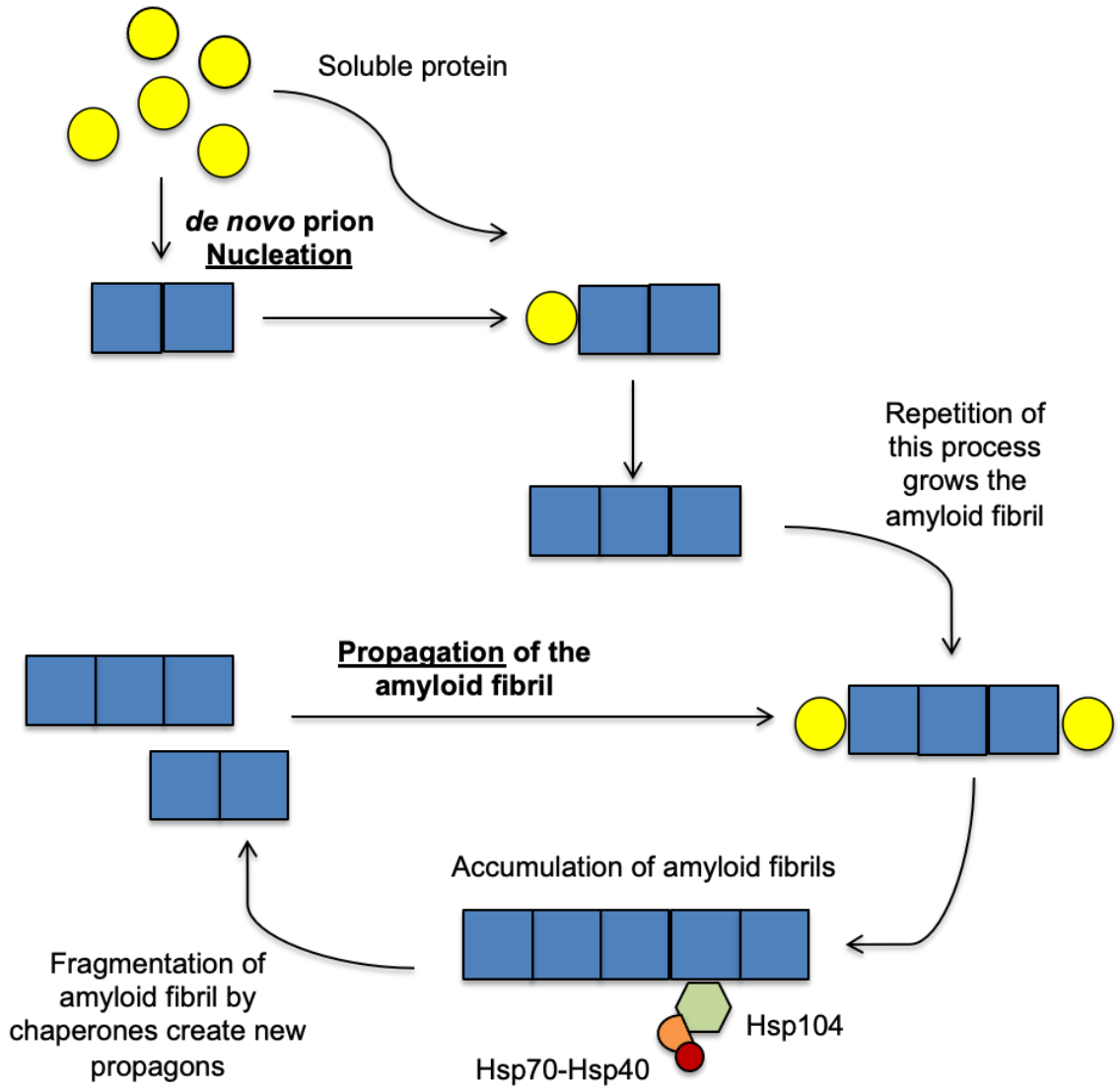

Figure 1.1 Amyloid life cycle. A soluble native or unfolded protein with an amyloidogenic domain undergoes a conformational conversion (driven either by mutation or sporadic) via nucleation and self assembles to form a prion polymer. The addition of monomers to the nuclei continues to grow the prion fibrils. Chaperones can interact with these large amyloid fibrils, sheering them into small subunits creating new propagons that can continue this process driving prion propagation.

symptoms associated with AD but do not target the underlying mechanism of protein misfolding [14]. As individuals affected by this disease are expected to increase in the near future, along with an increase in health care costs and the

burden to care givers, it becomes necessary for us to elucidate the mechanisms by which this protein misfolding begins. This will allow us to develop early detection and therapeutic strategies.

1.1.1.2 Aβ peptide and amyloid cascade model

The Aβ peptide is not an initial product of translation but is rather the result in the cleavage of the amyloid precursor protein (Figure 1.3) [15]. APP can be proteolytically cleaved by the group of enzymes known as α, β, and γ secretases. This process can occur by either of two mechanisms: non-amyloidogenic or amyloidogenic pathway. In the non-amyloidogenic pathway, which is the predominant pathway, APP is first cleaved by the α-secretase. This cleavage pathway prevents the formation of the Aβ peptide because the α secretase cleaves within the region for Aβ formation. In the amyloidogenic pathway, APP is first cleaved by β-secretase followed by further processing by the γ secretase. Cleavage by the γ secretase can lead to the formation of alternative Aβ products. One product is $A\beta_{40}$ and is the most common form produced. However, there is another variant known as $A\beta_{42}$ that can be produced and is known to have a higher rate of fibril formation compared to its $A\beta_{40}$ counterpart [16].

Since most of the cases of AD are sporadic it becomes important to understand what are the triggering mechanisms in the production of the Aβ peptide as early detection is key in preventing the AD onset and progression. The model that is currently dominant within the amyloid field when it comes to clinical and therapeutic research for AD is the amyloid cascade hypothesis (Figure 1.4) [17].

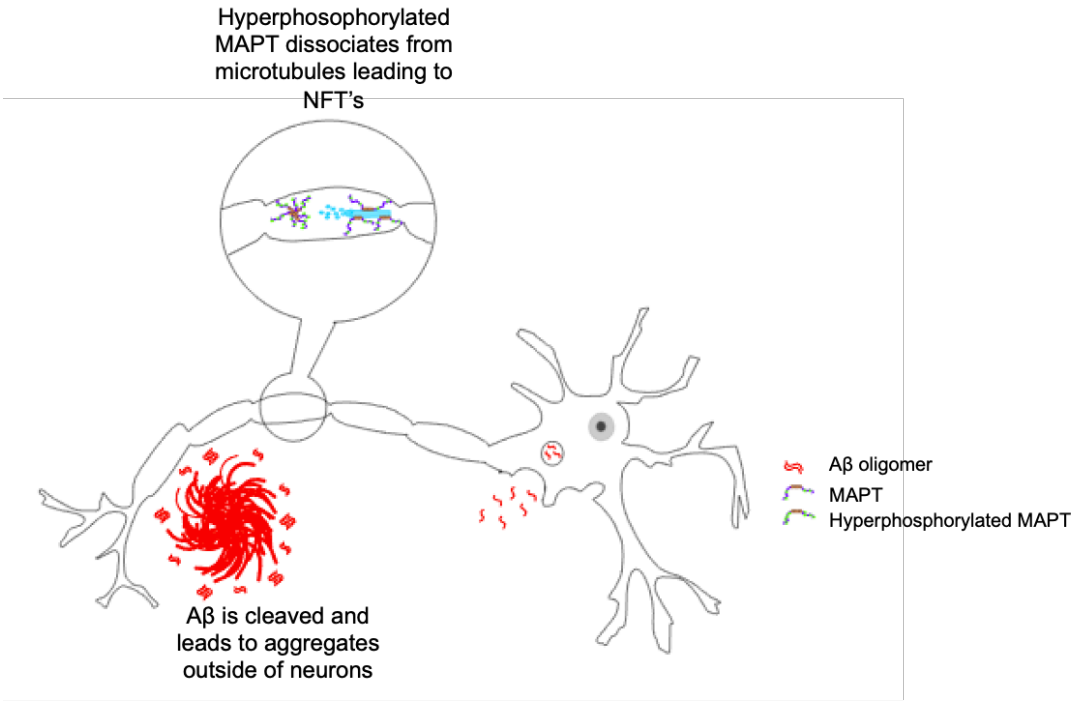

Figure 1.2 A diagrammatic representation of a neuron in an AD brain. Intracellular Aβ is secreted from cells leading to the accumulation of Aβ into large aggregates known as plaques outside of neurons while the hyperphosphorylation of MAPT leads to it dissociation to microtubules causing the formation of neurofibrillary tangles (NFT's).

This hypothesis states that the formation of the Aβ peptide and its aggregation into plaques within the brain is the initial triggering step that is required for the development of AD. The accumulation of Aβ into plaques may then lead to the triggering event of MAPT hyperphosphorylation, leading to NFTs [18]. The mechanism as to how this occurs is still highly debated and poorly understood since most of the Aβ that is sequestered exists in extracellular plaques while MAPT remains intracellular [19]. While there is evidence to show the coexistence of Aβ and MAPT aggregates in AD pathology, there is no clear link that this occurs via cross-seeding between Aβ and MAPT, rather this could occur by an alternative pathway [20]. The currently prevalent amyloid cascade model explains a majority

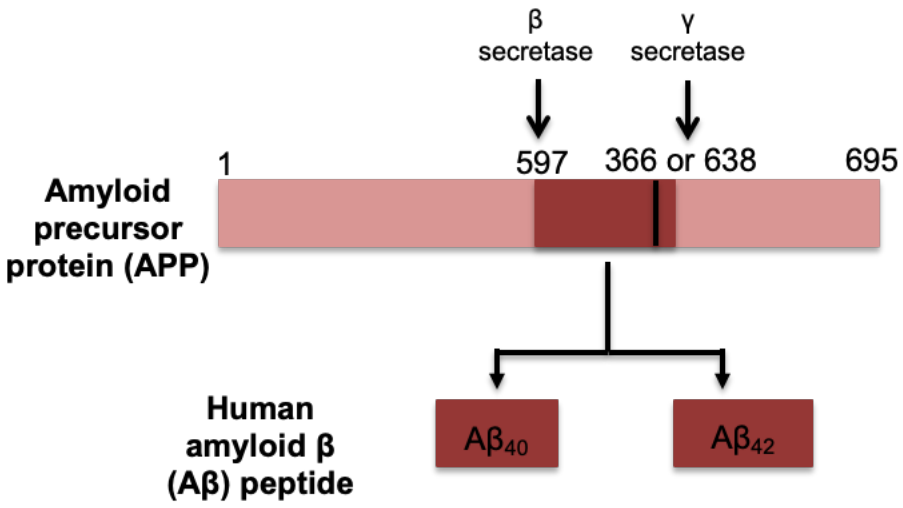

Figure 1.3 Structural organization of human Amyloid beta (Aβ) peptide. Aβ peptide is a product from proteolytic cleavage of the Amyloid precursor protein [15] by the β and γ secretases that can produce two isoforms – $A\beta_{40}$ and $A\beta_{42}$.

of current research, but it has reached much scrutiny. However, it is understood that the Aβ peptide is necessary for the development of AD and an understanding of the triggering event leading to its formation is of utmost importance in designing a therapy for AD.

1.1.1.3 Microtubule associated protein tau (MAPT)

MAPT is a member of the microtubule associated protein family that interacts with tubulin and promotes its assembly into microtubules and helps stabilize their structure [21]. MAPT contains repeat motifs in a proline-rich region, which are crucial for its association with other proteins. The phosphorylation of MAPT modulates its binding affinity to regulate the morphology of neurons and intracellular transport. However, the hyperphosphorylation of MAPT depresses this biological activity. In AD and a family of related neurodegenerative diseases, called

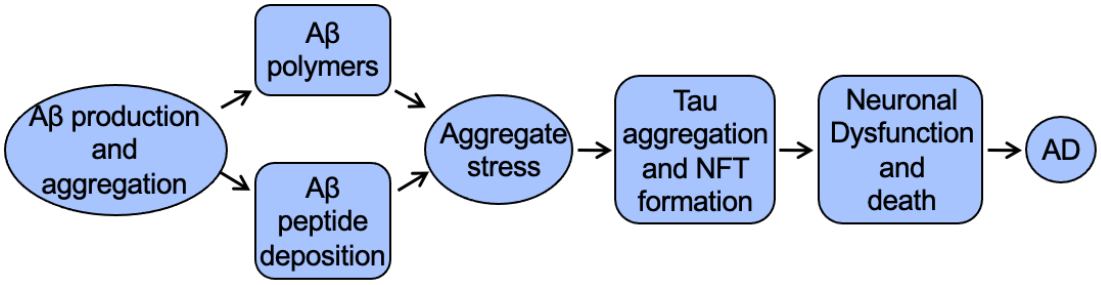

Figure 1.4 Amyloid cascade hypothesis. This model which has been the main explanation for AD pathogenesis starts with the accumulation of Aβ oligomers that can accumulate into large extracelluar plagues. Downstream of this event, by either physical interaction by intracellular Aβ oligomers or through extracellular Aβ causing activation of a signal cascade leads to the aggregation of Tau and its detachment from microtubules (leading to NTF formation). Both of these events work together to drive healthy neurons into the diseased state.

tauopathies, MAPT is abnormally hyperphosphorylated and aggregated into bundles of filaments that is polymerized into paired helical filaments, forming neurofibrillary tangles which are intracellular MAPT aggregates in AD brains (Figure 1.5) [22]. Mutations in or even close to the repeat region of MAPT have been shown to cause frontotemporal dementia and Parkinsonism linked to chromosome 17 (FTDP-17) [23]. It is now widely accepted that it is not the resulting fibrillary tangles produced by MAPT biology, but the process leading to its aggregation that is responsible for the toxicity associated with many tauopathies [24].

1.1.1.4 Other AD-associated proteins

U1-70k is a component of the spliceosomal U1 snRNP. The U1-snRNP is responsible for the recognition of the pre-mRNA 5' splice-site and is essential for the assembly of the spliceosome complex [25]. The spliceosome complex is responsible for the removal of introns from pre-mRNA, and has been found as

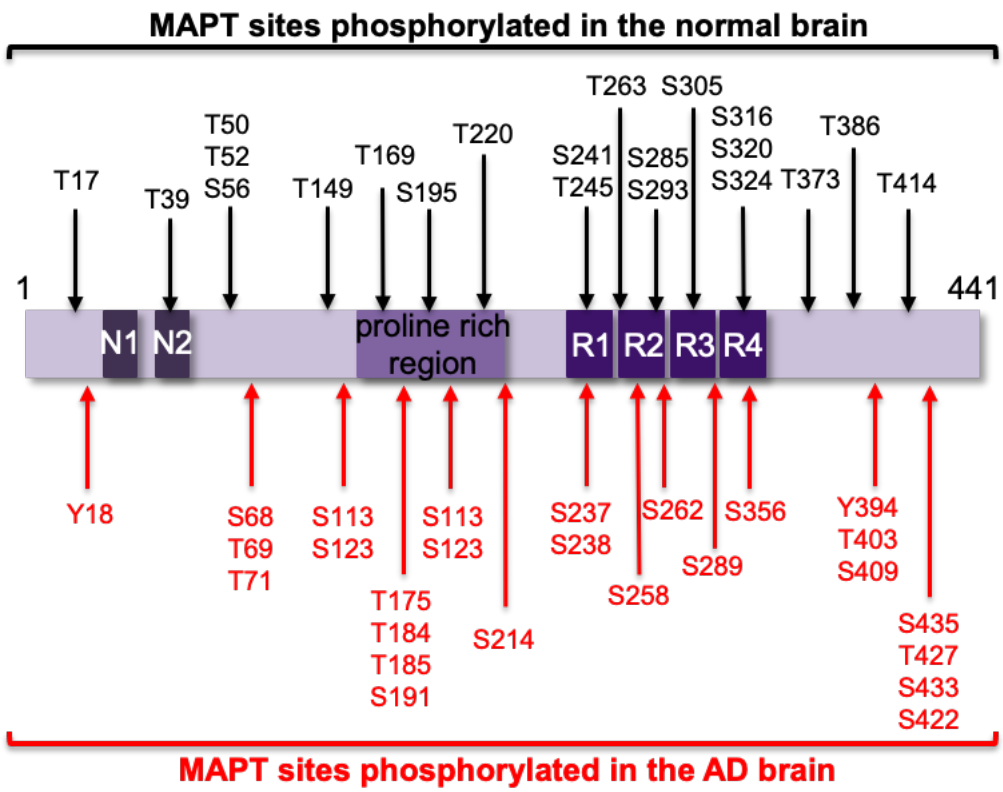

Figure 1.5 Acknowledged phosphorylation sites on MAPT. Black color denotes amino acid sites phosphorylated in the normal brain while red represents the AD brain. Note that there are more phosphorylated sites for both sample sets than what is denoted in figure.

cytoplasmic tangle-like aggregates in AD brains [26]. The aggregates containing U1-70k appear to be specific to AD, as its aggregation is not found in other neurodegenerative diseases such as ubiquitin-positive frontotemporal lobar degeneration (FTD) and amyotrophic lateral sclerosis (ALS) [26]. U1-70k harbors multiple low-complexity domains within its amino acid sequence [27]. LC domains are regions that contain repeats of single amino acids or short amino acid motifs, and have been implicated in the aggregation properties of numerous RNA-binding proteins [28]. Other RNA-binding proteins containing LC domains have been implicated in disease include hnRNPA1 (associated with multisystem

proteinopathy) and FUS, TDP-43 (both associated with Amyotrophic lateral sclerosis and frontotemporal dementia) [29, 30]. There are now close to 70 RNA-binding proteins that contain prion-like domains, and these domains are not only contributing to disease but are also playing a role in their normal RNA-binding function as well [31]. The LC domains of U1-70k are located within its C-terminus and are essential for U1-70k aggregation [32], however it should also be noted that in AD, it has been shown that U1-70k is N-terminally cleaved to a size of 40kDa [33]. The N40K fragment has been shown to have toxic effects in neurons suggesting this protein may play a role in neurodegeneration in AD patients.

1.2 Yeast prions

It is important to mention that animals are not the only ones affected by amyloid forming proteins, as such proteins exist in other domains of life as well. This includes bacteria, plants, and fungi. In yeast, amyloids manifest themselves as infectious proteins, termed yeast “prions” that are heritable via the cytoplasm (non-mendellian inheritance). Yeast prions are formed by what is called the prion domain (PrD) which is responsible for the intermolecular interactions that will form the core of the fiber (Figure 1.6). In most cases these PrD’s are generally separate from the other domains within the protein that are responsible for the major cellular function. Most (but not all) yeast prions also have easily detectable phenotypes (see examples in Table 1.2). This is typically due to the “loss of function” of the normal soluble protein due to its sequestration into an amyloid fiber. While some yeast prions can have “pathogenic properties” they are not all necessarily associated with a “diseased” state, rather a majority of them provide adaptive

characteristics that allow them to adapt to environmental stresses, which makes them differ from their mammalian counterparts [34, 35].

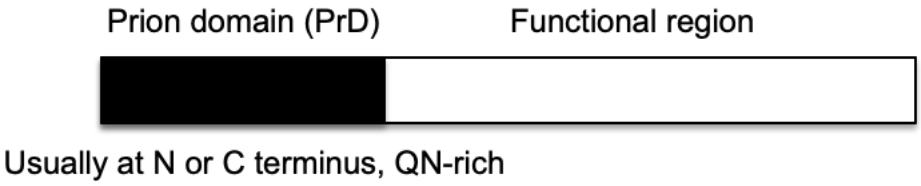

Figure 1.6 An example of a typical yeast prion protein. The prion domain (PrD) denotes the glutamine/asparagine-rich regions (shaded black in the figure, explained as QN-rich) that are located at the terminal ends of proteins, followed by a functional region that is responsible for the cellular function of the protein.

Sup35 and [PSI$^+$]

The most well studied yeast prion is [*PSI*$^+$], which is formed by the yeast protein Sup35, also known as eukaryotic release factor 3 (eRF3). In its normal soluble state (deemed [*psi*$^-$]), Sup35 works in conjunction with eRF1 and the ribosome as a GTPase to recognize stop codons and release newly synthesized polypeptide chains from the ribosome, thus terminating translation. The protein Sup35 consists of three domains – the Q/N rich N-terminal domain, which contains the PrD, the middle domain which contains charged residues and is responsible for the solubility of the protein, and the C-terminal domain which is responsible for its functions as a translation release factor (Figure 1.7A). In its amyloid state (deemed [*PSI*$^+$]), some of the endogenous Sup35 is incorporated into an amyloid aggregate, which leads to a “loss of function” phenotype. Specifically, in [*PSI*$^+$] cells, translation termination becomes less efficient resulting in reduced

Table 1.2 Examples of amyloid-based fungal prions.

Protein	Prion	Protein Function	Prion Phenotype
Sup35	[*PSI*$^+$]	Translation termination factor	Increases nonsense suppression
Rnq1	[*PIN*$^+$]/[*RNQ*$^+$]	Unknown	Increases *de novo* formation of other prions
Ure2	[*URE3*]	Regulatory protein in nitrogen metabolism	Use of poor nitrogen source
Swi1	[*SWI*$^+$]	Subunit of chromatin remodeling complex	Altered carbon source utilization
Cyc8	[*OCT*$^+$]	Transcriptional co-repressor	Altered carbon source utilization, flocculation
Mot3	[*MOT*$^+$]	Transcriptional co-repressor	Change in cell wall composition
Mod5	[*MOD*$^+$]	tRNA modification enzyme	Increased level of ergosterol and resistance to antifungals
Nup100	[*NUP100*$^+$]	FG-nucleoporin	Increases the rate of nuclear export
Lsb2	[*LSB*$^+$]	Binds and inhibits Las17, actin associated	Increases *de novo* formation of other prions [*PSI*$^+$]
HET-s*	[Het-s]	Unknown	Heterokaryon incompatibility

*All prions listed are found in *S. cerevisiae*, except for Het-S which is found in *P. anserina*.

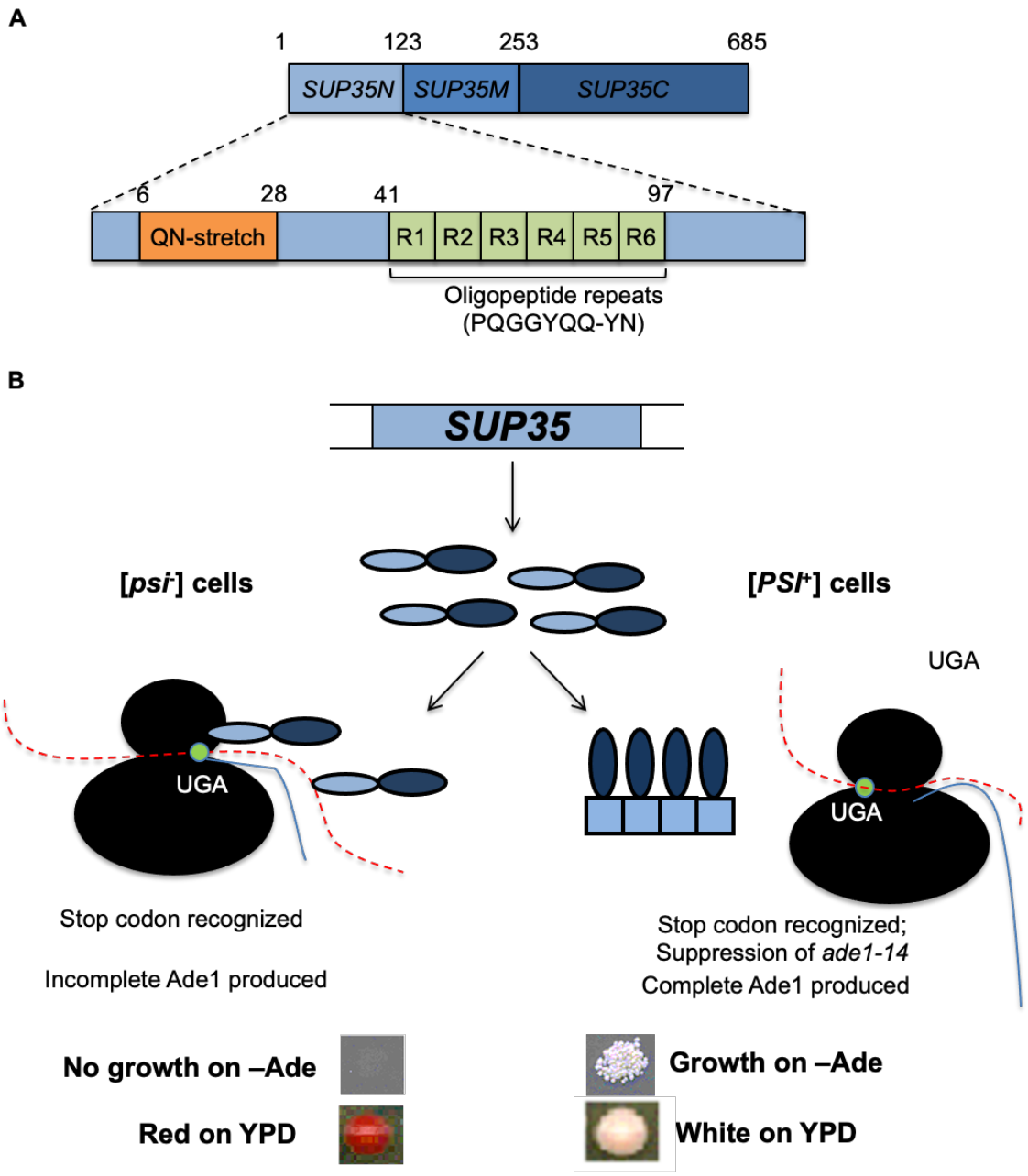

Figure 1.7 Structural composition of Sup35 and the [*PSI*$^+$] detection system. (A)The termination translation factor Sup35 is composed of the N, M, and C domains. Numbers correspond to amino acid positions. The QN refers to the asparagine, glutamine rich region. (B) In yeast containing the ade1-14 (UGA reporter), cells containing monomeric versions of Sup35 ([*psi*$^-$] cells) leads to termination at the premature UGA stop codon causing a truncated version of Ade1 to be produced. Because of this [*psi*$^-$] cells are unable to grow on medium lacking adenine and have a red pigment on YPD. When Sup35 is in the [*PSI*$^+$] state, the stop codon in ade1-14 is not recognized leading to full-length Ade1 to be produced allowing [*PSI*$^+$] cells to grow on –Ade medium and a white color on YPD.

suppression of nonsense codons. Termination suppression can be monitored phenotypically though the use of a read-through assay in strains incorporating nonsense mutations within genes responsible for macromolecule biogenesis. In our case specifically, we use a reporter system (Figure 1.7B) that contains a premature stop codon within *ADE1* [4]. In a [*psi*$^-$] cell, Sup35 is soluble and causes the correct termination of Ade1. This results in a truncated version of Ade1 that is nonfunctional causing cells to lack the ability to grow on media lacking adenine (-Ade medium). It also causes growth on YPD medium to be red due to the buildup of SAICAIR in the vacuole. In [*PSI*$^+$] cells, Sup35 is incorporated into aggregates (the soluble level of Sup35 is decreased to less than 1% as to that of [*psi*$^-$] cells [4]), causing inefficient translation termination. This leads to readthrough of the premature stop codon and production of Ade1. This allows for growth on -Ade medium and normal color (whitish or light pink) growth on YPD [36].

Strains and variants

A remarkable feature in prion biology is the strain phenomenon. This is where prion particles composed of the same protein leads to phenotypically distinct transmissible states [37]. To reconcile the existence of strains with the 'protein-only' hypothesis of prion transmission, it has been proposed that a single protein can misfold into multiple distinct infectious forms, one for each different strain [37]. This helps to explain the pathological heterogeneity observed in AD[38]. It has been shown that prion proteins (including mammalian PrP and yeast Sup35) of one and the same sequence can form various amyloid conformations with distinct structures – prion "strains" (usually called "variants" in

yeast), and that these different strains have different disease manifestation in mammals or phenotypic characteristics in yeast (Figure 1.8) [39].

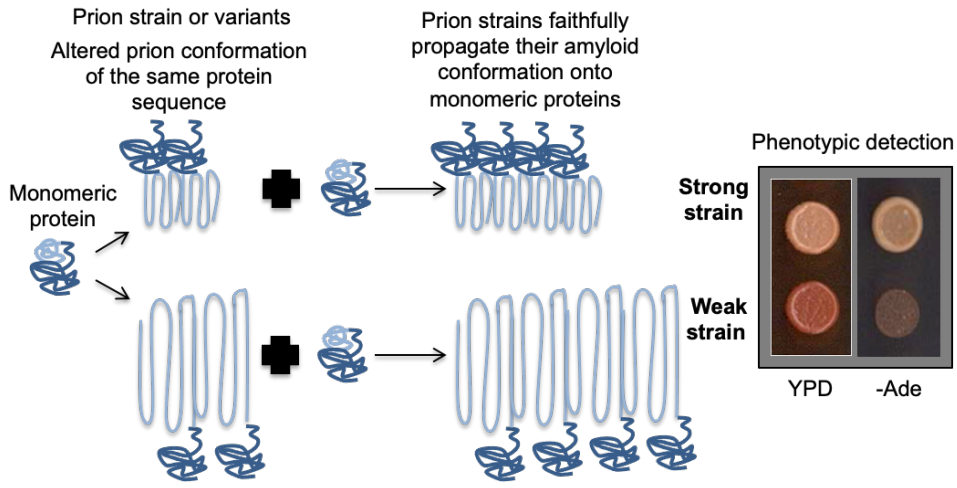

Figure 1.8 Prion strains. Confirmational changes in the misfolding of the protein during the nucleation step allows for the formation of prion strains (or variants in yeast). Once formed, these strains faithfully propagate their misfolded confirmation onto monomers of the same amino acid sequence. In yeast, these different strains can be monitored phenotypically. Strong variants have a whitish color on YPD and strong growth on –Ade medium, while weak variants have a darker pink color on YPD and weaker growth on –Ade.

For the yeast prion [*PSI*$^{+}$], it is known to exist in several different variant states caused by different confirmations of Sup35 fibrils and their interactions with chaperones (*e.g* Hsp104) leading to phenotypic differences. One of them is deemed the “strong” variant which is characterized by white growth on YPD and strong growth on -Ade medium. This is due to it being easily fragmented by the chaperone Hsp104, leading to more propagons causing more efficient immobilization of newly synthesized Sup35. In contrast the weak variant, consist of a larger prion core, leading to less disaggregation by Hsp104, causing a phenotype of a pinkish color on YPD and less efficient growth on -Ade medium.

1.3 Yeast models for Aβ and MAPT

Budding yeast have served as a powerful tool for studying complex eukaryotic mechanisms. The reason being is that many of the cellular mechanisms including replication, recombination, cell division, and metabolism is conversed between yeast and other eukaryotes, including mammals. This has held true for the study of prion proteins, as the same features that effect protein misfolding in mammals also holds true in yeast [40]. Yeast have been very crucial in the understanding the molecular mechanism of prions/amyloids as disease manifestation in humans and other mammals has long incubation periods which has made it hard for traditional mammalian models for identification of aggregation factors and drug screening. While many of the genes associated with these neurodegenerative diseases caused by amyloids/prions do not have homologs in yeast, the other proteins influencing their aggregation behavior do and their heterologous overexpression can be phenotypically characterized and have led to major breakthroughs into novel therapeutic targets and drugs [41, Miller-Fleming, 2008 #25]. Here I will briefly examine some of the yeast models in Table 1.3 and Table 1.4 that have helped in the better understanding in amyloid formation and propagation of both Aβ and MAPT.

Table 1.3 Summary of yeast models for studying Aβ.

Mode of Action	Model Features	Pitfalls	Reference Paper
Aβ fused to fluorophores	Both forms of Aβ ($A\beta_{40}$ and $A\beta_{42}$) fused to fluorophores (*e.g* GFP) form detergent resistant aggregates in yeast and allow for microscopic detection	Since Aβ instantly aggregates, these models cannot be used address amyloid formation	(Rubel *et. al.* 2013)
Fluorophores fused to Aβ	Here the fluorophore is fused in front of Aβ (e.g. GFP-Aβ) and aggregation suppresses fluorescence. Useful for drug screening.	Again, Aβ is always present as aggregates, so these models can only address further Aβ aggregation and cannot address amyloid nucleation and polymerization	(Caine *et. al.* 2007), (Macreadie, 2008)
Aβ with the addition of secretion peptides fused to fluorophores	Here the addition of a secretory signal allows for Aβ to be exocytosed into the periplasmic space (a hallmark of AD is accumulation of Aβ aggregates outside of neurons)	Toxicity of Aβ might not be relevant to human AD and screening targets do not address Aβ aggregation, the triggering factor of AD.	(Matlack *et. al.* 2014), (D'Angelo *et. al.* 2013)
Substitution of Aβ for the PrD of Sup35	$A\beta_{42}$ fused to the M and release factor domain of Sup35, which allows for more easy phenotypic detection of Aβ aggregation based on readthough assay of Sup35 (Figure1.4)	$A\beta_{42}$ fusion constructs instantly aggregates which prevents the monitoring between monomeric and aggregated Aβ, the triggering event in AD.	(Park *et. al.* 2011), (von der Haar *et. al.* 2007)
PrD of Sup35 fused to Aβ	$A\beta_{40}$ and $A\beta_{42}$ fused to PrD of Sup35 also allows for phenotypic detection, however here it is monitored separately via aggregation of another protein Sup35	Only monitors the nucleation step of aggregation formation, does not address propagation.	(Chandramowlishwaran *et. al.* 2018)

Table 1.4 Summary of yeast models for studying MAPT.

Mode of Action	Model Features	Pitfalls	Reference Paper
Yeast shuttle vectors containing MAPT	Overexpression of isoforms of MAPT in both WT and gene deletion yeast strains	Only allows for the monitoring of MAPT aggregation via biochemical techniques	(De Vos *et. al.* 2011)
MAPT in yeast surface display vector	Expression of MAPT on the yeast cell surface	Only allows for studying protein-protein interactions and does not address the phosphorylation and aggregation of MAPT, its hallmarks in AD.	(Wang *et. al.* 2020)

1.4 Objectives

Prior to this work, our lab had established a yeast assay for studying the propagation step in prion formation for the protein Aβ_{42}, associated with AD. In this assay it was previously shown that Aβ_{42} is capable of forming a prion and that its switch between its soluble and aggregated state can be easily monitored using a phenotypic assay. Here our objective is to continue some of the previous work in establishing the model, specifically demonstrating the ability of the Aβ peptide to form and maintain a prion in yeast is controlled exclusively by the Aβ peptide. We will also use this assay to determine if Aβ isolated from different patients suffering from AD are capable of forming variants.

Also associated with AD, are the proteins MAPT and U1-70k. Previous studies have shown that MAPT is capable of forming aggregates in yeast, but not whether these aggregates are amyloid in nature. Using both *in vivo* and *in vitro*

techniques we would like to determine if aggregates formed by MAPT are amyloid fibrils. Specifically, we will use plasmids expressing different domains of MAPT to determine specific sequence factors that control its aggregation, along with determining if any other cellular factors such as kinases can influence its aggregation capabilities. We will also employ similar techniques to study U1-70k, which to date has not been specifically studied in yeast, to determine if the same sequence factors that control aggregation in humans, also holds true in yeast.

Our lab has also established a yeast model for studying the nucleation step in amyloid formation for mammalian amyloidogenic proteins. This assay has shown that the same sequence elements that drive amyloid formation in humans, remains the same in yeast. Here we will build off of those original studies to study protein or peptide sequences that have not been clearly linked to disease. Specifically, we will use our assay to study proteins or peptide sequences that have been demonstrated to have amyloid-like properties either experimentally or computationally. We will also use this assay to study novel synthesized chemical compounds to determine if they can prevent the initial nucleation of Aβ, the triggering event in AD.

CHAPTER 2. MATERIALS AND METHODS

2.1 Materials

Strains

The genotype of *Saccharomyces cerevisiae* strains used in this study are listed in Appendix Table A. The haploid [*PSI*$^+$][*PIN*$^+$] strain GT81-1C is a meiotic spore of the homozygous autodiploid GT81. The [*psi*$^-$][*pin*$^-$] strain GT409 was obtained from GT81-1C via curing by guanidinium hydrochloride (GuHCl), while the [*psi*$^-$][*PIN*$^+$] strain GT159 was obtained via curing GT81-1C of [*PSI*$^+$] using excess Hsp104. The [*psi*$^-$][*pin*$^-$] strains GT671 and GT680 were used as the source for making the [*ABE*$^+$] strains and checking plasmid functionality in the shuffle experiments in Chapter 3 and are the haploid derivatives of GT81. Both GT671 and GT680 contained a *sup35Δ::HIS3* transplacement on the chromosome and was maintained alive by a Sup35-expressing plasmid. GT671 contains the pASB2 plasmid, with a *LEU2* marker, while GT680 contains the pYCH-U2 plasmid, with a *URA3* marker.

Plasmids

Appendix Table B provides a list of all plasmids constructed or used for this work together with their descriptions. Chapters 3 through 6 each contain a section titled “Plasmids” and also contains a brief description along with construction strategy if applicable for each plasmid used in specific work for each chapter.

Primers

Appendix Table C provides a list of all primers used for this work with their sequences and descriptions.

Enzymes and antibodies

Enzymes used for molecular cloning, PCR, ligation, and site-directed mutagenesis, including restriction endonucleases: *Bam*HI, *Eco*RI, *Xba*I, *Not*I, *Sac*I, *Xho*I, *Pst*I, Mung Bean nuclease, Taq polymerase, and T4 DNA ligase, were purchased from New England Biolabs. Antibody to Sup35C was a gift of Dr. D. Bedwell (Department of Biochemistry and Molecular Genetics, University of Alabama at Birmingham). GFP antibody was purchased from Sigma. The Rpl3 antibody was used as a loading control and was a gift from Dr. J.R. Warner (Department of Cell Biology, Albert Einstein College of Medicine). The MAPT specific antibodies PHFI, MCI, and CP13 were a gift of Dr. Lary Walker (Department of Neurology, Emory University).

2.2 Genetic and microbiological techniques

Standard yeast media and growth conditions

Yeast media and protocols were as described previously (Sherman 2002) [42]. Rich organic medium (YPD) contained 1% yeast extract, 2% peptone, and 2% dextrose. Organic YPG medium containing glycerol (3%) instead of glucose was used to identify respiratory incompetent (Pet-) transformants that arose due to loss of mitochondrial DNA during transformation and were eliminated from

further analysis. Synthetic dropout (SD) media were designated by the supplements that are missing (e.g -Ade for the synthetic medium lacking adenine) and contained 0.17% yeast nitrogen base without amino acids or ammonium sulfate, 0.5% ammonium sulfate, 2% glucose and 13 nutritional supplements (adenine, arginine, histidine, isoleucine, leucine, lysine, methionine, phenylalanine, threonine, tryptophan, tyrosine, uracil, and valine) unless noted for dropout. Standard medium contains 3 μM copper sulfate ($CuSO_4$); it was supplemented with 10, 50, 100, 150, or 300 μM $CuSO_4$ as indicated to induce higher expression of genes under the P_{CUP1} promoter. Yeast cultures were grown at 30°C. Liquid cultures were grown with at least at least a 1/5 media/flask volumetric ratio in a shaking (200-250 rpm) incubator at 30°C. Optical densities of yeast cultures were measured at 600 nm using Shimadzu UV-2450 spectrophotometer.

In order to examine phenotype of each yeast strain, single colonies from purified yeast cultures were patched to YPD and grown at 30°C overnight. This primary plate was then used to velveteen the same colonies to various media in order to examine the metabolic phenotype for each colony. Velveteening was performed by placing a piece of sterile velveteen fabric onto a replicating block, the placing the primary plate over the velveteen face-down in order for the cells from the plate to transfer onto the velveteen. The plate was then removed and the plates for metabolic testing were placed on the velveteen, one at a time, in order to transfer some of the cells to each plate. Each phenotype screening profile began

with YPG and ended with YPD in order to verify that viable cells were still available for growth, as useable colonies should grow on both these media types.

Bacterial transformation procedure

Chemically competent DH5α *Escherichia coli* were transformed using standard laboratory protocols [43].

Yeast transformation procedure

Transformation of yeast cells was preformed similarly to the previously described method (Gietz *et. al.* 1992) [44]. Briefly, a pre-culture of the desired yeast strain was grown overnight in 10 mLs of YPD. This preculture was used to inoculate a 50 mL flask of YPD the following day and incubated at 30°C for 2-4 hours. The culture was then transferred to two sterile Oakridge tubes and spun down at 3,000 rpm for 10 minutes, the supernatant poured off, the cells were washed with water, then spun down again. The water was removed, and the cells were re-suspended in 10 mLs of 0.1 M lithium acetate Tris-EDTA buffer (LiAc-TE) then incubated at 30°C for 60 minutes with shaking. Cells were then centrifuged again, the supernatant was removed, and the cells were re-suspended in 0.5-1.0 mL of 0.1 M LiAc-TE (depending on number of transformations, 100 μL per transformation). For each transformation, 100 μL of cells was placed into a microcentrifuge tube along with 10 μg of transforming DNA and 20 μg of carrier DNA. For each transformation attempt, one transformation had no transforming DNA (negative control). Transformations were incubated for 30 minutes at 30°C,

then 700μL of Lithium acetate-Polyethelene glycate-Tris-EDTA buffer (LiAc-PEG-TE) was added to each tube, and tubes were incubated for an additional 60 minutes at 30°C. Cultures were heat shocked at 42°C for 6 minutes, then placed at 4°C overnight. The following day, cultures were spun down at 3000 rpm for 2 minutes, the supernatant was mostly removed. Approximately 200μL of supernatant was used to re-suspend cells and plated onto appropriate selective media. Plates were incubated 3-4 days to obtain transformative colonies.

2.3 DNA analysis and plasmid construction

E.coli small-scale DNA isolation protocol

Alkaline lysis method was used for quick isolation of small amount of plasmid DNA from *E. coli* for obtaining DNA. *E. coli* was patched onto LB plates containing antibiotics selective for the target plasmid. Wooden toothpicks were used to collect cells that were then resuspended in 100μL of Solution I (25 mM Tris-HCl, 10 mM EDTA, 50 mM glucose, pH 8.0). 200μL of Solution II (0.2 M NaOH, 1% sodium dodecyl sulfate (SDS)) was added and mixed by inversion, and samples were kept on ice. 150μL of Alkaline Lysis Solution III (5M potassium acetate, pH 5.0) was added and mixed by inversion. The sample was then incubated on ice for 5 minutes and centrifuged at 15,000 rpm for 5 minutes to pellet the cell debris. The supernatant was collected in a new microcentrifuge tube, and 2 volumes of 95% ethanol was added, followed by vortexing to mix, and incubated on ice for 5 minutes. The sample was again centrifuged at 15,000 rpm for 5 minutes, and the supernatant was discarded. The pellet was washed with 70% ethanol and vortexed

briefly. The sample was centrifuged again at 15,000 rpm for 5 minutes, and the supernatant was discarded. The DNA pellet was dried thoroughly and resuspended in 50μL of TE (or water) containing 10 μg/mL RNase A. The sample was incubated at 37°C for 30 minutes for RNA removal. Isolated plasmid DNA was stored at -20°C.

DNA extraction from agarose gels

DNA fragments generated from restriction digestion or PCR reaction were separated by running the fragments on a 1% TBE agarose gel stained with ethidium bromide. DNA bands corresponding to desired products were visualized using a UV transilluminator (Fischer Biotech 321nm Variable Intensity Transilluminator) and excised with a scalpel and were purified using an IsoPure DNA Purification Prep Kit (Denville).

DNA sequencing

DNA was purified for sequencing using an IsoPure DNA Purification Kit (Denville) and was eluted in water. Purified DNA and subsequent sequencing primers were diluted to specified concentrations for Sanger sequencing performed by Eurofins MWG Operon Sequencing (Huntsville, AL).

2.4 Protein Analysis

Yeast total protein isolation and Bradford assay

For total yeast protein isolation and purification, cultures were grown in a liquid medium overnight before collection by centrifugation at 3000 rpm for 10 minutes. Pelleted cells were resuspended in 100-300 μL of ice-cold lysis buffer (25 mM Tris pH 7.5, 0.1 M NaCl, 10 mM EDTA, 100 μg/ml cycloheximide, 2 mM benzamidine, 20 μg/ml leupeptin, 4 μg/ml pepstatin A, 1 mM N-ethylmaleimide, 1x protease inhibitor cocktail from Roche Diagnostics, 2 mM PMSF) along with one volume glass beads. Cells were agitated for 8 minutes using the disruptor genie in the 4°C cold room. Cell debris was pelleted by centrifugation at 3,000 rpm for 3 minutes. The supernatant was transferred to a clean microcentrifuge tube and the concentration of protein in the sample was determined using the colorimetric Bradford protein assay (BioRad), which was normalized using the aforementioned lysis buffer. Concentration was based on an absorbance shift of the dye Coomassie Brilliant Blue G-250 using the Shimadzu UV-2450 spectrophotometer at an absorbance of 595 nm.

SDS-PAGE and western blotting

For denaturing polyacrylamide gel electrophoresis (SDS-PAGE) and Western analysis, protein samples were incubated with 0.25x volume of 4x loading buffer (240 mM Tris-HCl pH 6.8, 8% SDS, 40% glycerol, 12% 2-mercapthoethanol and 0.002% bromophenol blue) at room temperature, boiled for 10 minutes, and

run in a 10% SDS-polyacrylamide gel with 4% stacking gel in Tris-Glycine running buffer (25 mM Tris, 192 mM glycine, 0.1% SDS, pH 8.3), followed by electrotransfer to a Hybond-ECL nitrocellulose membrane (GE Healthcare Life Sciences), pre-blocking with 5% non-fat milk made in 0.1% TBS-Tween, and probed with the appropriate antibody overnight at 4°C. The following day the membrane was thoroughly washed in 0.1% TBS-Tween 3 times with gentle shaking for 10 minutes each wash, before probing with appropriate secondary horseradish peroxidase-conjugated antibody for 1 hour with gentle shaking. Visualization of the reaction was detected using the chemiluminescent detection reagents as described in the GE Healthcare protocols.

SDD-AGE

Analysis of protein aggregation was achieved by running protein samples on a semi-denaturing detergent-agarose gel (SDD-AGE) as described in Bagrianstev *et. al.* 2006 [45]. Protein extracts were incubated with 0.25 volume of 4x loading buffer (240 mM Tris-HCl pH 6.8, 8% SDS (or sarkosyl), 40% glycerol, and 0.002% bromophenol blue) at room temperature for 10 minutes and run in a 1.8% Tris-Acetate EDTA (TAE)-based agarose gel with 0.1% SDS in running buffer for 2-2.5 hours at 80V in the 4°C cold room followed by protein transfer to a nitrocellulose membrane by capillary blotting. Membranes were reacted to appropriate antibodies after pre-blocking in 5% non-fat milk. Chemiluminescent detection was completed as described previously.

2.5 Prion curing assay

Prion curing by GuHCl

To determine whether strains could be cured of respective prions by passage on guanidine hydrochloride (GuHCl), each strain was first streaked onto YPD for single colonies. Single colonies were then patched onto YPD containing 5 mM GuHCl, grown for 3 days at 30°C, then serially patched to YPD + GuHCl an additional 2 times. The final patch of growth for each culture was then streaked onto YPD for individual colonies, grown 1 day, velveteened to YPD and -Ade medium, and visually examined and counted to determined curing via color on YPD (red if cured) and growth on -Ade (growth indicating non-cured). Tested colonies were simultaneously passaged on YPD medium as a control.

2.6 Microscopy

General fluorescence microscopy and colocalization

To visualize protein aggregates tagged by GFP, YFP, and CFP fluorophores, respective cultures were grown according to the procedures discussed above. 500 µl samples were taken from cultures at specified time points following expression, and spun down at 3000 rpm for 2 min, after which the supernatant was removed and the cells were resuspended in 30–50 µl of water. 10 µl of each sample was then placed onto a microscope slide and sealed with clear nail polish to prevent drying. Fluorescence was detected under a BX41 microscope (Olympus) at 100× (oil immersion) using the appropriate emission

filter. For colocalization analysis, the haploid [*psi*$^-$][*pin*$^-$] strain GT409 was transformed with the desired plasmids and co-expressed. Samples were prepared and analyzed in the same way as above using appropriate filters for imaging. Images were taken using an Olympus DP-71 camera, and were overlaid using the program DP manager (Olympus) to determine colocalization.

Hexanediol analysis

The yeast cultures (1 ml) were pelleted at 3000 x g for 3 min and the supernatant was discarded. The cells were then resuspended in 200 μl of medium (SD(+13), 0.1% Triton X100, 10% 1,6-Hexanediol). Media excluding 1-6, hexanediol was used as the control. The cells were incubated at room temperature for 10 minutes. The cells were again pelleted (12-13 sec short centrifugation) to concentrate them on the bottom of a microcentrifuge tube. The supernatant was not discarded. The pellet was gently resuspended on the bottom of the microcentrifuge tube and 5-10 μl of the dense suspension was used for slide preparation and was imaged by fluorescence microscopy.

2.7 Statistical analysis

Experimental means are depicted in graphs, with error bars typically representing standard deviations (unless stated otherwise), which were calculated according to a standard formula (McDonald 2009) [46]. These numbers are shown in tables either in the main text or located in the supplemental text. In some instances, in the fluorescence microscopy data, error bars represent standardized errors (SDs), calculated according to binomial or polynomial distribution formula

(SE_p = sqrt [p(1−p)/n], where p is the frequency of the given class, and n is the total number of cells in the sample). Statistical significance of differences was determined by Student's t-test. Differences with $P \leq 0.05$ were considered significant.

CHAPTER 3. CHARACTERIZATION OF AMYLOID STRAINS DEPENDENT ON Aβ PEPTIDE IN YEAST

This chapter includes data published in

Deckner, Z., Chandramowlishwaran, P., Kulichikhin, KY., Li, NX., Walker, LC., Lynn, DG., Chernoff, YO. Propagation of amyloid beta strains in yeast. (In preparation.)

3.1 Summary

Our lab has previously established a yeast model for studying the propagation of the amyloid protein $A\beta_{42}$ associated with AD [47]. To do this, a portion of the prion forming domain of Sup35, specifically the glutamine and asparagine (QN) rich region of the N-terminal domain of Sup35 was replaced by the $A\beta_{42}$ peptide. This chimeric protein is functional in translation termination and can spontaneously switch to a non-functional polymeric state, generating a prion isoform deemed [*ABE*$^{+}$]. Previous data shown in Chandramowlishwaran *et al.* 2018 demonstrates that the [*ABE*$^{+}$] prion is capable of adopting differing prion isoforms, termed variants, that can be monitored through color and growth on yeast media using a readthrough assay [47]. She also was able to demonstrate that amyloid "seeds" composed of *in vitro* produced $A\beta_{42}$ are capable of seeding the conversion of the chimeric protein monomers, leading to the formation of a spectrum of prion variants. Here we are applying this model to studying $A\beta_{42}$ strains produce in brains of AD patients to determine if there is a link between $A\beta_{42}$ strains and phenotypic diversity seen in AD.

3.2 Specific materials and methods

Materials

Strains, plasmids, and oligonucleotide primers used in this study are described in Appendix tables A, B and C respectively.

3.2.1.1 Strains

The *S. cerevisiae* strains used in this study are shown in Appendix A. The [*abe*$^{-}$] (strain GT2126) and the spontaneous [*ABE*$^{+}$] strains: [*ABE*$^{+}$-25] (GT2306), [*ABE*$^{+}$-10] (GT2217), and [*ABE*$^{+}$-9] (GT2216) were previously obtained and shown in Chandramowlishwaran et. al. 2018 [47]. [*ABE*$^{+}$] strains that were made via transfection (procedure discussed in methods section) were derived from the [*abe*$^{-}$] strain and transfected with either *in vitro* produced Aβ_{42} or protein extracts enriched for Aβ_{42} from patients diagnosed with AD, along with an empty *LEU2* plasmid that was subsequently lost.

The [*psi*$^{-}$][*pin*$^{-}$] yeast strain GT680 containing the chromosomal deletion of *SUP35* and kept alive via a *URA3* plasmid containing wild-type Sup35 under its own promoter was used for evaluating the functionality of the constructs [*LEU2 SUP35NR-MC*] and [*LEU2 Aβ$_{42}$-SUP35NR-MC*] used in the direct and reverse shuffle experiments discussed in section 3.5.

3.2.1.2 Plasmids and primers

The *S. cerevisiae - E. coli* shuttle plasmids and primers used in this study are shown in Appendix Tables B and C respectively. The plasmid P_{SUP35}-$A\beta_{42}$-*SUP35NR-MC (URA3)* used in this study are previously described in Chandramowlishwaran *et. al.* 2018 and shown in Figure 3.1 [47]. The P_{CUP1}-$A\beta_{42}$-*SUP35NR-MC (URA3)* plasmid was constructed by removing the $A\beta_{42}$-*SUP35NR-MC* fragment using the *Bam*HI and *Sac*I enzymes and placed into plasmid pMCUP1 using the same enzymes. The P_{CUP1}-$A\beta_{42}$-*SUP35NR-MC (LEU2)* plasmid was constructed by removing the entire cassette (promoter and genes) from the *URA3* plasmid using the *Xho*I and *Sac*I enzymes and placed into plasmid pRS415 (*LEU2*) using the same enzymes. The control plasmid P_{CUP1}-*SUP35NR-MC* (*URA3*) was received from the Amyloid Biology Lab at St. Petersburg University, St. Petersburg Russia. It was then subsequently digested using the *Xho*I and *Sac*I enzymes to remove the cassette and placed it into the pRS415 backbone constructing the P_{CUP1}-*SUP35NR-MC* (*LEU2*) plasmid.

3.2.1.3 Antibodies

The Sup35C antibody used in this study is described in Chapter 2.

3.2.1.4 Protein aggregates used for transfection

In vitro aggregated $A\beta_{42}$ was prepared from two different sources. We purchased lyophilized $A\beta_{42}$ from GenicBio and aggregates were prepared by Aditi Sharma from Dr. Andreas Bommarius research lab (School of Chemical and

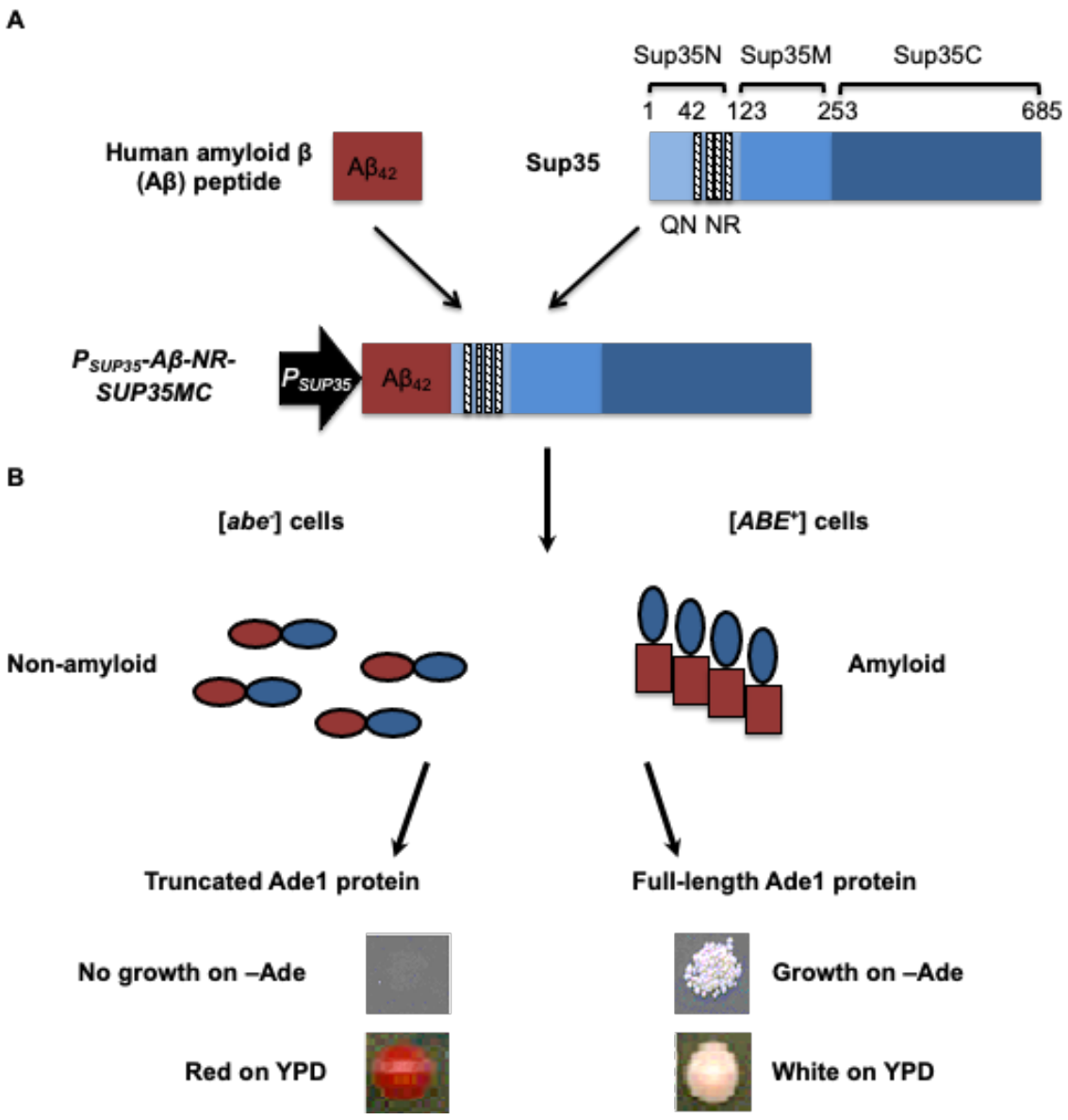

Figure 3.1 Scheme of construction of chimera Aβ-NR-MC and readthrough assay to determine prion status in yeast. (A) The region coding for the first 42 amino acids of the N-terminal domain of Sup35 was substituted with the region coding for human Aβ version 42. The NQ and NR region in Sup35 refers to the asparagine, glutamine rich region and oligopeptide repeat region respectively. In yeast strains containing ade1-14 (UGA) reporter and a deletion of Sup35 on the chromosome, defects in translation termination caused by [*ABE*$^{+}$] is detectable on by growth on –Ade medium or by color on YPD media, due to the accumulation of a red pigment within the yeast vacuole, an intermediate in adenine biosynthesis.

Biomolecular Engineering, Georgia Tech). The other was synthesized in the lab of Dr. David Lynn (Department of Chemistry, Emory University) and aggregates were prepared by his graduate student Noel Xiang' An Li. N. Li and C. Gordon in David Lynn's lab also prepared the samples containing $A\beta_{42}$ derived from human brain extracts. Cortical brain extracts from patient samples from the Emory Brain Bank were kindly provided by Maria Gearing through Lary Walker (Department of Neurology, Emory University). Brain extracts arose from different classifications of patients, based on manifestation of clinical symptoms, and will be referred to as either regular or rapid progress AD cases. Brain samples were treated to increase the amount of $A\beta_{42}$ within the sample while removing other brain tissue. Here, samples termed rapid-progress AD are determined by a steep decline in test scores from year to year; this is particularly evident just before death, not by the usual definition as diagnosis to death in 2 or 3 years. Samples termed *in vitro* $A\beta_{42}$ seeded by brain extracts were made by taking extracts derived from AD patient samples to be used as an initial "seed" to template the conversion of *in vitro* $A\beta_{42}$ into an aggregated state.

Methods

Standard protocols were used for DNA isolation, gel electrophoresis, restriction digestion, gel extraction, ligation, and bacterial transformation as described in Chapter 2 for plasmid construction. Standard yeast media and standard procedures for yeast cultivation, phenotypic analysis, and transformation were used and are also described in Chapter 2. The procedures for the plasmid

shuffle experiment are described in the results section (section 3.3.5). The method for the guanidine hydrochloride curing experiment is described in Chapter 2 and the method for transfection of protein material is described below.

3.2.2.1 Transfection procedure

Aggregated protein containing $A\beta_{42}$ either from in vitro or from brain extracts was transfected into [*abe*$^-$] yeast cells containing the [*URA3 Aβ$_{42}$-SUP35NR-MC*] plasmid using our modified protocol described by Tanaka *et al.* 2006 [48] (Figure 3.2). Our modifications differed from the published protocol as follows: 1) 1 M dithrothreitol was added separately to the SCE buffer (1 M sorbitol, 100 mM sodium citrate, 10 mM EDTA, pH 5.8) to a final concentration of 10 mM; 2) PEG buffer was prepared with 44% PEG 4000; 3) the top agar concentration was 0.8% and incubated at 42°C to prevent solidification after autoclaving; and 4) an empty plasmid containing a *LEU2* marker was transformed together with the transfected protein material as a marker for material uptake. Cells were plated on sorbitol media lacking leucine to identify transformants (having plasmid uptake and therefore, potential protein uptake). Colonies that grew in the top agar lacking leucine were characterized further for the Ade$^+$ phenotype indicating successful protein uptake.

3.2.2.2 Colony purification of Ade$^+$ colonies

As a step during the transfection procedure, colony purification is performed to lose the *LEU2* plasmid used as a marker. For this, the original Ade$^+$ transfectant

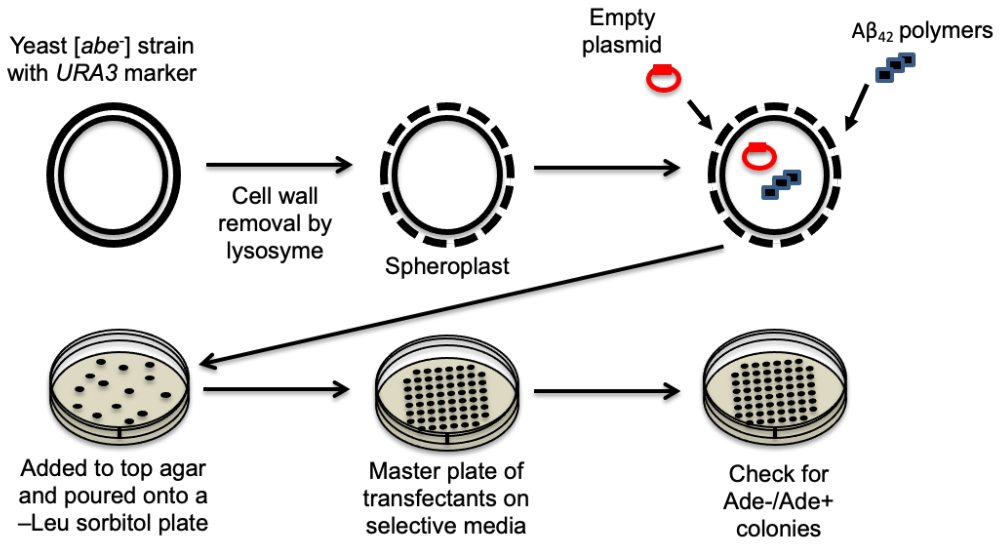

Figure 3.2 Scheme of transfection procedure.

analyzed was streaked out onto -Ura medium to cause the spontaneous loss of *LEU2* plasmids. These streaked out plates were then velveteened to the following medium: YPD, -Ura, and -Leu. Colonies were then selected from the -Ura plate that grew on both YPD and -Ura medium, but not on -Leu, indicating the loss of the *LEU2* plasmid. Eight colonies were selected from the -Ura plate and patched onto a new -Ura plate and allowed to grow for 2 days. This plate was subsequently velveteened to both YPD and -Ade to check for stability of the Ade^+ phenotype of the original Ade^+ transfectants.

3.3 Results

Transfection of yeast strains by unseeded and extract seeded by Aβ, and directly by human brain AD extracts.

Some Ade$^+$ [*ABE*$^+$] strains generated spontaneously or via transfection with *in vitro* produced $A\beta_{42}$ were previously analyzed and shown in Chandramowlishwaran *et. al.* 2018 [47]. Here, they showed that such [*ABE*$^+$] strains derived by either approach resulted in colonies displaying different phenotypic characteristics (as seen by growth on -Ade and color on YPD) indicative of prion variants (Figure 3.3A). It is known that in the case of the prion protein, the molecular differences between different variants are controlled by the prion protein itself [49]. These variants were classified into three groups designated as “strong”, “intermediate”, and “weak” which were based upon growth and color. Here, we expanded upon this previous research to determine if: a) brain-derived $A\beta_{42}$ aggregates can seed the $A\beta_{42}$-Sup35NR-MC protein into a prion form in yeast; b) *in vitro* self-seeded and brain-derived or brain-seeded $A\beta_{42}$ aggregates produce the same or different spectra of prion strains in yeast, and c) $A\beta_{42}$ aggregates from patients with different levels of severity of AD (regular versus “rapid progress” cases) produce the same or different spectra of prion strains in yeast.

To do this, the [*abe*$^-$] strain carrying the [*URA3 Aβ$_{42}$-SUP35NR-MC*]

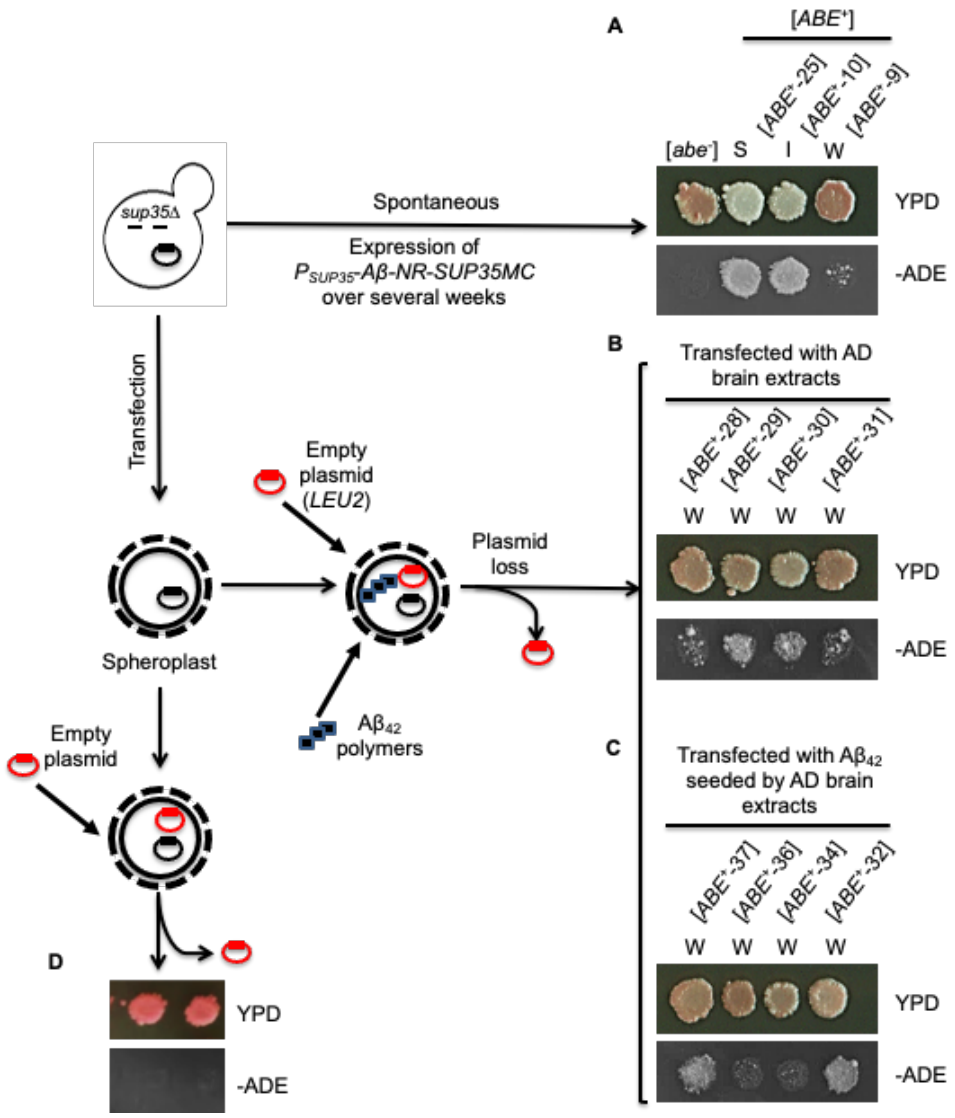

Figure 3.3 Generation of [*ABE*$^+$] colonies spontaneously and after transfection. (A) Representative Ade$^+$ colonies after long incubation of the P_{SUP35}-Aβ-NR-Sup35MC (*URA3*) plasmid. Note the S indicates strong, I indicates Intermediate, and W indicates weak [*ABE*$^+$] variant phenotype. Here the [*abe*$^-$] strain is a strain expressing the plasmid but never became Ade$^+$. (B) Representative Ade$^+$ transfectants obtained after transfection with brain extracts from different patients into a [*abe*$^-$] strain containing the [*Aβ-NR-MC URA3*] using the procedure outlined in Figure 3.2. Transfected colonies were checked for their Ade$^+$ phenotype after 14 days growth, in which colonies of different stringencies could be seen by color on YPD media and by growth on –Ade media. This process was also completed with samples of synthetic $A\beta_{42}$ that was seeded by brain extracts from various brain regions (C). (D)Colonies only transfected with the empty plasmid for selection remain [*abe*$^-$].

Table 3.1 Total Ade$^+$ colonies from transfection before colony purification.

Origin of Aβ_{42} sample	Total Ade$^+$ before colony purification	Total colonies tested
In vitro, unseeded	109	395
In vitro seeded by AD brain extracts	46	195
AD brain extracts	39	285
Control (no Aβ_{42})	1	220

Table 3.2 Classification of Ade$^+$ colonies generated in transfection experiments after colony purification.

Origin of Aβ_{42} sample	Strains of Ade$^+$ transfectants			Total Ade$^+$
	Strong	Intermediate	Weak	
In vitro, unseeded	40	34	35	109
In vitro seeded by AD brain extracts	0	0	46	46
AD brain extracts	0	0	30	30
Control (no Aβ_{42})	0	1	0	1

plasmid was transfected with $A\beta_{42}$ aggregates, derived from either human brain extracts or synthetic $A\beta_{42}$ seeded by human brain extracts using the transfection procedure described previously. As shown in Figure 3.3B, colonies transfected with material derived directly from brain extracts also show different levels of growth on -Ade and different colors on YPD as compared to strains derived spontaneously in Figure 3.3A. The same was also true for colonies transfected with aggregates of $A\beta_{42}$ seeded by brain extracts (Figure 3.3C). Cells transfected with only the empty *LEU2* plasmid remained [*abe*$^{-}$] as seen by red color on YPD and lack of growth on -Ade media (Figure 3.3D). The resulting Ade^{+} colonies derived by transfection for each sample type is summarized in Table 3.1 and their variant classification in Table 3.2.

In comparison to spontaneously derived [*ABE*$^{+}$] strains, transfectants derived from brain extracts or $A\beta_{42}$ seeded by brain extracts appeared different. Transfectants derived from brain extracts or *in vitro* $A\beta_{42}$ seeded by brain extracts formed only the “weak” class of variants (Figure 3.3A-C) as determined by growth on -Ade. However, these transfectants formed different variants of “weak” as seen by color on YPD and growth on -Ade. These ‘weak” variants were further classified as “subtype 1”, “subtype 2”, and “subtype 3” as seen by growth on -Ade as shown in Figure 3.4A-B and summarized in Table 3.4.

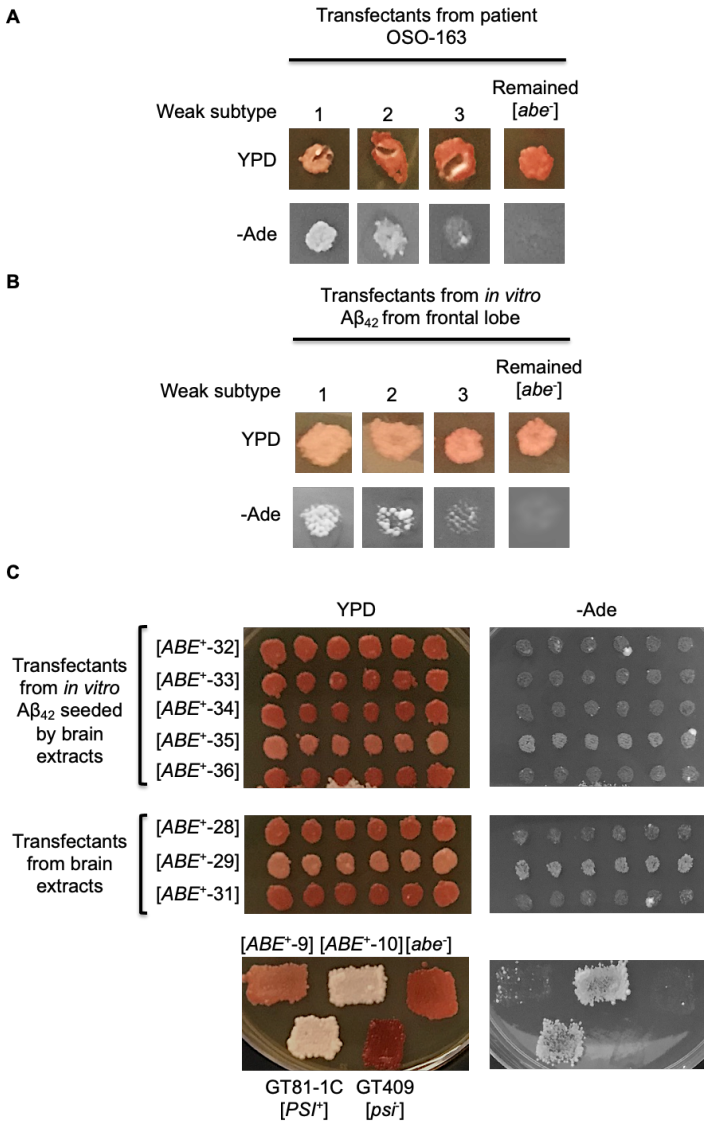

Figure 3.4 Classification and stability of weak subtypes of samples derived from brain extracts. Examples demonstrating the different subtypes of weak transfectants derived from brain extracts. Examples shown in A are from brain extracts from patient OSO-163 and examples shown in B are transfectants from *in vitro Aβ42* seeded by brain extracts from the frontal lobe. The images from the YPD plates and -Ade plates for each sample set are from the same plate, but have been cropped to place samples next to each other for comparison. (C) Ade^+ colonies from transfections were streaked out and six colonies were patched to a YPD plate and velveteened to YPD and -Ade medium to check for color and growth respectively. Colonies derived from both transfections from *in vitro* $A\beta_{42}$ seeded by brain extracts and direct brain extracts all grow on -Ade medium indicating stability. Control strains and transfection strains from brain extracts are the same plate, only cropped for labeling. Control strains for transfections seeded by *in vitro* $A\beta_{42}$ seeded by brain extracts are not shown.

Table 3.3 Stability of Ade$^+$ phenotype of transfectants derived from AD brain extracts after colony purification.

Type of AD case	Patient ID of transfecant origin	Ade$^+$ after colony purification	Ade$^-$ after colony purification	Total colonies tested
Rapid progress cases	E14-14 colony #1	1	7	8
	E14-14 colony #2	0	8	8
	E14-14 colony #3	8	0	8
	E10-64 colony #1	0	8	8
	E10-169 colony #1	0	8	8
	E10-169 colony #2	1	7	8
Regular AD case	OSO-300 colony #1	6	0	6
	OSO-300 colony #2	6	0	6
	OSO-300 colony #3	6	0	6
	OSO-159 colony #2	6	0	6
	OSO-163 colony #3	6	0	6

Table 3.4 Summary of weak subtypes generated after transfection from samples derived from AD brain extracts.

Patient ID	Weak Strains of Ade$^+$			Total Ade$^+$
	Subtype 1	Subtype 2	Subtype 3	
OSO-159	1	7	3	11
OSO-300	1	2	5	8
OSO-163	2	4	4	10
E14-14	0	1	0	1
Totals	4	14	12	30

Comparison of phenotypes of the [ABE+] strains obtained by transfection from regular AD cases and rapid progress AD cases

All tested Ade$^+$ colonies produced by brain extracts from regular AD cases or by $A\beta_{42}$ seeded from regular AD cases remained stable after colony purification as seen in Figure 3.4C and summarized in Table 3.3. In contrast, most transfectants derived from samples with rapid progress AD have lost Ade$^-$ phenotype after colony purification, with only occasional Ade$^+$ colonies remaining, that points to high mitotic instability of respective prion isolates in yeast (Figure 3.5 and Table 3.3). This points to the differences in the $A\beta_{42}$ seeds formed in the brains of regular and rapid progress AD patients.

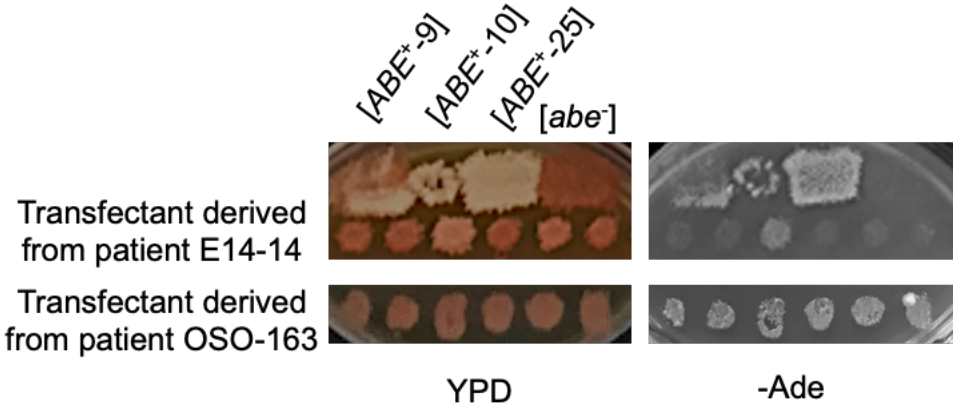

Figure 3.5 Transfectants derived from rapid progress AD cases are not stable. Initial screening from transfections of samples of both normal and rapid progress AD led to initial Ade$^+$ colonies, however after streaking out the initial colony on YPD medium to lose the empty *LEU2* vector, the colonies derived from the rapid progress cases (example patient E14-14) remain unstable as compared to those from normal AD cases (example patient OSO-163). Colonies shown are from the same plates, but are cropped for comparison. Data shown are from the same transfection experiments.

Biochemical characterization of Ade$^+$ colonies derived both spontaneously and via transfection

Proteins were harvested using our standard extraction procedure describe in Chapter 2 from representative Ade$^+$ strains generated either spontaneously or via transfection and expressing $A\beta_{42}$-Sup35N-MC. Protein extracts were normalized using the Bradford assay prior to running on a 10% SDS-PAGE gel. As per our data, differences in prion stringencies are not due to differences in the $A\beta_{42}$-Sup35NR-MC protein levels (Figure 3.6). However, it should be noted one of

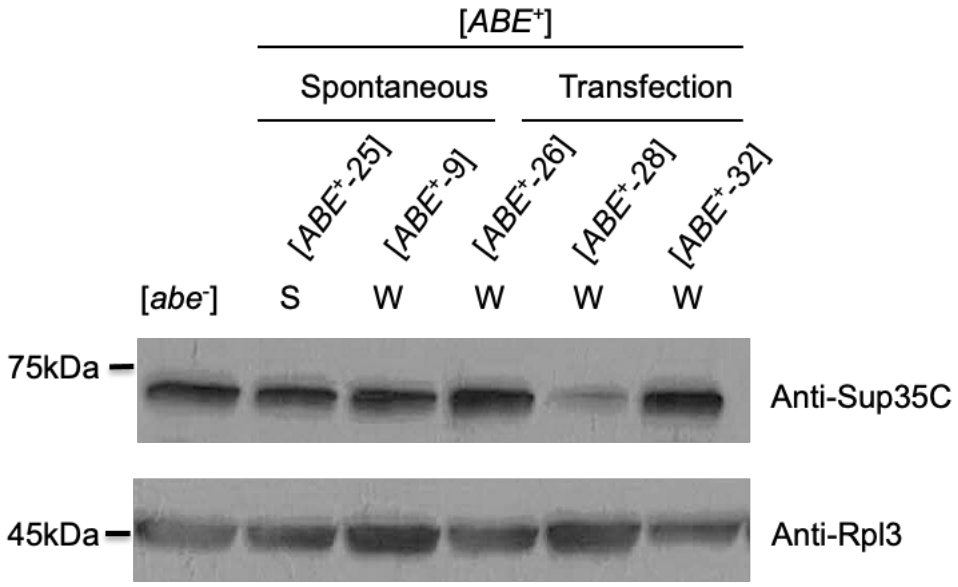

Figure 3.6 Expression of Aβ-NR-Sup35MC is the same between [*ABE*$^+$] colonies of different variants. The Aβ-NR-MC chimeric protein is expressed as the same size protein in each transfection strain indicating that difference seen are not due to the chimeric plasmid, but rather from the initial material templating the chimeric protein. Proteins were isolated and ran on 10% SDS-PAGE gel, followed by Western blotting and reaction to the anti-Sup35C antibody. The membrane was striped and then re-probed with the anti-Rpl3 antibody as a loading control.

the strains, [*ABE*$^{+}$-28], generated by transfection from a regular AD brain extract, produced detectable chimeric protein at a lesser level to [*abe*$^{-}$] and other [*ABE*$^{+}$] strains. Possible explanations could be that either protein in this strain is more proteolytically unstable, or forms very rigid aggregates that are not even solubilized by boiling in detergent in the conditions used in our experiments. In addition, we characterized representative [*ABE*$^{+}$] strains of different stringencies by employing semi-denaturing detergent agarose gel electrophoresis (SDD-AGE) as described in Chapter 2. As expected, [*ABE*$^{+}$] strains produced detergent resistant polymers, a characteristic of amyloids, on SDD-AGE (Figure 3.7). Moreover, polymers from the strong and weak strains run in different ways, showing the differences in polymer distribution between these strains.

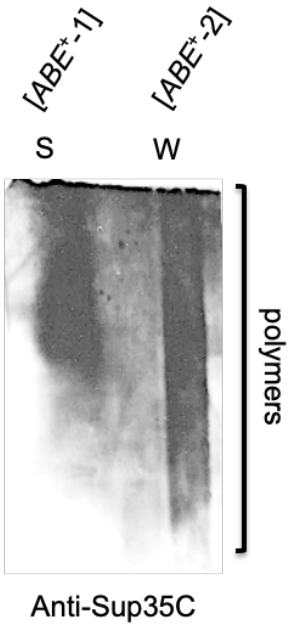

Figure 3.7 Biochemical characterization of different [*ABE*$^{+}$] variants. The semi-denaturing detergent agarose gel electrophoresis (SDD-AGE) shows that $A\beta_{42}$ is capable of forming different strains (or variants).

Guanidine hydrochloride treatment of [ABE+] colonies

Guanidine hydrochloride (GuHCl) is a known agent that cures a majority of yeast prions, including [*PSI*$^{+}$] [50-52]. GuHCl's curing mechanism is not due to prevention of the aggregation of Sup35 or destruction of [*PSI*$^{+}$] aggregates. Rather, millimolar concentrations of GuHCl blocks the generation of new "propagons" (proliferating prion subunits), thus antagonizing the ability of yeast prions to be passed on to daughter cells and decreasing their mitotic stability [53]. This is achieved via inhibition of Hsp104, the crucial chaperone involved in aggregate fragmentation and propagon generation [54]. Here, we investigated the effects of GuHCl on the proliferation of the [*ABE*$^{+}$] prion using the GuHCl curing procedure outlined in Chapter 2. Following the third passage, strains were streaked out onto a YPD plate to check for the appearance of red colonies (indicative of prion curing). Growth of these colonies on -Ade was also tested. The [*PSI*$^{+}$] yeast strain GT81-1C was used as a positive control for curing. As shown in Figure 3.8, among the eight [*ABE*$^{+}$] strains tested, generated either spontaneously or via transfection, none was curable of a prion state by GuHCl. In contrast, the [*PSI*$^{+}$] control GT81-1C was efficiently cured of the [*PSI*$^{+}$] prion following passaging on the GuHCl (but not after passaging on control YPD) medium. Results of this experiment are summarized in Table 3.5.

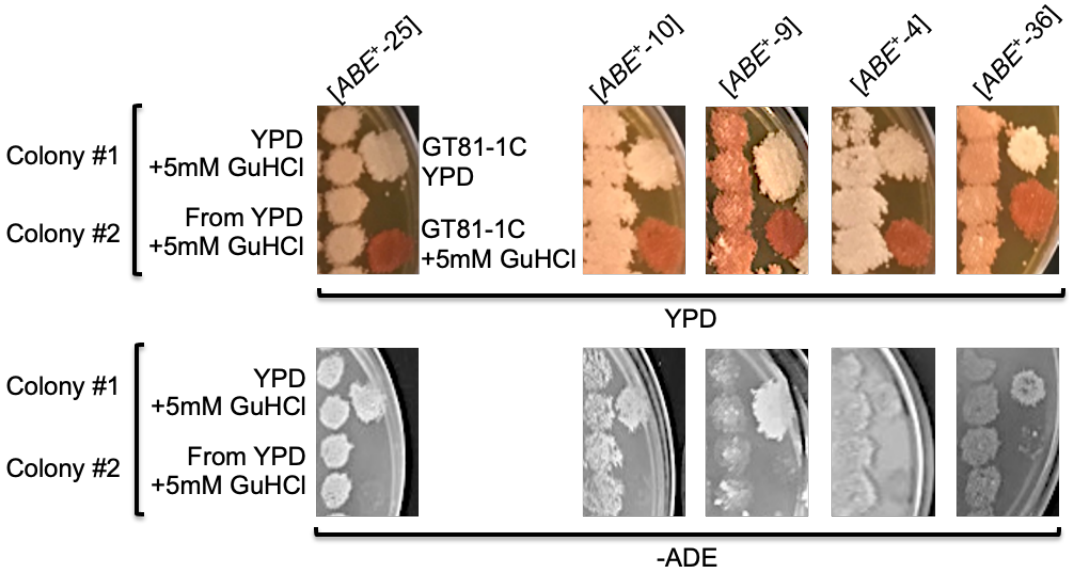

Figure 3.8 [*ABE*$^+$] strains are not curable by GuHCl. The [*ABE*$^+$] prion of different stringencies and formed both spontaneously and from transfection maintain their Ade$^+$ phenotype after 20-40 generations in the presence of 5mM guanidine hydrochloride (GuHCl), an agent antagonizing the propagation of some yeast prions. The [*PSI*$^+$] strain GT81-1C was used as a control.

Evidence that [ABE$^+$] strain propagation requires the Aβ42 portion of a chimeric protein.

To eliminate the possibility that the prion established (either spontaneously or by transfection) is not dependent on the NR portion of Sup35 present in our chimeric plasmid, we employed a plasmid shuffle procedure to demonstrate that the presence of $A\beta_{42}$ is necessary to keep the [*ABE*$^+$] prion present in these strains. First, we checked if the Sup35NR-MC (Figure 3.9A) protein produced is efficient in translation termination in the absence of complete Sup35. Poor termination efficiency could mimic the presence of a prion, and therefore could be confused with a prion phenotype. For checking protein functionality, the *P_{CUP1}-Sup35NR-MC*

Table 3.5 Summary of [*ABE*$^+$] strains checked by GuHCl.

[*ABE*] strain number	Strain Name	Number of colonies passaged through YPD or YPD + 5 mM GuHCl	Number of colonies streaked after 3rd passage on YPD or YPD + 5 mM GuHCl	Number of subcolonies checked from colonies passaged through YPD	Number of subcolonies checked from colonies passaged through YPD + 5 mM GuHCl
[*abe*$^-$]	GT2126	6	4	24	24
[*ABE*$^+$-25]	GT2036	6	4	24	24
[*ABE*$^+$-10]	GT2217	6	4	24	24
[*ABE*$^+$-9]	GT2216	6	4	24	24
[*ABE*$^+$-4]	GT2170	6	4	24	24
[*ABE*$^+$-37]	GT2387	6	4	24	24
[*ABE*$^+$-30]	GT2380	6	4	24	24
[*ABE*$^+$-26]	GT2376	6	4	24	24
N/A	GT409 [*psi*$^-$] control	1	1	8	8
N/A	GT81-1C [*PSI*$^+$] control	1	1	8	8

plasmid was transformed into a [*psi*$^-$][*pin*$^-$] strain containing the chromosomal deletion of Sup35 (*sup35Δ*). This strain also contained a *URA3* plasmid containing Sup35 under its own promoter as *SUP35* is an essential gene and cannot be deleted. These strains also contain the *ade1-14* reporter system allowing for the detection of nonsense suppression as indicated by growth on -Ade medium (Figure 1.7). The plasmid containing Sup35NR-MC was fully efficient at terminating translation, in the presence of Sup35, however only when overexpressed in the presence of 150 μM $CuSO_4$ (Figure 3.9B). We also tested termination efficiency

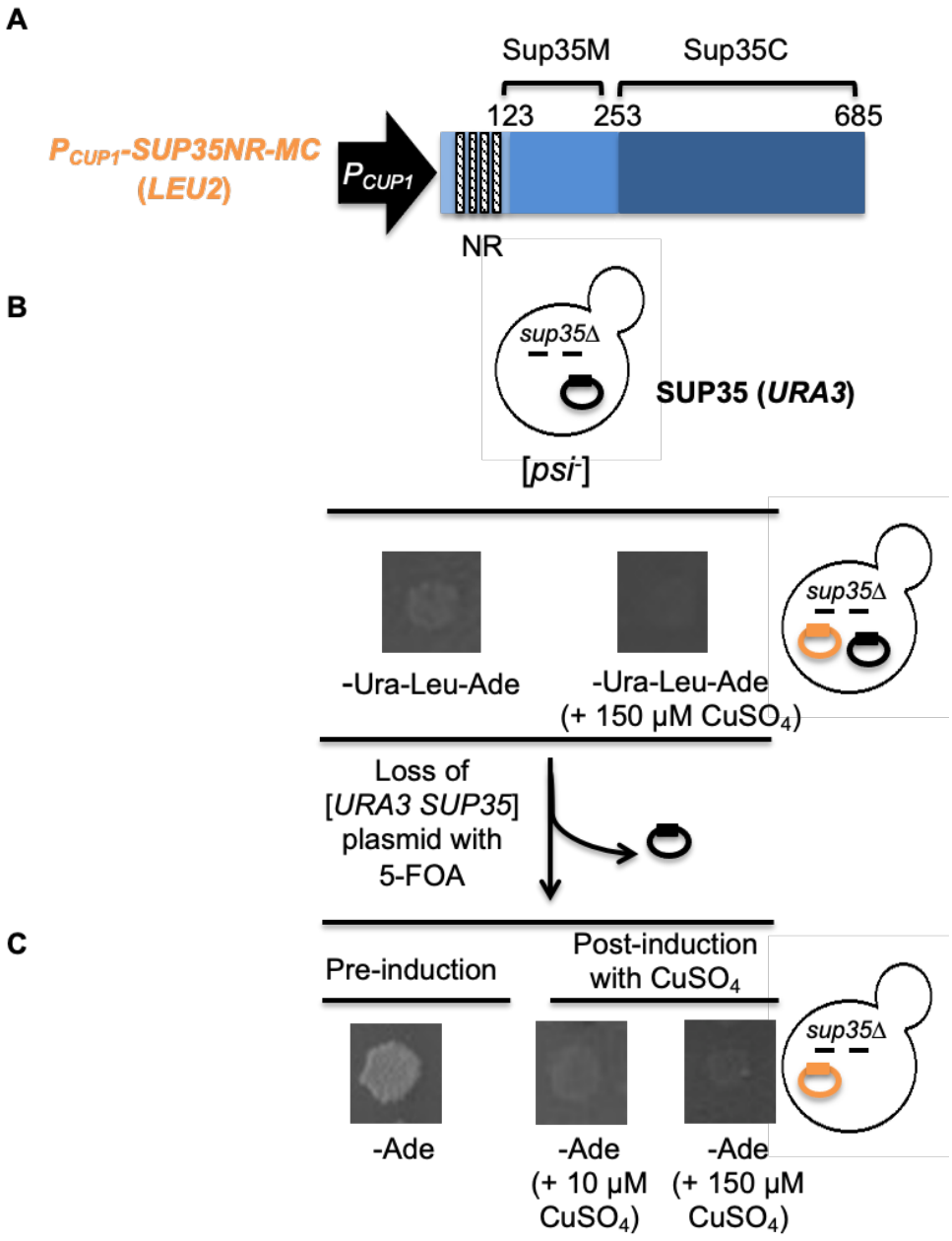

Figure 3.9 Functionality of plasmid *P_{CUP1}-SUP35NR-MC* (*LEU2*). (A) Diagram showing the structure of the P_{CUP1}-SUP35NR-MC (LEU2) plasmid. The region coding for the first 42 amino acids of the N-terminal domain of Sup35 has been removed. (B) The [*psi*$^-$][*pin*$^-$] strain simultaneously expressing both Sup35 protein (chromosomal copy of *SUP35* is deleted by *HIS3*, cells are kept viable by a *URA3* plasmid containing *SUP35* under its endogenous promoter) and Sup35NR-MC protein, do not cause nonsense suppression. (C) After losing Sup35 *(URA3)* by plasmid shuffle, Sup35NR-MC *(LEU2)* remains capable of nonsense suppression with the addition of 150μM $CuSO_4$ (copper is required to increase the abundance of Sup35NR-MC since the plasmid is under the copper promoter).

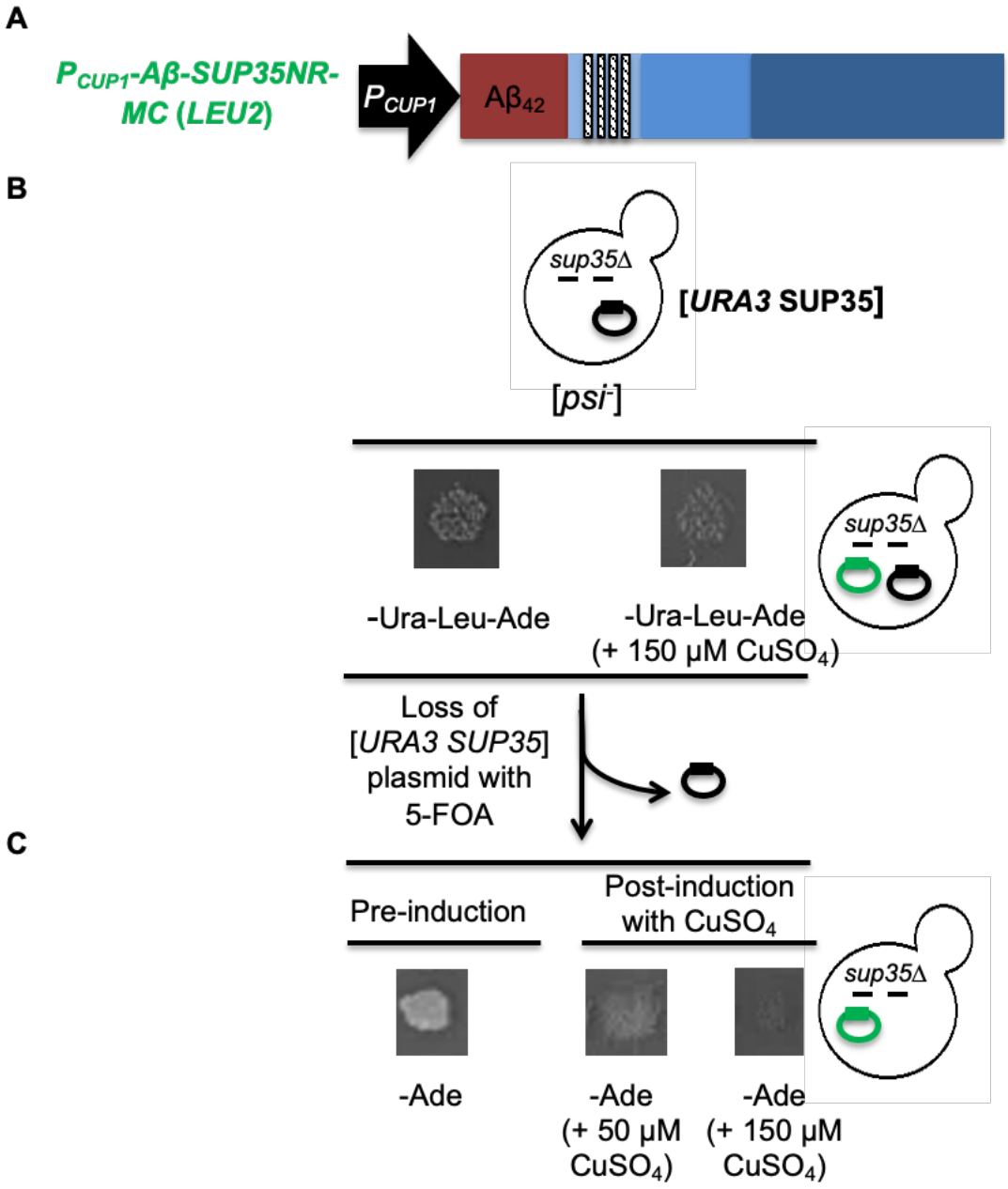

Figure 3.10 Functionality of plasmid P_{CUP1}-Aβ-SUP35NR-MC (LEU2). (A) Diagram showing the *Aβ-SUP35NR-MC* cassette moved to the P_{CUP1} promoter in a plasmid backbone with a *LEU2* marker. (B)The [*psi*$^-$][*pin*$^-$] strain simultaneously expressing both Sup35 protein (chromosomal copy of *SUP35* is deleted by *HIS3*, cells are kept viable by a *URA3* plasmid containing *SUP35* under its endogenous promoter) and Aβ-Sup35NR-MC protein, causes slight nonsense suppression. (C) After losing Sup35 *(URA3)* by plasmid shuffle, Aβ-Sup35NR-MC*(LEU2)* remains capable of nonsense suppression with the addition of 150μM $CuSO_4$ (copper is required to increase the abundance of Aβ-NR-Sup35MC since the plasmid is under the copper promoter).

after loss of the P_{SUP35}-*SUP35* URA3 plasmid by using 5-FOA. Again, Sup35NR-MC was able to terminate translation but only on media containing additional copper (Figure 3.9C). The same was true for the *LEU2* plasmid containing $A\beta_{42}$-NR-Sup35MC under the P_{CUP1} promoter (Figure 3.10).

For checking the maintenance of the [*ABE*$^+$] prions in the shuffle experiments, the control [*abe*$^-$] strain along with several [*ABE*$^+$] strains of various origins (Figure 3.11A and Table 3.5) were transformed with either the [*LEU2 SUP35NR-MC*] or [*LEU2 Aβ$_{42}$-SUP35NR-MC*], generating two-plasmid combinations (Step I). Then, the original [*URA3 Aβ$_{42}$-SUP35NR-MC*] plasmid was lost using 5-FOA media (Step II). Growth of resulting single-plasmid colonies on -Leu-Ade medium with 150 μM $CuSO_4$ was then checked. The Ade$^+$ phenotype disappeared in the colonies originating from [*ABE*$^+$] now containing only the plasmid [*LEU2 SUP35NR-MC*] (data not shown). They have become indistinguishable from the [*abe*$^-$] control, indicating that the prion state was not transferred to the Sup35NR-MC protein. However, all [*ABE*$^+$]-derived colonies containing the [*LEU2 Aβ$_{42}$-SUP35NR-MC*] construct grew on -Ade with $CuSO_4$, in contrast to those derived from the [*abe*$^-$] control (data not shown).

To ensure that the Ade$^+$ phenotype has indeed disappeared after transfer to Sup35NR-MC and could not be restored by reintroducing the plasmid containing $A\beta_{42}$-Sup35NR-MC protein, we transformed the strains from Step II with the *URA3 Aβ$_{42}$-NR-Sup35MC* plasmid (Step III), and then streaked resulting transformants on -Ura media containing an additional 150 μM $CuSO_4$ in order to lose the *LEU2*

Table 3.6 [*ABE*$^+$] strains checked via direct/reverse shuffle.

[*ABE*] strain number	Strain Name	Aβ variant phenotype	Origin	Transfection Sample	Patient ID
[*abe*$^-$]	GT2126	N/A	N/A	N/A	N/A
[*ABE*$^+$-25]	GT2036	Strong	Spontaneous	N/A	N/A
[*ABE*$^+$-10]	GT2217	Intermediate	Spontaneous	N/A	N/A
[*ABE*$^+$-9]	GT2216	Weak	Spontaneous	N/A	N/A
[*ABE*$^+$-4]	GT2170	Strong	Transfection	*In vitro* $A\beta_{42}$	N/A
[*ABE*$^+$-37]	GT2387	Weak	Transfection	Synthetic $A\beta_{42}$ seeded by brain extract from parietal lobe	N/A
[*ABE*$^+$-30]	GT2380	Weak	Transfection	Brain extract	OSO-159
[*ABE*$^+$-26]	GT2376	Weak	Transfection	Brain extract	OSO-163

plasmid. Ura$^+$ Leu$^-$ colonies resulting from such a reverse shuffle were identified (Step IV). Selected colonies were patched onto -Ura media and allowed to grow for 2 days. These plates were then velveteen replica plated to -Ura medium containing an additional 150 μM $CuSO_4$ to induce expression of the *$A\beta_{42}$-SUP35NR-MC* construct, and allowed to grow for three days, followed by velveteen replica plating to -Ura-Ade media containing 150 μM $CuSO_4$. As shown on Figure 3.11B, colonies that previously originated from Step II derivatives containing the *SUP35NR-MC* plasmid maintained the Ade$^-$ phenotype after reintroduction of the plasmid containing *$A\beta_{42}$-SUP35NR-MC*, independently of whether they have originated from [*abe*$^-$] or [*ABE*$^+$] strains. This shows that [*ABE*$^+$]

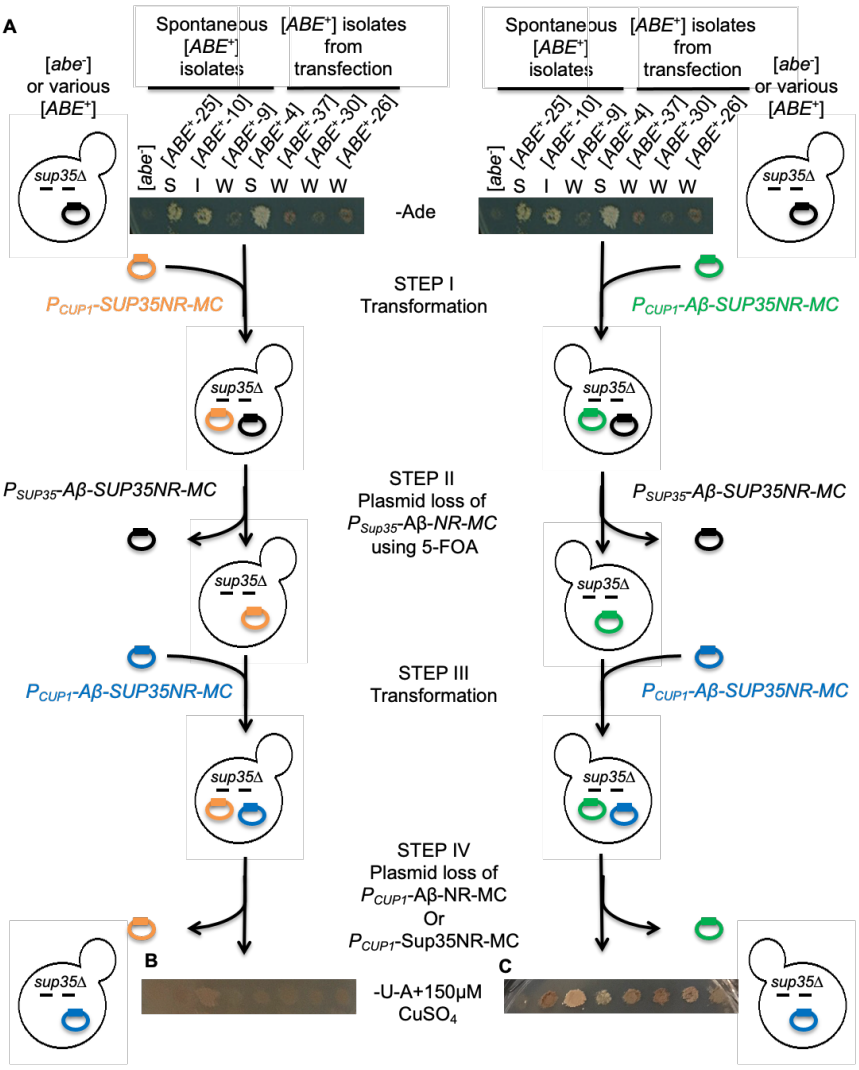

Figure 3.11 Analysis of [*ABE*$^+$] isolates by direct and reverse plasmid shuffle. Step I. The Ade$^+$ colonies generated from both spontaneous and transfection experiments were transformed with either the plasmid [P_{CUP1}-*SUP35NR-MC LEU2*] or [P_{CUP1}-*Aβ-SUP35NR-MC LEU2*]. (A) Representative colonies from each experimental type and of different stringencies chosen to be tested by direct shuffle Step II. Colonies underwent plasmid loss procedure using 5-FOA media to generate cells containing only either [P_{CUP1}-*SUP35NR-MC LEU2*] or [P_{CUP1}-*Aβ-SUP35NR-MC LEU2*]. Step III. Cells generated from Step II were transformed with plasmid [P_{CUP1}-*Aβ-SUP35NR-MC URA3*] to generate colonies of either [P_{CUP1}-*SUP35NR-MC LEU2*] and [P_{CUP1}-*Aβ-SUP35NR-MC URA3*] (left column) or [P_{CUP1}-*Aβ-SUP35NR-MC LEU2*] and [P_{CUP1}-*Aβ-SUP35NR-MC URA3*] (right column). Step IV. The *LEU2* plasmids placed into the strain during STEP I was lost spontaneously by streaking out on –URA media containing 150 μM $CuSO_4$. Colonies were velveteened to both –URA and –LEU media to select colonies only containing the *URA3* plasmid for analysis. (B) Step IV of reverse shuffle transformed with P_{CUP1}-*Aβ-SUP35NR-MC URA3* continue to show no growth on -Ade with 150 μM $CuSO_4$, as the [*ABE*$^+$] prion was lost previously during Step II of direct shuffle. (C) The original [*ABE*$^+$] strains maintain the Ade$^+$ phenotype with only the P_{CUP1}-*Aβ-SUP35NR-MC URA3* plasmid, as the Aβ region was maintained thought Step II of direct shuffle to allow for the continual propagation of the [*ABE*$^+$] prion.

prion was lost after shuffle to Sup35NR-MC and could not be recovered in yeast after reintroduction of $A\beta_{42}$-Sup35NR-MC. However, the colonies originated from Step II derivatives containing the *$A\beta_{42}$-SUP35NR-MC* plasmid retained Ade^+ phenotype, if they have originated from [*ABE*$^+$], after reintroduction of the *URA3 $A\beta_{42}$-SUP35NR-MC* construct plasmid (Figure 3.11C). Only Step IV derivatives originated from the control [*abe*$^-$] strain stayed Ade^-. These results demonstrate the [*ABE*$^+$] prions generated either spontaneously or via transfection require $A\beta_{42}$ to maintain the Ade^+ phenotype.

3.4 Discussion

The phenomenon of amyloid/prion variants describes the difference in phenotypic manifestation for both mammalian and yeast amyloids that cannot be explained by differences in protein sequence. The strain concept postulates that the differences between amyloid variant are fully determined by the particular structure of nuclei or “seeds” that establish and propagate the amyloid state. Once a particular variant structure has been established it is then faithfully propagated onto all joining monomers of the same protein sequence [55, 56]. The transfection procedure has previously been used in yeast to provide proof for the “protein only” information transfer upon infection by a prion protein, demonstrating that seeds of different variants maintain the respective phenotypes after transfection [37, 57]. Thus, transfection becomes a powerful tool for studying amyloid strains of different origins. For [*PSI*$^+$] prion, different variant stringencies correlate with varying ratios

of aggregated versus non-aggregated protein. This results in differing levels of translational readthrough, leading to different levels of pigment accumulation due to the lack of Ade1 in the *ade1-14* reporter system as discussed in Chapter 1 section 1.3.1 and shown in Figure 1.7B. Strains that have a higher abundance of aggregated protein and have more translational readthrough (appear white) and are termed strong variants while those with less aggregated protein and less translational readthrough (appear pinker) and are termed weak variants [55, 58]. Here, we took advantage of the same translational readthrough system to study the variants produced by $A\beta_{42}$ containing chimeric protein, $A\beta_{42}$-Sup35NR-MC. Previous (Chandramolishwaran *et. al.* 2018 [47]) and new (presented in this work) data show that $A\beta_{42}$ produced *in vitro* and transfected into an [*abe*$^{-}$] strain is capable of converting resident $A\beta_{42}$-Sup35NR-MC protein into a variety of [*ABE*$^{+}$] phenotypes as seen by both color on YPD and growth on -Ade (Figures 3.3 and 3.4, and Table 3.2) [47].

We furthered this initial study by studying [*ABE*$^{+}$] isolates, produced by aggregated $A\beta_{42}$ that is derived from brains of AD patient samples classified as having various forms of AD (either regular or rapid progress AD). We show that aggregated $A\beta_{42}$ from AD patient brains is indeed able to seed the conversion of the chimeric protein $A\beta_{42}$-Sup35NR-MC into the prion form, [*ABE*$^{+}$] (Figure 3.3). Moreover, spectra of [*ABE*$^{+}$] strains transfected from brain extracts, or by *in vitro* aggregated $A\beta_{42}$ that was seeded by brain extracts, are different in comparison to those formed spontaneously and those transfected with *in vitro* self-aggregated $A\beta_{42}$. Essentially all [*ABE*$^{+}$] isolates originated from brain extracts are weak as

judged from color on YPD and growth on -Ade medium, while self-aggregated $A\beta_{42}$ can produce [*ABE*$^{+}$] isolates of different classes (weak, intermediate or strong) as shown in Figure 3.3 and summarized in Table 3.2. A possible explanation for this is that the “strong” or “intermediate” strains cannot propagate in human brains with AD, so that interactions of $A\beta_{42}$ with the chaperone machinery and/or other proteins within the AD brain preferentially dictate $A\beta_{42}$ to adopt a weaker amyloid variant.

It should be noted that even though $A\beta_{42}$ from AD brains produces weak [*ABE*$^{+}$] strains in yeast, they are not all the same. Careful phenotypic analysis as shown in Figure 3.4, A and B and Table 3.4 confirms that these weak strains can be divided into at least three different subtypes. Moreover, [*ABE*$^{+}$] strains obtained by transfection from “rapid progress” AD cases differ drastically from those originating from regular AD cases, because rapid progress AD derived [*ABE*$^{+}$] isolates show extremely high mitotic instability in yeast (Figure 3.5 and Table 3.3). This enables us to establish a link between the patterns of an AD case and characteristics of the [*ABE*$^{+}$] strain obtain after transfection of respective amyloids into the yeast cells. While molecular foundations of these differences are still to be determined, these correlations demonstrate a usefulness of the yeast model for the propagation of disease-related patterns of $A\beta_{42}$ amyloids.

Complete removal of the N-domain, would completely eliminate the possibility of Sup35 from converting to a [*PSI*$^{+}$] state. However, this resulted in the instant aggregation of $A\beta_{42}$-Sup35MC demonstrating that it was poorly functional in terminating translation as shown in Park *et. al.* 2011 and confirmed in Chandramowlishwaran *et. al.* 2018 [47, 59]. In order to prevent the instant

aggregation of $A\beta_{42}$ in our system, the NR portion of Sup35N domain needed to be retained. As previously discussed, the N-domain of Sup35 contains a portion of the PrD of Sup35. However, it should be mentioned that the glutamine/asparagine rich region which is crucial for prion formation of [*PSI*$^+$] is absent in our $A\beta_{42}$-Sup35NR-MC construct. Thus, the possibility remains that the Ade$^+$ phenotype formed by our chimeric construct could be maintained by the large portion or the PrD of Sup35 that remains. Here we show that through plasmid shuffle, when only the Sup35NR-MC protein is present, the Ade+ phenotype is lost. Subsequent transformation with the plasmid containing $A\beta_{42}$-Sup35NR-MC did not re-establish the Ade$^+$ phenotype, thus the NR-domain of Sup35 is not capable of maintaining the prion established by $A\beta_{42}$ (Figure 3.11B).

It has been shown in the case of [*PSI*$^+$] variants produced by Sup35 that weak variants are less easily fragmented and present as larger average polymer size on SDD-AGE gels, while strong variants of [*PSI*$^+$] are more easily fragmented and present as smaller average polymer size. The inverse seems to be true for $A\beta_{42}$. As seen in Figure 3.7, strong [*ABE*$^+$] strains run as a larger polymer size, while weak strains contain more small polymers. This result was also previously seen in Chandramowlishwaran *et. al.* 2018 [47]. Both strong and weak [*ABE*$^+$] variants were also resistant to GuHCl (Table 3.5), so differences in polymer size seems unlikely to be driven by interaction with chaperone machinery as is the case in [*PSI*$^+$], at least in yeast. It seems plausible that difference could be that the prion fiber formed by $A\beta_{42}$ could be compositionally different in different variants. This could be due to the initial formation of distinct nuclei.

Our data demonstrate that $A\beta_{42}$ is capable of substituting for the aggregation portion of the Sup35 PrD, so that the respective chimeric protein can form and propagate a prion state termed [*ABE*$^{+}$] in yeast. This ability, coupled with the use of transfection procedure enables us to amplify and characterize the brain-derived amyloid state of $A\beta_{42}$ in yeast. Moreover, our yeast assay can potentially be used as a screening platform to look for proteins or chemical screens that influence the propagation of $A\beta_{42}$ and may be employed in the development of new therapeutic strategies for AD.

3.5 Conclusions

- Human $A\beta_{42}$ can substitute for aggregation-prone region domain of the Sup35 prion domain, leading to the conversion of a chimeric protein into a partly non-functional prion state, and propagating distinct prion strains.
- Aβ amyloids, produced *in vitro* or originated from human brains, can generate self-propagating strains of the chimeric $A\beta_{42}$-Sup35NR-MC protein after transfection into yeast cells.
- The spectrum of yeast Aβ-based prion strains seeded from brain extracts is different from those produced spontaneously in yeast cells or *in vitro.*
- Yeast Aβ-based prion strains seeded from “regular” or “rapid progress” Alzheimer’s disease cases differ from each other by mitotic stability.
- $A\beta_{42}$-region is required for the maintenance of prion state by the chimeric Aβ-NR-MC protein.

CHAPTER 4. CHARACTERIZATION OF THE AGGREGATION PROPERTIES OF TAU PROTEIN IN YEAST

4.1 Summary

The previous chapter focused on developing a yeast model for studying the amyloid properties of Aβ. Here we will shift our attention to microtubule associated protein tau [60], another protein associated with AD. Previously reported yeast models developed for studying tau have been limited in scope, and do not address the broad array or properties surrounding tau's aggregation. For this work, we constructed plasmids containing either full length tau (MAPT), or different domains of tau (TauRD), including the C-terminal repeat regions that have been associated with the amyloid properties of tau and fused them to a YFP fluorophore under different promoters. High expression of these constructs from plasmids in yeast leads to the formation of aggregates that can be detected using fluorescent microscopy techniques. Furthermore, our data demonstrates that these aggregates are also detergent-resistant, a characteristic of amyloids, and that these aggregates are phosphorylated. Another advantage of our model is that it is applicable to studying other factors that can either promoter or inhibit tau's aggregation, such as mutations related to disease as well as the presence or absence of particular kinases that have been shown to phosphorylate tau. In this chapter we will describe a yeast model for studying the amyloid properties of tau using both *in vivo* and biochemical techniques.

4.2 Specific materials and methods

Materials

Strains, plasmids, and oligonucleotide primers used in this study are described in Appendix tables A, B and C respectively.

4.2.1.1 Strains

The [*psi*$^-$][*pin*$^-$] strain GT409 of the GT81 strain series was used extensively for this study and was previously described in Chernoff *et al.* 2000 [61]. The wild-type haploid strains of the BY4741 series containing the *mds1Δ* and *pho85Δ* are from the Invitrogen collection. The double deletion strain *mds1Δ pho85Δ* was obtained using the Pringle method, described in Longtine *et al*. 1998, as shown in Figure 4.1, specifically by adding the *pho85Δ* to the BY4741 *mds1Δ* strain. To do this, primers were designed with gene specific sequences at the 5' end and tags for deletions to the 3' end. PCR was preformed using these primers and the respective marker from a plasmid as template (in this case *HIS3* was used) [62]. The PCR product was transformed via lithium acetate transformation, as previously described in Chapter 2, and plated onto selective media (-His), and incubated 3-4 days at 30°C. Transformants were restreaked on selective media to purify colonies, and single colonies were chosen and patched onto selective media to determine phenotype. Potentials with desired phenotype (identical to BY4741 strain with *mds1Δ* except growth on the medium for the selectable transplacement marker - in this case, -His) were checked via PCR to determine whether the desired

gene had been successfully deleted. It should also be noted that the *pho85Δ* leads to an increase in mitophagy conferring a petit phenotype in yeast colonies.

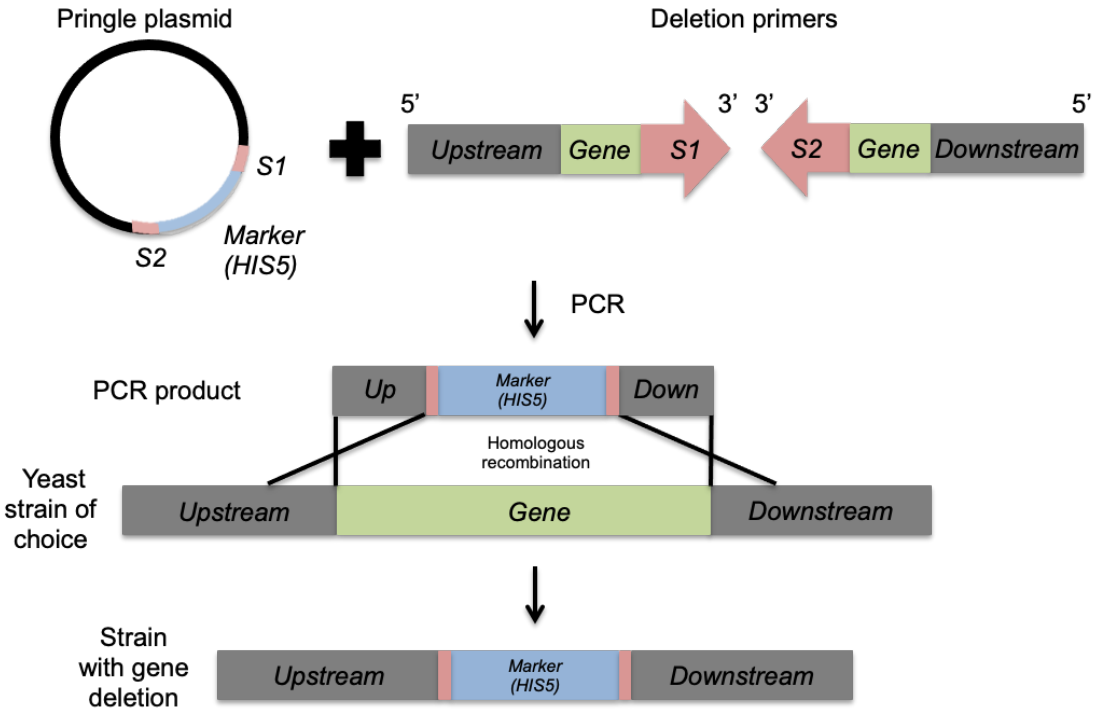

Figure 4.1 Pringle method of gene deletion. Deletion primers were designed to include either just upstream/downstream of the gene being deleted through the start codon and a sequence homologous to sequence on the Pringle plasmid. During PCR, this creates a fragment with approximately 40bp homology to just upstream/downstream and approximately 20bp slightly internal to the gene being deleted, and the marker from the plasmid, in this case *HIS5*. When transformed into the desired strain, homologous recombination causes the gene to be replaced with the marker, *HIS5*. The loci of the deletion can be checked using a separate set of primers that are both upstream and downstream of the gene that was deleted, and this strain will also now be His^+.

4.2.1.2 Plasmids and primers

The overall scheme for construction of the MAPT genes and repeat domains of tau (Figure 4.2) is described in detail as follows. The P_{GPD}-YFP and CFP plasmids were received from the Laboratory of Amyloid Biology at St.

Petersburg University, St. Petersburg Russia, and are previously described by Rubel *et al.* 2013 [63]. The P_{GPD}-TauRD-YFP plasmid was constructed using PCR to add the restriction sites *BamHI* and *SacII*. The plasmid containing the amino acid coding region of 244-372 of TauRD (containing 4 repeat regions of tau) received from Dr. Marc Diamond at Washington University was used as a template. The PCR product was digested and ligated into the P_{GPD}-YFP using the same enzyme sites. The P_{GPD}-TauRDpro-YFP plasmid was constructed similarly to the wild-type plasmid, however the template plasmid containing TauRD with mutations P301L and V337M, which confers the autosomal dominant tauopathy, FTDP-17, also received from Dr. Marc Diamond was used as a template for PCR. The P_{GPD}-Aβ_{42}-CFP plasmid was also constructed by using PCR, digestion, and ligation using the same enzyme sites as previously described for the other P_{GPD} plasmids.

The P_{CUP1}-YFP and CFP plasmids were also received from the Amyloid Biology Laboratory. The CFP plasmid was constructed using the centromeric plasmid P_{CUP1}-GFP, received from Dr. Susan Lindquist (Whitehead Institute, MIT), by replacing the gene for *GFP* with that for *CFP*. The backbone of this plasmid is based upon pRS316 plasmid. The YFP plasmid was constructed by removing the P_{CUP1}-CFP cassette and switching out the CFP fluorophore for that of YFP into the pRS315 backbone to give a *LEU2* marker allowing for colocalization studies using both the CFP and YFP fluorophores under different markers. The P_{CUP1}-MAPT-YFP plasmid was constructed using PCR to amplify the full-length version of MAPT (containing 2N4R) and add restriction sites for cloning. The PCR product was

digested and ligated using the same enzyme sites. All plasmids were confirmed via enzyme digestion and sequencing.

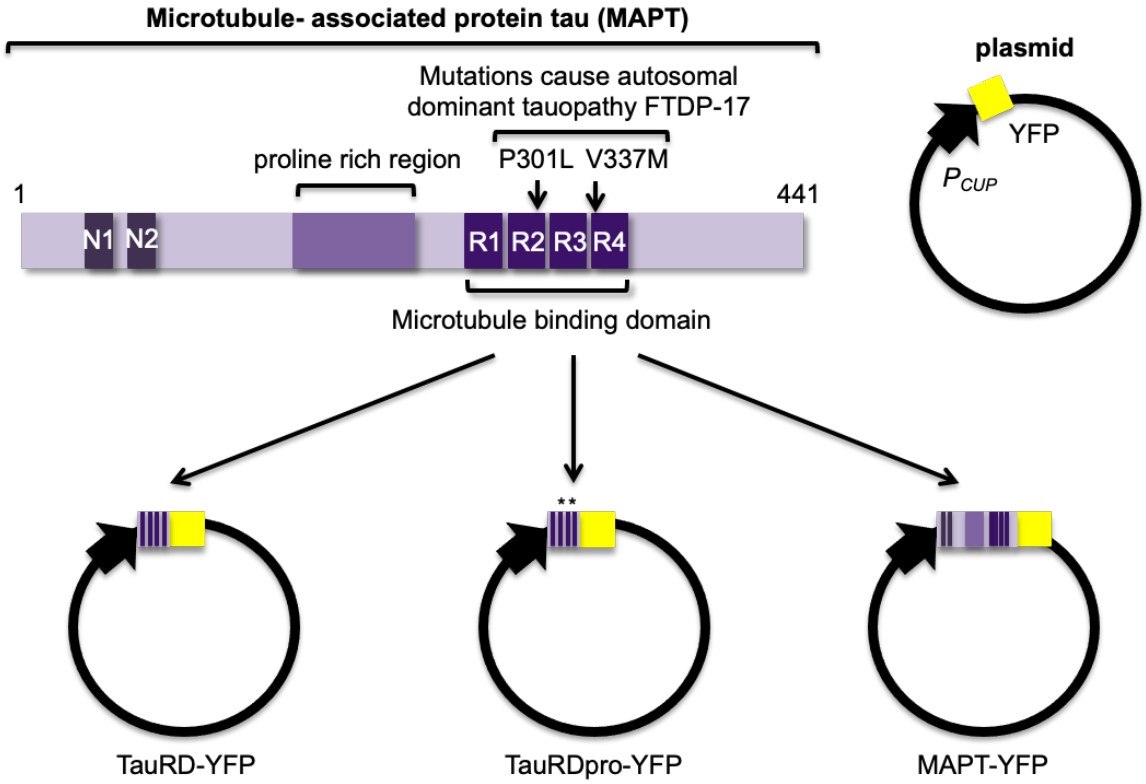

Figure 4.2 Scheme of the construction of plasmids with MAPT protein or its repeat domains, fused to fluorophores. Schematic diagram of the protein domains of tau and highlights certain features as it is related to specific amyloid properties.

4.2.1.3 Antibodies

The antibodies to GFP, PHFI, MC1, and CP13 used in this study are described in Chapter 2. PHF1, MC1 and CP13 were gifts from Dr. Lary Walker (Department of Neurology, Emory University).

Methods

Standard protocols were used for DNA isolation, gel electrophoresis, restriction digestion, gel extraction, ligation, and bacterial transformation and are described in Chapter 2. Standard yeast media and standard yeast cultivation and transformation were used and also described in Chapter 2. The methodology for fluorescent microscopy experiments along with the use of 1,6-hexanediol is also found in the methods chapter.

4.3 Results

Microscopic detection of aggregation of fluorophore tagged Tau-derived constructs in yeast

Considering that previous data indicates the role of the C-terminal repeat domain (TauRD; amino acids 244-372) on tau's ability to aggregate, we enquired whether the expression of this protein domain alone would lead to the formation of protein aggregates in yeast. High expression alone of TauRD resulted only in the appearance of diffuse fluorescence, however the addition of pro-aggregation mutation associated with FTDP-17 (TauRDpro) results in detectable foci (Figure 4.3A). Quantitative data showing the percentage of cells with aggregates is provided in Figure 4.3B and summarized in Table 4.1. We also studied the aggregation properties of full-length tau (MAPT). Again, upon high expression of TauRD alone results in only the appearance of diffuse fluorescence (Figure 4.4A), which is consistent with our previous result. Surprisingly, high expression of wild-type MAPT-YFP from the P_{CUP1} promoter, induced by $CuSO_4$ results in the

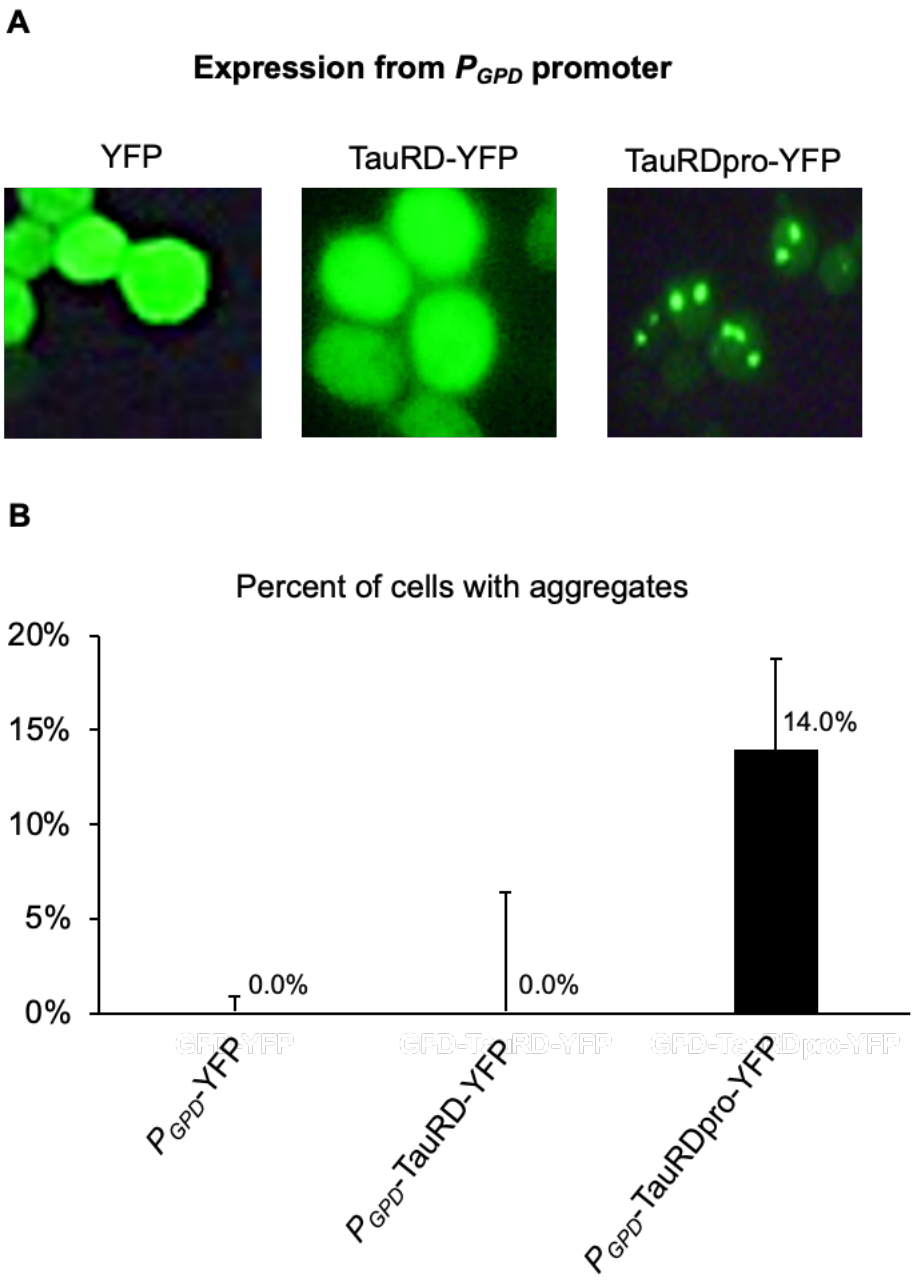

Figure 4.3 Microscopic detection of the aggregation of tau repeat domains under the P_{GPD} promoter. (A) Aggregation of the control plasmid (YFP), and experimental plasmids containing either 4 repeats of Tau (TauRD), and the same region with the pro-aggregation mutations of P301L and V337M (TauRDpro) under the P_{GPD} promoter in a [*psi*$^-$][*pin*$^-$] strain (GT409). (B) Comparison of the percent aggregation between plasmids. Three colonies were analyzed for each strain/plasmid combination after six hours of growth. Error bars depict standard deviations. Numbers for this experiment are shown in Table 4.1.

Table 4.1 Microscopic detection of the aggregation of tau repeat domains under P_{GPD} promoter.

Strain	Protein Expressed	Cells with aggregates relative to all cells with fluorescence			
		Analyzed colony	% aggregation	SD Range	Number of colonies analyzed
GT409 [*psi*$^-$][*pin*$^-$]	YFP	Colony #1	0		193
		Colony #2	0		71
		Colony #3	0		78
		Average	**0**	**0 – 0.9**	**342**
	TauRD-YFP	Colony #1	0		28
		Colony #2	0		24
		Colony #3	0		101
		Average	**0**	**0 – 6.4**	**153**
	TauRDpro-YFP	Colony #1	14.3		63
		Colony #2	18.6		70
		Colony #3	8.9		56
		Average	**14%**	**9.2 – 18.8**	**189**

Data for Figure 4.3B

formation of detectable foci, in contrast to wild-type TauRD, expressed from the same promoter (Figure 4.4A). Quantitative data showing the percentage of cells with aggregates is provided in Figure 4.4B and summarized in Table 4.2. We also checked if the high expression of TauRD could be toxic in yeast and thus result in its inability to aggregate. Here, we show that high expression of TauRD (Figure 4.5A), TauRDpro (Figure 4.5A) or MAPT (Figure 4.5B) are not toxic in yeast.

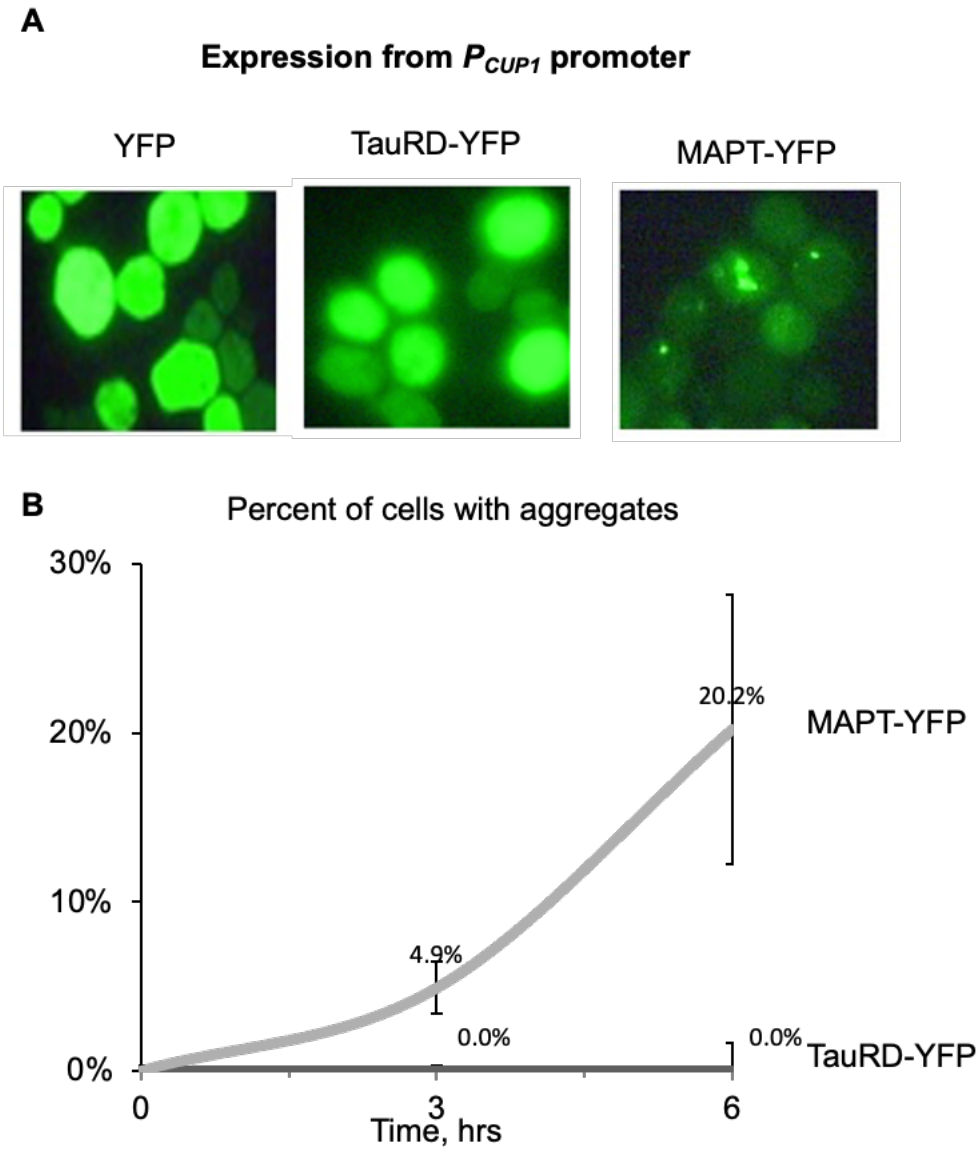

Figure 4.4 Microscopic detection of the aggregation of MAPT under the P_{CUP1} promoter. (A) Aggregation of the control plasmid (YFP), and the experimental plasmids containing either 4 repeat of Tau (TauRD), or full-length tau (MAPT). All plasmids were transformed into a [*psi*$^-$][*pin*$^-$] strain (GT409). (B) Comparison of the percent aggregation between plasmids. Three colonies were analyzed for each strain/plasmid combination after six hours of expression. Error bars depict standard deviations. Numbers for this experiment are shown in Table 4.2.

Table 4.2 Microscopic detection of the aggregation of Tau protein under P_{CUP1} promoter.

Strain	Protein expressed	Time	Cells with aggregates relative to all cells with fluorescence			
			Analyzed colony	% aggregation	SD range	Number of colonies analyzed
GT409 [*psi*$^-$][*pin*$^-$]	YFP	0 hr	Colony #1	0		211
		0 hr	Colony #2	0		90
		0 hr	Colony #3	0		166
		0 hr	**Average**	**0**	**0 – 0.2**	**467**
		3 hrs	Colony #1	0		225
		3 hrs	Colony #2	0		124
		3 hrs	Colony #3	0		82
		3 hrs	**Average**	**0**	**0 – 0.2**	**431**
		6 hrs	Colony #1	0		260
		6 hrs	Colony #2	0		195
		6 hrs	Colony #3	0		150
		6 hrs	**Average**	**0**	**0 – 1.6**	**605**
	TauRD-YFP	0 hr	Colony #1	0		181
		0 hr	Colony #2	0		78
		0 hr	Colony #3	0		212
		0 hr	**Average**	**0**	**0 – 0.3**	**471**
		3 hrs	Colony #1	0		255
		3 hrs	Colony #2	0		125
		3 hrs	Colony #3	0		167
		3 hrs	**Average**	**0**	**0 – 0.2**	**547**
		6 hrs	Colony #1	0		207
		6 hrs	Colony #2	0		178
		6 hrs	Colony #3	0		149
		6 hrs	**Average**	**0**	**0 – 0.3**	**534**
	MAPT-YFP	0 hr	Colony #1	0		197
		0 hr	Colony #2	0		92
		0 hr	Colony #3	0		168
		0 hr	**Average**	**0**	**0 – 0.3**	**457**
		3 hrs	Colony #1	3.1		257
		3 hrs	Colony #2	5.8		292
		3 hrs	Colony #3	5.7		294
		3 hrs	**Average**	**4.9**	**3.3 – 6.5**	**843**
		6 hrs	Colony #1	17.1		211
		6 hrs	Colony #2	14.29		77
		6 hrs	Colony #3	29.3		140
		6 hrs	**Average**	**20.2**	**12.3 – 28.1**	**428**

Data for Figure 4.3D

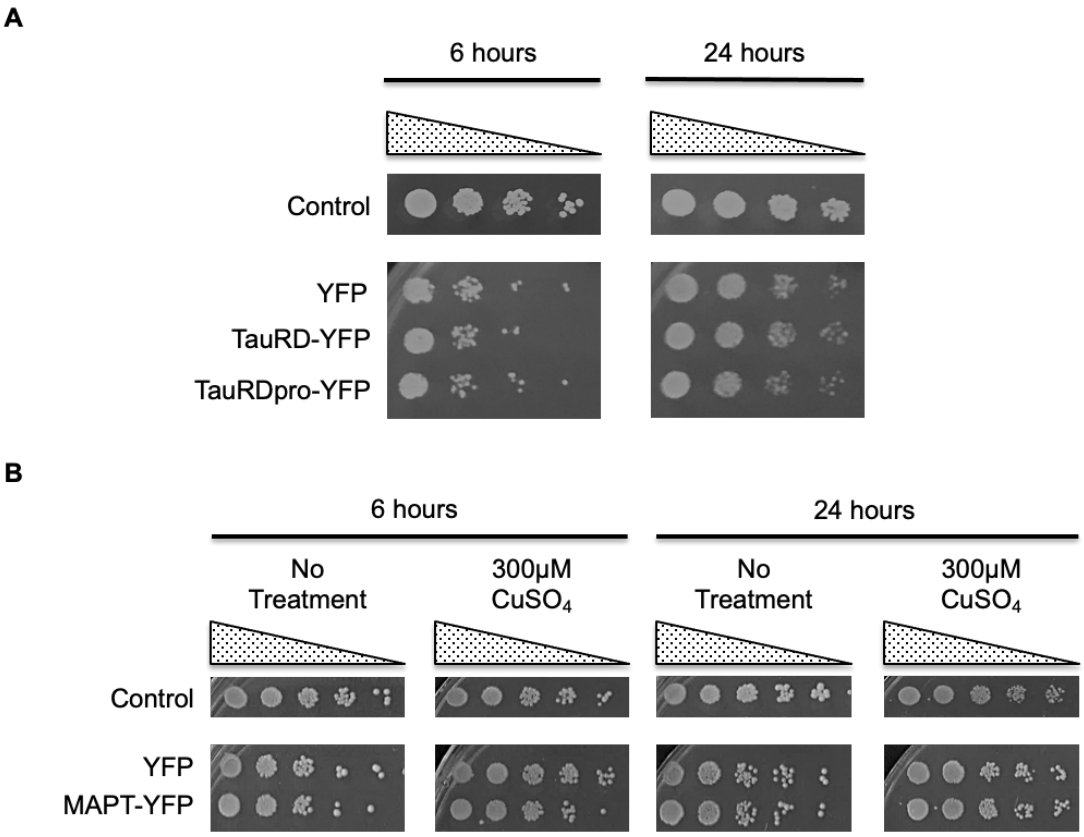

Figure 4.5 Effects of Tau plasmids on growth in a [*psi*$^-$][*pin*$^-$] background. Overnight precultures were diluted to an OD_{600} of 0.1 in selective medium. Serial dilutions were prepared after both 6 hours and 24 hours to check for toxicity of the plasmids. (A) Shows results from P_{GPD} expression plasmids and (B) shows plasmid under the P_{CUP1} plasmid. For those under the P_{CUP1} plasmid it is compared between no additional copper and medium containing 300 μM $CuSO_4$.

Biochemical characterization of Tau-derived aggregates in yeast

One possible explanation for the lack in ability of TauRD to induce aggregation could be due to low levels of expression as compared to TauRDpro. However, in fact, levels of TauRD are higher when compared to TauRDpro, indicating such a simple explanation does not apply (Figure 4.6A). MAPT's expression level is equal to the YFP control as shown in Figure 4.6B.

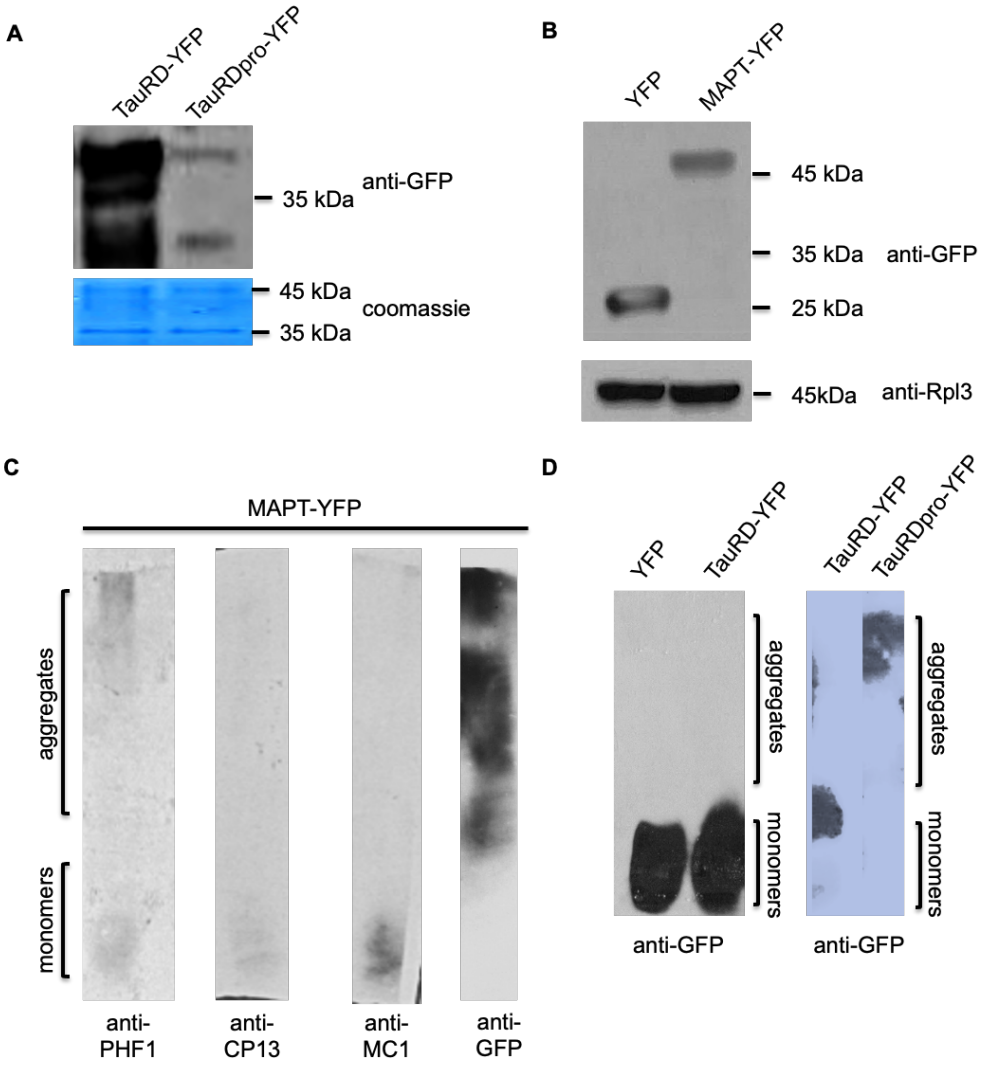

Figure 4.6 Biochemical detection of aggregates formed by Tau. (A) The repeat domains of Tau (TauRD and TauRDpro) expression in yeast. Proteins were isolated after 6 hours of growth and ran on 10% SDS-PAGE gel, followed by Western blotting and reaction to the anti-GFP antibody. Another gel was ran simultaneously was ran with the same protein extracts and strained in coomassie as a loading control. (B) Expression of full-length MAPT after six hours of expression in 300 μM $CuSO_4$. Here, the membrane after probing with the anti-GFP antibody was striped and then reprobed with the anti-Rpl3 antibody as a loading control. (C) The semi-denaturing detergent agarose gel electrophoresis (SDD-AGE) of MAPT in the presence of sarkosyl. The same protein extract was ran in 4 individual lanes on the same gel and transferred to the same membrane. The membrane was then cut and probed with the following antibodies: anti-PHF1, anti-CP13, and anti-MC1, and anti-GFP. (D) SDD-AGE of TauRD and TauRDpro in the presence of sarkosyl following high expression in yeast. These membranes were probed using the anti-GFP antibody.

Next, we wanted to determine if the aggregates seen as fluorescent foci were amyloid in nature or another type of protein aggregate. To date, data only shows that tau is capable of aggregating in yeast, but not if these are amyloid aggregates or another type of protein aggregate. To do this, we employed the technique termed semi-denaturing detergent agarose gel electrophoresis (SDD-AGE) as described in chapter 2. Detergent resistance is a characteristic of amyloid aggregates, but not those of other types (*e. g* stress granules or liquid-liquid phase separation condensates). Per our data, MAPT is able to form detergent-resistant aggregates as shown in Figure 4.6C. Notably, these aggregates also react to antibodies that recognize specific phosphorylation sites or specific tau species found in AD, or a combination of both. We show that aggregates of MAPT reacted to the PHF-1 antibody, who's epitope recognizes paired helical filaments (PHF) that is phosphorylated at both serine 396 and 404 residues [64]. However, MAPT species that are phosphorylated at serine 202, were detected only as monomers by the CP13 antibody. The CP13 antibody's epitope recognizes phosphoserine 202. We also show that only monomers of MAPT are detected by the MC1 antibody. The MC1 antibody recognizes a specific conformation of pathological tau associated with AD, involving the intramolecular conformation involving portions of the N and C-terminal domains of tau [65]. Our data also shows that TauRDpro, which contains pro-aggregation mutations, forms detergent-resistant aggregates as compared to TauRD which is only detected as a monomer as shown in Figure 4.6D. Overall, our biochemical data supports what is seen by microscopy.

Analysis of the sensitivity of Tau-based aggregates to hexanediol

To further characterize the aggregates formed by both TauRDpro and MAPT, we employed 1,6-hexanediol, an aliphatic alcohol that weakens hydrophobic interactions and can inhibit liquid-liquid phase separation (LLPS). LLPS is associated with the formation of membraneless bodies, which are important in a myriad of cellular functions [66-68]. While the involvement of LLPS is still poorly understood in its role in the formation of amyloids, there is a general consensus that LLPS could serve as a possible driver to nucleating aggregation [69].

As a control we first studied 1,6-hexanediol's effect on Sup35N (the PrD of Sup35) fused to GFP. The overexpression of Sup35N results in the formation of [*PSI*$^{+}$], the prion isoform of Sup35, but only in the presence of a pre-existing prion, such as [*PIN*$^{+}$] formed by the Rnq1 protein. In Figure 4.7A, we confirm that the overexpression of Sup35N-GFP in a [*psi*$^{-}$][*PIN*$^{+}$] strain leads to the formation of amyloid aggregates that can be microscopically detected. This is an expected result as multiple labs have confirmed the appearance of fluorescent foci following the expression of the PrD of Sup35 as long as the strain contains either [*PIN*$^{+}$] or is already [*PSI*$^{+}$] [70, 71]. We also show that these aggregates remain resistant 10 minutes post treatment with hexanediol. Furthermore, Sup35N-GFP is able to form a biocondensate when expressed at high levels in the [*psi*$^{-}$][*pin*$^{-}$] cells, however, these aggregates are not amyloid in nature, as they disappear following the 10-min hexanediol treatment (Figure 4.7B). This confirms data by A.V. Grizel and Y.O. Chernoff (personal communication) showing that Sup35N-YFP forms

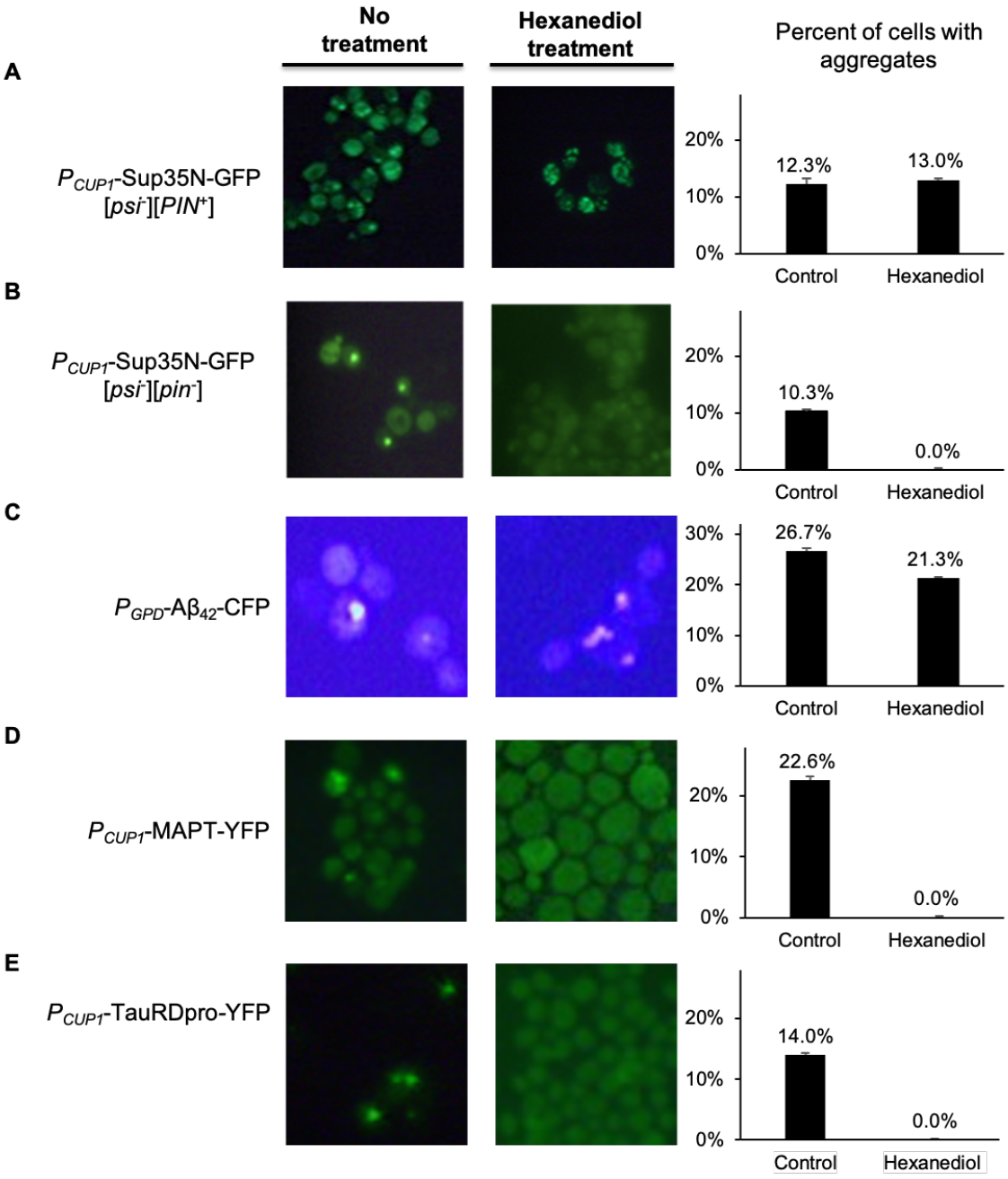

Figure 4.7 Hexanediol treatment with Tau and Aβ$_{42}$ plasmids. Cells transformed with plasmids (A) Sup35N-GFP in a [*psi*$^-$][*PIN*$^+$] strain, (B) Sup35N-GFP in a [*psi*$^-$][*pin*$^-$] strain, (C) Aβ$_{42}$-CFP in a [*psi*$^-$][*pin*$^-$] strain, (D) MAPT-YFP in a [*psi*$^-$][*pin*$^-$] strain, and (E) TauRDpro-YFP in a [*psi*$^-$][*pin*$^-$] strain were visualized by fluorescence microscopy following either 10 minutes of no treatment (control) or with hexanediol. Graphs depict pairwise comparisons within one experiment, however three cultures were analyzed, showing a difference in the same direction. Error bars depict standard error.

Table 4.3 Hexanediol treatment with plasmids.

Strain	Protein expressed	Treatment	Cells with aggregates relative to all cells with fluorescence***		
			Average %	SE range	Number
[*psi*$^-$][*PIN*$^+$] GT159	Sup35N-GFP	Control	12.3	11.8 – 12.8	57
		Hexanediol	13	12.99 – 13.01	54
[*psi*$^-$][*pin*$^-$] GT409	Sup35N-GFP	Control	10.3	10.2 – 10.4	107
		Hexanediol	0	0 – 0.05	88
	Aβ_{42}-CFP	Control	26.7	26.5 – 26.9	30
		Hexanediol	21.3	21.2 – 21.4	61
	MAPT-YFP	Control	22.6	22.57 – 22.63	62
		Hexanediol	0	0 – 0.01	40
	TauRDpro-YFP	Control	14	13.99 – 14.01	43
		Hexanediol	0	0 – 0.01	94

Data for Figure 4.7

***Experiment shows pairwise comparison of one colony. Three colonies were examined showing a difference in the same direction. Standard error was calculated by binomial distribution.

LLPS biocondensates rather than amyloids in [*psi*$^-$][*pin*$^-$] cells. We also examined the effects of hexanediol on another amyloidogenic protein, Aβ_{42}. We have previously shown that the aggregation Aβ_{42} leads to the formation of fluorescent foci and that these aggregates are also detergent resistant [63, 72]. Here, we also show that these aggregates are also hexanediol resistant (Figure 4.7C).

Next we studied both MAPT (Figure 4.7D) and TauRDpro (Figure4.7E), both of which formed fluorescent aggregates and were detergent resistant. However, 10 minutes post-treatment with hexanediol aggregates by both domains of tau were dissolved. This data indicates that aggregates formed by tau in yeast cells combine properties of both amyloids (detergent resistance) and LLPS biocondensates (hexanediol sensitivity). While this is somewhat a surprising result,

it does highlight the unique features of tau aggregates that are different from both $A\beta_{42}$ Sup35N aggregates.

Colocalizaiton of Tau derived aggregates with Aβ42

The coexistence of Aβ plaques and neurofibrillary tangles in the brain is a histopathological hallmark of AD. As previously discussed in Chapter 1, the amyloid cascade hypothesis has been guiding AD research for the past several decades [73, 74]. In short, it states that Aβ as the causative agent of AD pathology, and that the accumulation of tau into neurofibrillary tangles is a direct result of Aβ's deposition. While there is consensus that both proteins aggregate during AD progression, the molecular link between Aβ and tau still remains poorly understood. To check to see if there is a possible interaction between Aβ and tau, we co-expressed YFP tagged either TauRDpro or MAPT along with CFP-tagged Aβ. Following high expression, cells containing both plasmids showed colocalization of either TauRDpro (Figure 4.8A) or MAPT (Figure 4.8B) with Aβ. Numbers for the quantitative analysis are shown in Figure 4.8C and summarized in Table 4.4.

Effects of protein kinases on Tau aggregation

Phosphorylation events are important in regulating tau's normal cellular function in regulating microtubule dynamics. Dysregulation of phosphorylation, as is found in AD, can lead to tau dysfunction and mislocalization, possibly contributing to its polymerization. Previous data has shown that tau is

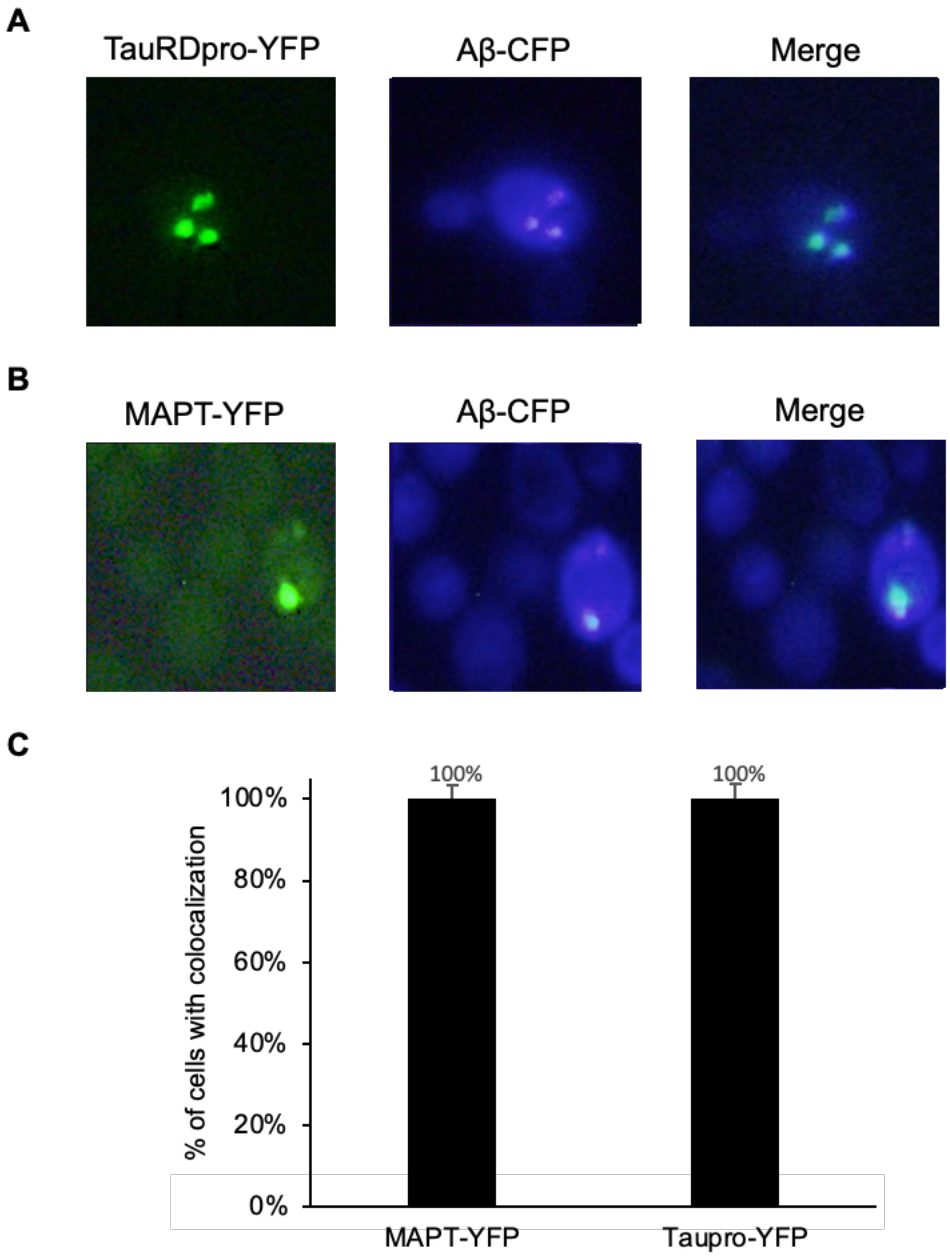

Figure 4.8 Colocalization of MAPT-YFP or TauRDpro-YPF with $A\beta_{42}$-CFP. (A) [*psi*$^-$][*pin*$^-$] strain co-expressing both TauRDpro-YFP and $A\beta_{42}$-CFP tagged plasmids visualized by fluorescence microscopy following 6 hours expression. (B) MAPT-YFP and $A\beta_{42}$-CFP co-expressed in a [*psi*$^-$][*pin*$^-$] strain and visualized by fluorescence microscopy following 6 hours expression with additional 300 μM $CuSO_4$. (C) Quantitation of YFP (either MAPT or TauRDpro) and $A\beta_{42}$-CFP colocalization. Percentages of colocalized dots detected in cells containing both types of aggregates are shown. Error bars depict standard deviations.

Table 4.4 Colocalization of MAPT-YFP or TauRDpro-YFP with Aβ$_{42}$-CFP.

Strain	Protein expressed	Cells with aggregates relative to all cells with fluorescence		
		Average %	SD range	Number
[*psi*$^{-}$][*pin*$^{-}$] GT409	TauRDpro-YFP and Aβ$_{42}$-CFP	100	96.3 - 100	30
	MAPT-YFP and Aβ$_{42}$-CFP	100	96.6 – 100	23

Data for Figure 4.8

phosphorylated in yeast. Specifically, purified MAPT from yeast strains containing the deletion of *PHO85,* the homolog of Cdk5 in humans, showed a decrease of sarkosyl-soluble tau as compared to that found in wild-type, indicating a link between phosphorylation and its ability to aggregate [75].

To further explore the aggregation patterns of tau in yeast and to determine if aggregation was influenced by phosphorylation in our yeast model, we expressed MAPT in the BY4741 background strain (WT), along with strains containing single kinase deletions (either *mds1Δ* or *pho85Δ)*. The strain containing both deletions was also used in these experiments. Here, we show that deletion of *MDS1* leads to an increase in aggregation of MAPT as seen in both *mds1Δ* and *mds1Δ pho85Δ* strains as compared to the wild-type strain, while deletion of *PHO85* had no noticeable effect (Figure 4.9C). In order to determine if this increase in aggregation was due to changes in phosphorylation, we conducted this same experiment using the peptide Aβ$_{42}$ that also aggregates in AD, but its aggregation pattern is not linked to phosphorylation in either yeast or mammals. Following high

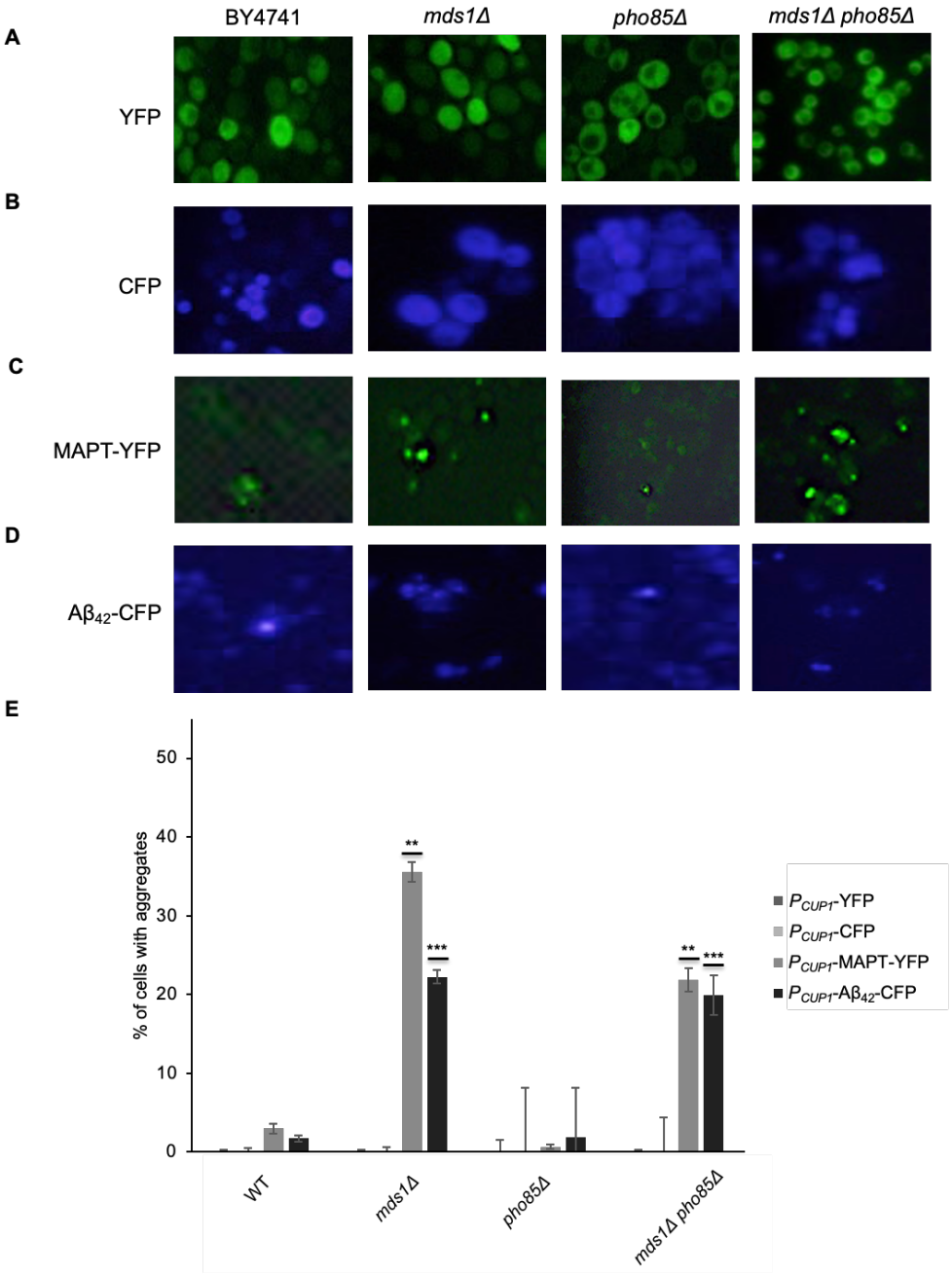

Figure 4.9 Studies on MAPT and Aβ42 aggregation in kinase deletion strains. Yeast strains of the BY4741 series expressing either the control plasmids (A) PCUP1-YFP or (B) PCUP1-CFP and experimental plasmids (C) PCUP1-MAPT-YFP or (D) PCUP1-Aβ42-CFP. Cells with transformed plasmids were visualized by fluorescence microscopy after 6 hours following expression with 300 μM CuSO4.(E) Percent of cells with aggregates following high expression of plasmid after 6 hours, as detected by fluorescence microscopy. Numbers of cells for this experiment are shown in Table 4.4. Error bars depict standard deviations and statistical calculations indicating differences in p-values are shown in Table S4.1.

Table 4.5 Studies on MAPT and Aβ42 in kinase deletion strains.

Strain	Protein expressed	Cells with aggregates relative to all cells with fluorescence**		
		Average %	SD range	Number
WT (BY4741)	YFP	0	0 – 0.2	895
	CFP	0	0 – 0.3	833
	MAPT-YFP	2.9	1.4 – 4.4	1258
	Aβ42-CFP	1.7	1.5 – 1.9	839
mds1Δ	YFP	0	0 – 0.5	472
	CFP	0	0 – 0.6	176
	MAPT-YFP	35.6	19.4 – 51.8	262
	Aβ42-CFP	22.2	18.9 – 25.5	443
pho85Δ	YFP	0	0 – 0.6	400
	CFP	0	0 – 1.3	228
	MAPT-YFP	0.6	0.3 – 0.9	2000
	Aβ42-CFP	1.8	0.3 – 3.3	813
mds1Δ pho85Δ	YFP	0	0 – 0.42	287
	CFP	0	0 – 0.88	198
	MAPT-YFP	21.8	15.5 – 28.1	648
	Aβ42-CFP	19.9	17.4 – 22.4	508

Data for Figure 4.9.

**Three colonies were analyzed for each strain/plasmid combination.

expression of Aβ42 in the kinase deletion strains, we observed the same trend as seen with MAPT. Aβ42's aggregation increased in strains containing the *mds1Δ* as compared to wild-type, while *pho85Δ* had no noticeable effect (Figure 4.9D). This indicates that while this specific kinase deletion does effect protein aggregation in yeast, it does not appear to be specific to tau, nor does it appear to be increasing aggregation due to changes in phosphorylation patterns. Quantitative data for this analysis is shown in Figure 4.9 and summarized in Table 4.5 and S4.1.

Further analysis by Western blotting demonstrated differences in the abundance of MAPT in the kinase deletion strains. Here, we show that in strains containing the deletion of *MDS1,* MAPT is in higher abundance as compared to

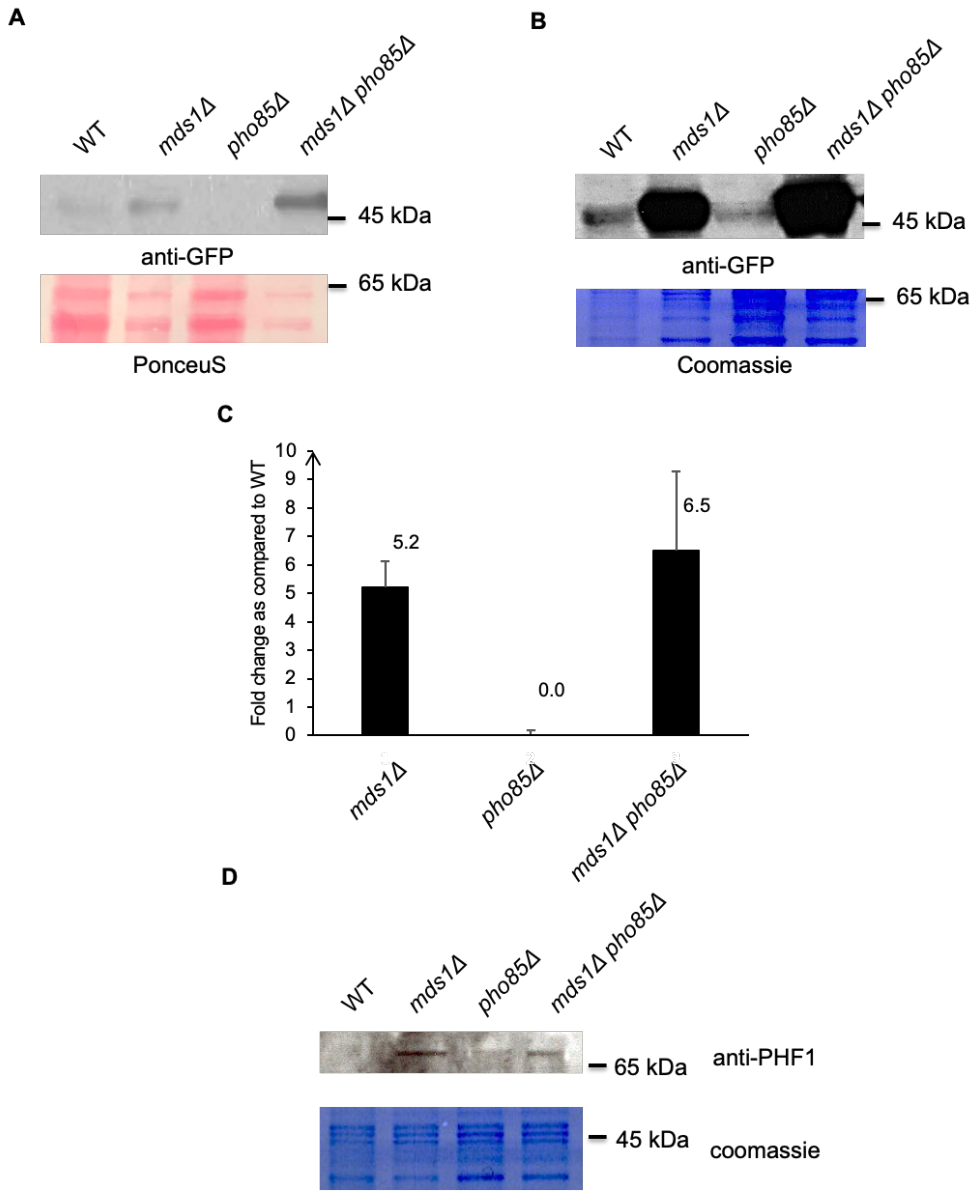

Figure 4.10 Biochemical detection of aggregates formed by Tau. (A) MAPT is in higher abundance in strains containing the *mds1Δ*. Proteins were isolated after 6 hours of expression in media supplemented with 300 μM $CuSO_4$ and ran on 10% SDS-PAGE gel, followed by Western blotting and reaction to the anti-GFP antibody. The membrane was stained with Ponceau S prior to probing with antibody as a loading control. (B) Second gel showing same conditions as shown in A, however Coomassie was used as a loading control. (C) Fold change relative to the level of MAPT in the wild-type strain. Results are averaged from 3 repeats. Error bars depict standard error. (C) SDS-PAGE gel with the same protein extracts as depicted in A, however, probed using the anti-PHF1 antibody to detect phosphorylation of MAPT in the kinase deletion strains. A separate gel ran with the same extracts was ran and stained with coomassie as a loading control.

WT, while in strains containing the deletion of *PHO85*, it is less abundant (Figure 4.10A). Differences in protein abundance may explain the effects of respective deletions on aggregation. Notably, *mds1Δ* is epistatic to *pho85Δ* in regard to both aggregation (Figure 4.9C) and abundance (Figure 4.10A) of tau-based constructs. Moreover, tau levels are even higher in the double *mds1Δ pho85Δ* deletion, compared to both WT and any single deletion (Figure 4.10B). Interestingly, phosphorylation of MAPT was not abolished at serines 396 and 494 as determined by the PHF1 antibody (Figure 4.10C), however further analysis would be required to determine if overall changes to phosphorylation occur in the kinase deletion strains. Despite altered protein levels, high expression of MAPT is not toxic to *mds1Δ* strain, as compared to wild-type. Here, we show that the *PHO85* deletion on its own decreases growth as compared to WT, this could be related to its altered respiration pattern as discussed previously (Figure 4.11A). The *MDS1* deletion has no noticeable effect on growth. The added expression of either MAPT (Figure 4.11B) or $A\beta_{42}$ (Figure 4.11C) are not toxic in strains harboring these kinase deletions.

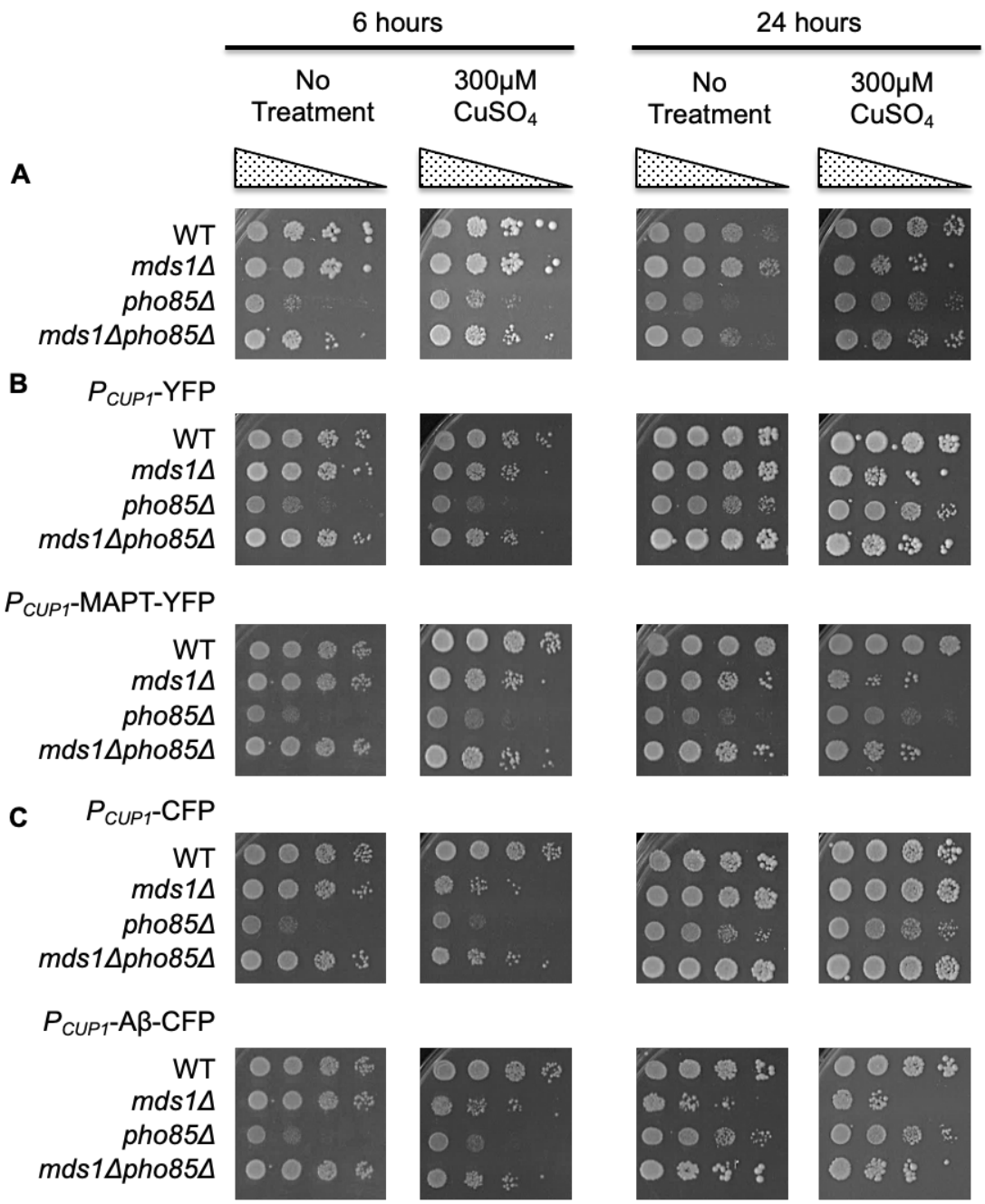

Figure 4.11 Toxicity of Tau and Aβ42 in kinase deficient strains. Overnight precultures were diluted to an OD600 of 0.1 in selective medium. Serial dilution were prepared after both 6 hours and 24 hours to check for toxicity of the plasmids. (A) Shows results of strains containing no plasmids. (B) Shows result for plasmids containing the YFP fluorophore and (C) shows results for plasmids with the CFP fluorophore. Comparison is shown between samples treated with no additional copper and medium containing 300μM $CuSO_4$.

4.4 Discussion

Our data demonstrates that we are able to recapitulate the conditions necessary for tau to aggregate in yeast. Previous studies of tau in yeast have only pointed to changes in phosphorylation, not its aggregation. Specifically, they have only shown by western blotting that partial amounts of tau are present in the sarkosyl-insoluble fraction, possibly indicating the presence of aggregates [76-78]. With our model we are able to visualize these cytoplasmic aggregates and confirm that they are indeed detergent resistant using subsequent biochemical techniques.

While yeast does not have a tau homolog, the phosphorylation machinery that targets tau is highly conserved between yeast and humans. This is useful as post-translational modifications (specifically phosphorylation) of tau are thought to be critical to the biology behind is normal and toxic gain of functions. In the normal soluble form of tau, phosphorylation is crucial for the regulation of microtubule dynamics [79-81]. Alterations in the phosphorylation patterns of tau have been shown to prevent its normal function (its ability to bind to microtubules), however, hyperphosphorylated versions are found in the deposits in AD brains [82]. It should be mentioned that the actual role of hyperphosphorylation in tau's aggregation remains unclear.

By using tau specific antibodies, we were able to detect full-length tau aggregates that were phosphorylated. Specifically, we showed this via the PHF1 antibody, as its epitope as previously discussed recognizes the phosphoserines at position 396 and 404. While this result is not unique to our model, as other studies

in yeast have also shown that tau is phosphorylated [76], it shows the relevance of the yeast system to processes in human cells.

Also, since most of the machinery for the phosphorylation of tau is conserved in yeast [76, 77], it makes yeast models powerful tools in being able to address questions if kinases and phosphatases also play a role in tau's ability to aggregate. In our model, we investigated the role of both Mds1 (Gsk-3β) and Pho85 (Cdk5) on tau's ability to aggregate. Here, we show that the deletion of *MDS1* does increase both levels and aggregation of tau as compared to wild-type, while the deletion of *PHO85* decreases them. Previous studies have only investigated the effects of kinase deletions on phosphorylation alterations, not directly on changes in aggregation. However, it should be mentioned that in Vandebroek *et. al.* 2005, they showed an increase in tau species detected by MC1 in the *pho85Δ* strain as compared to wild-type, suggesting an increase in aggregation [77].

Overall, our data suggest that kinases modulate levels of tau protein rather than directly influencing its aggregation. It should also be noted that *mds1Δ* increases aggregation of Aβ, not known to be phosphorylated. It is therefore possible that effects of kinases on tau are at least in part due to phosphorylation of other (yet unknown) proteins influencing aggregation of both tau and Aβ, rather than due to direct phosphorylation of tau protein itself.

While our current data cannot fully address questions surrounding if changes in phosphorylation are driving aggregation in our yeast model, we can

show that we have a system in which future experiments could address these questions, as our yeast model is able to replicate the phosphorylation of tau. Also due to its design, our model could easily be adapted to incorporate downstream approaches such as mass spectroscopy to address large scale changes in phosphorylation patterns in yeast which to date have not be completed.

Tau has also been demonstrated to be able to undergo LLPS [83, 84]. LLPS are drivers in the formation of many membraneless compartments with the cell [69, 85]. These types of biocondensates can also be detected visually as a type of aggregate, so alternative techniques are necessary in order to decipher between those that are amyloid or other types of protein aggregates, such as stress granules. LLPS have been shown to drive the amyloid formation of other amyloidogenic proteins such as FUS [86-88] and hnRNPA1 [89], however conflicting data has been shown for tau, and it remains unclear on whether LLPS is necessary to drive tau's aggregation [90]. To our knowledge, this is the first time that tau aggregates have been examined in yeast using hexanediol. To date, this type of assay has only been performed on purified tau protein aggregates. Previous studies involving hexanediol have shown that tau aggregates formed under high salt conditions were dissolved in the presence of hexanediol [84, 91], while those that were electrostatically driven were not [91]. This indicates that tau forms aggregates of different types under different conditions. This is also suggested by data in which our SDD-AGE data demonstrates tau is detergent-resistant (Figure 4.6C), a characteristic of amyloids, but our hexanediol data suggests otherwise (Figure 4.7D). To date there is no published example of a

protein aggregate being both detergent resistant and hexanediol sensitive, although it is known that multi-protein complexes such as stress granules may include both detergent-resistant hexanediol-sensitive components [92]. One possibility is that tau may form aggregates of the mixed composition in yeast cells, so-that amyloid-type detergent resistant protofibrils are assembled into the cytologically detectable complexes via interactions with other molecules undergoing phase separation. It should also be mentioned that hexanediol should be used with caution when applied to live cells as it changes the permeability of membranes and thus can lead to additional artifacts (Kroschwald 2017).

It is shown in specific models that the aggregation of Aβ happens first, followed by the deposition of tau into NFT's within the AD brain [60, 93-95]. While the molecular mechanism behind the ability of Aβ to cross-seed tau remains elusive, there have been data to indicate that this is possible. With our model, we have been able to demonstrate that aggregates of $A\beta_{42}$ and tau are found colocalized in the yeast cell. This does provide potential credence to the hypothesis that tau could be directly cross-seeded by Aβ, although of course this does not prove it [38, 96]. While more work would be necessary to demonstrate cross-seeding in our system, our model is able to address such questions. Notably, constructs based on the wild-type tau repeat domain region (TauRD) remain soluble in yeast even at high levels of expression (Figure 4.3 and 4.4). As previously shown in Chapter 3, we also have a system in which we can control the aggregation of Aβ. Merging these two approaches would allow us the ability to study if aggregates of Aβ are able to cross-seed the aggregation at least of TauRD.

Overall, our data strongly supports the notion that a yeast-based model can be used for studying the amyloidogenic properties of tau. Both MAPT and TauRDpro have the ability to form aggregates following high expression, along with preliminary evidence showing that tau phosphorylation is maintained in yeast indicating that our model could be used in future studies in unraveling the properties and conditions that control amyloidogenic features of tau.

4.5 Conclusions

- Full-length MAPT protein fused to a fluorophore forms microscopically detectable aggregates in yeast, while the repeat domain (TauRD) does not.
- Tauopathy-associated mutations P301L and V337M confer aggregation capacity to TauRD expressed in yeast.
- Aggregates formed by both MAPT and TauRDpro are detergent-insoluble, as typical of amyloids.
- Aggregates formed by both MAPT and TauRDpro are dissolved following 10 minute treatment with hexanediol.
- Aggregates of $A\beta_{42}$ peptide colocalize with aggregates of either full-length wild-type MAPT or mutant TauRD in yeast, supporting the amyloid cascade model for Alzheimer's disease.
- Deletion of the gene coding for the protein kinase Mds1 (homologous to human tau phosphorylating kinase GSK3β) increases abundance and aggregation of MAPT in yeast while MAPT, while deletion of the

gene coding for the protein kinase Pho85 (homologous to human tau phosphorylating kinase cdk5) decreases them.

- Effect of *mds1Δ* on protein aggregation is not specific to tau as it also seen for $A\beta_{42}$ which is not known to be phosphorylated.

CHAPTER 5. CHARACTERIZATION OF THE AGGREGATION PROPERTIES OF THE U1 RIBONUCLEOPROTIEN 70

5.1 Summary

A newly identified protein found to be aggregated within the AD proteome is the U1 small nuclear ribonucleoprotein-70k [97]. It is a spliceosome component of the U1 snRNP. This protein is of interest to us, as there are now other examples of other RNA-binding proteins found aggregated in other neurodegenerative diseases such as TDP-43 and FUS that have also been studied in yeast. As with other proteins, expression of these proteins in yeast are able to recapitulate key features of proteinopathy [97, 98]. For this work, we constructed plasmids containing different domains of U1-70k and fused them to a YFP fluorophore under a P_{CUP1} promoter. High expression of these plasmids in yeast leads to the formation of aggregates that can be detected using fluorescent microscopy techniques. Furthermore, our data demonstrates that only the U1-70kC domain, which harbors two low-complexity domains, forms aggregates which are also detergent-resistant. In this chapter we will demonstrate a yeast model for studying the amyloid properties of the domains of U1-70k using both *in vivo* and biochemical techniques.

5.2 Specific materials and methods

Materials

Strains, plasmids, and oligonucleotide primers used in this study are described in Appendix tables A, B and C respectively.

5.2.1.1 Strains

The [*psi*$^-$][*pin*$^-$] strain GT409 of the GT81 strain series was used extensively for this study and was previously described in Chernoff *et al.* 2000 [61].

5.2.1.2 Plasmids and primers

The overall scheme for construction of the U1-70k domains (Figure 5.1) fused to fluorophores are described in detail as follows. The P_{CUP1}-YFP and CFP vectors were previously described in Chapter 4. Plasmids containing the full coding region of U1-70k were received from Dr. Nicholas Seyfried (Department of Biochemistry, Emory University) and used as templates. For these studies we used the N-terminal domain (U1-70kN), amino acids 1-99, the middle domain (U1-70kM) encompassing amino acids 100-181, and the C-terminal domain (U1-70kC) which includes amino acids 182-437. A plasmid containing both the N-terminal and middle domains together (U1-70kNM) was also included. PCR was used to amplify the coding region of each domain along with adding the restriction sites for *Bam*HI and *Xba*I. The PCR product was digested and ligated into the P_{CUP1}-YFP plasmid using the same enzyme sites. All plasmids were confirmed via digestion and subsequent sequencing. The CFP fusion plasmids were constructed by removing

the promoter and U1-70k coding domain via enzyme digestion and subsequent ligation.

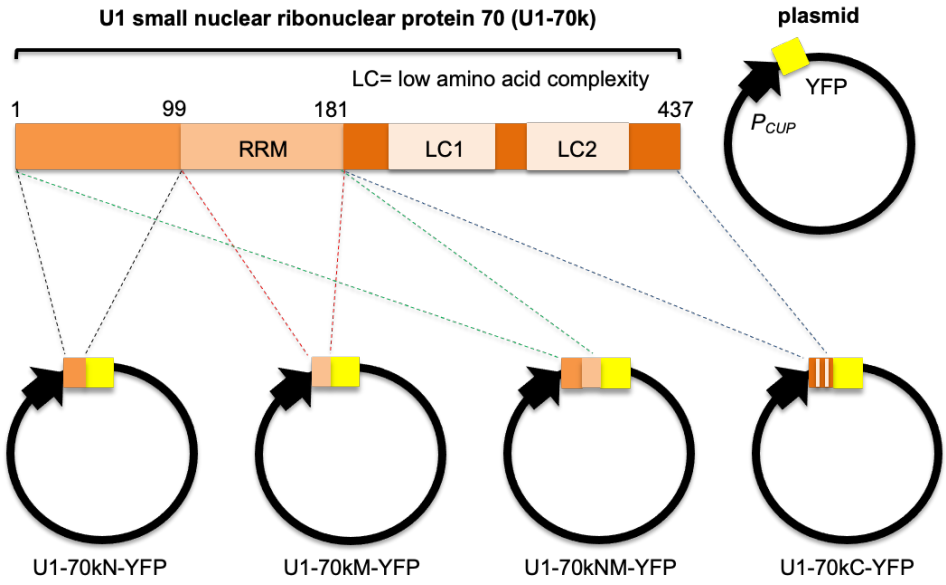

Figure 5.1 Scheme of construction of plasmids with U1-70k domains fused to fluorophores. Schematic diagram of the protein domains of U1-70k and highlights certain features as it is related to specific amyloid properties.

5.2.1.3 Antibodies

The GFP antibody used in this study is described in Chapter 2.

[redacted]*Methods*

Standard protocols were used for DNA isolation, gel electrophoresis, restriction digestion, gel extraction, ligation, and bacterial transformation and are described in Chapter 2. Standard yeast media and standard yeast cultivation and transformation were used and also described in Chapter 2. The methodology for

fluorescent microscopy experiments along with the use of 1,6-hexanediol is also found in the methods chapter.

5.3 Results

Characterization of aggregation properties of the domains of U1-70k by fluorescence microscopy

Previous data has shown that U1-70k has amyloid-like properties and is found aggregated in AD brains [32, 99]. In order to better understand the aggregation patterns of this protein and the properties that drives its aggregation, we expressed plasmids harboring different domains of U1-70k in yeast to determine if any were capable of forming aggregates. High expression of the YFP control leads to diffuse fluorescence as expected (Figure 5.2A). The N-terminal domain of U1-70k is intrinsically disordered. While not all disordered domains are PrD, there are several RNA-binding proteins that contain disordered domains that are also known to have amyloid-like properties. Interestingly, the high expression of U1-70kN (Figure 5.2B) leads to the appearance of only diffuse fluorescence.

In AD brains it is known that U1-70k can be N-terminally cleaved, resulting in a smaller protein product (denoted N40k) that includes both the N-terminal domain and the middle domain [100]. Here, we investigated to see if further protein sequence was necessary in order to lead to protein aggregation besides the N-terminal domain alone. For this, we expressed both the middle domain (U1-70kM) alone and a plasmid containing both the N-terminal and middle domains (U1-70kNM) together. High expression of both U1-70kM (Figure 5.2C) and U1-70kNM

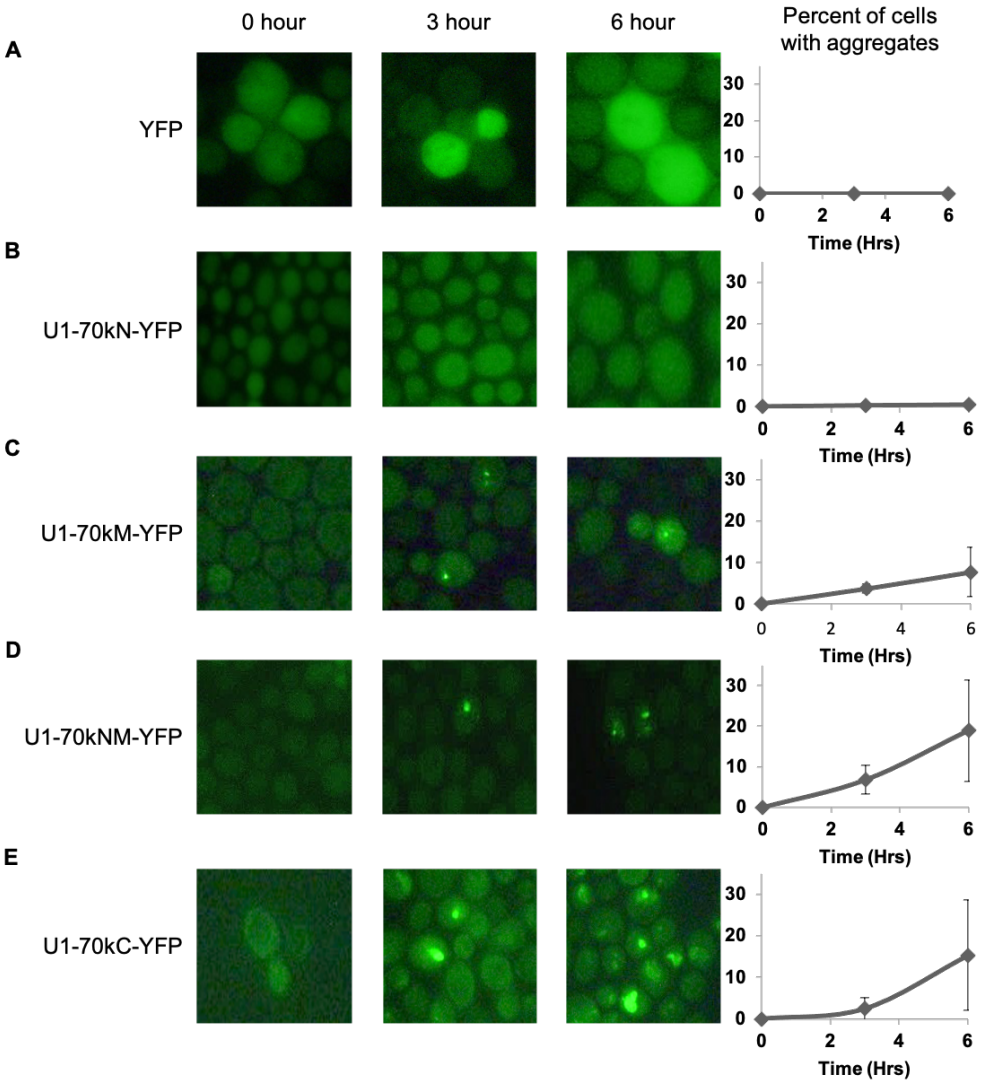

Figure 5.2 Characterization of the aggregation properties of U1-70K domains by fluorescence microscopy. (A) Fluorescent microscopy of the YFP control and different domains of U1-70k (B) U1-70kN, (C) U1-70kM, (D) U1-70kNM, and (E) U1-70kC expressed under the P_{CUP1} promoter in a [*psi*$^-$][*pin*$^-$] strain. Overnight pre-cultures of cells were diluted to on OD_{600} of 0.5 and supplemented with 300 μM $CuSO_4$. At each time point 0, 3, and 6 hours, cells were harvested, washed with water, and the plated onto microscopy slides for imaging. Each panel shows were three colonies were analyzed for each strain/plasmid combination after expression. Error bars depict standard deviations. Numbers for this experiment are shown in Table 5.1.

Table 5.1 Characterization of the aggregation properties of U1-70k domains by fluorescence microscopy.

Strain	Transformed plasmid	Time	Cells with aggregates relative to all cells with fluorescence**		
			(Average %)	SD Range	Number
[*psi*$^-$][*pin*$^-$] GT409	YFP	0 hrs	0	0 – 0.2	467
		3 hrs	0	0 - 0.2	473
		6 hrs	0	0 – 0.2	605
	U1-70kN-YFP	0 hrs	0	0 - 0.3	635
		3 hrs	0	0 – 0.6	432
		6 hrs	0	0 – 0.2	771
	U1-70kM-YFP	0 hrs	0	0 – 0.4	204
		3 hrs	3.67	2.57- 4.77	720
		6 hrs	7.75	1.85 – 13.65	309
	U1-70kNM-YFP	0 hrs	0	0 – 0.3	447
		3 hrs	2.44	0 – 5.04	508
		6 hrs	15.35	2.15 – 28.55	592
	U1-70kC-YFP	0 hrs	0	0 – 1.6	61
		3 hrs	6.77	3.27 – 10.27	404
		6 hrs	18.9	6.5 – 31.3	566

Data for Figure 5.2

**Three colonies were analyzed for each strain/construct combination.

(Figure 5.2D) both lead to the formation of cytoplasmic detectable foci, indicating a possible involvement of the M-domain to be necessary for aggregation.

Lastly, we examined the C-terminal domain's ability to aggregate. The C-domain contains LC domains, which are regions that contain repeats of single amino acids or short amino acid motifs, and have been implicated in the aggregation properties of numerous RNA-binding proteins [28]. Here, we show that high expression of U1-70kC (Figure 5.2E) also leads to the formation of cytoplasmic detectable foci, indicating that multiple domains of U1-70k are capable of forming aggregates in yeast.

We also wanted to determine if the high expression of U1-70k domains could be toxic in yeast and thus result in its inability to aggregate. Here, we show that the high expression of the domains of U1-70k do not result in any toxic effects in yeast as shown in Figure 5.3.

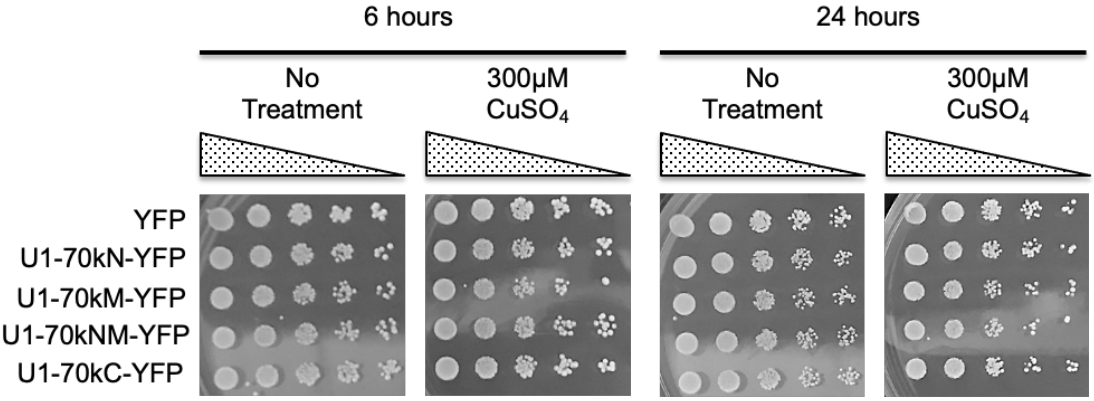

Figure 5.3 Growth effects of U1-70k domain plasmids in a [*psi*$^-$][*pin*$^-$] background. Overnight precultures were diluted to an OD_{600} of 0.1 in selective medium. Serial dilutions were prepared after both 6 hours and 24 hours to check for toxicity of the plasmids and plated onto –Ura medium. Media supplemented with 300 μM $CuSO_4$ was used for plasmid expression and compared to culture grown in medium lacking additional copper.

Biochemical detection of aggregates formed by domains of U1-70k

We again compared the expression levels of our fusion plasmids to determine if there were altered protein levels between protein domains. Previously, we did see a difference between domains of MAPT in Chapter 4. When comparing U1-70kN, a domain that does not aggregate, to that of U1-70kC, a domain that does, there is a decrease in expression for U1-70kC as compared to U1-70kN (Figure 5.4A). We previously saw a decrease in protein levels between TauRD

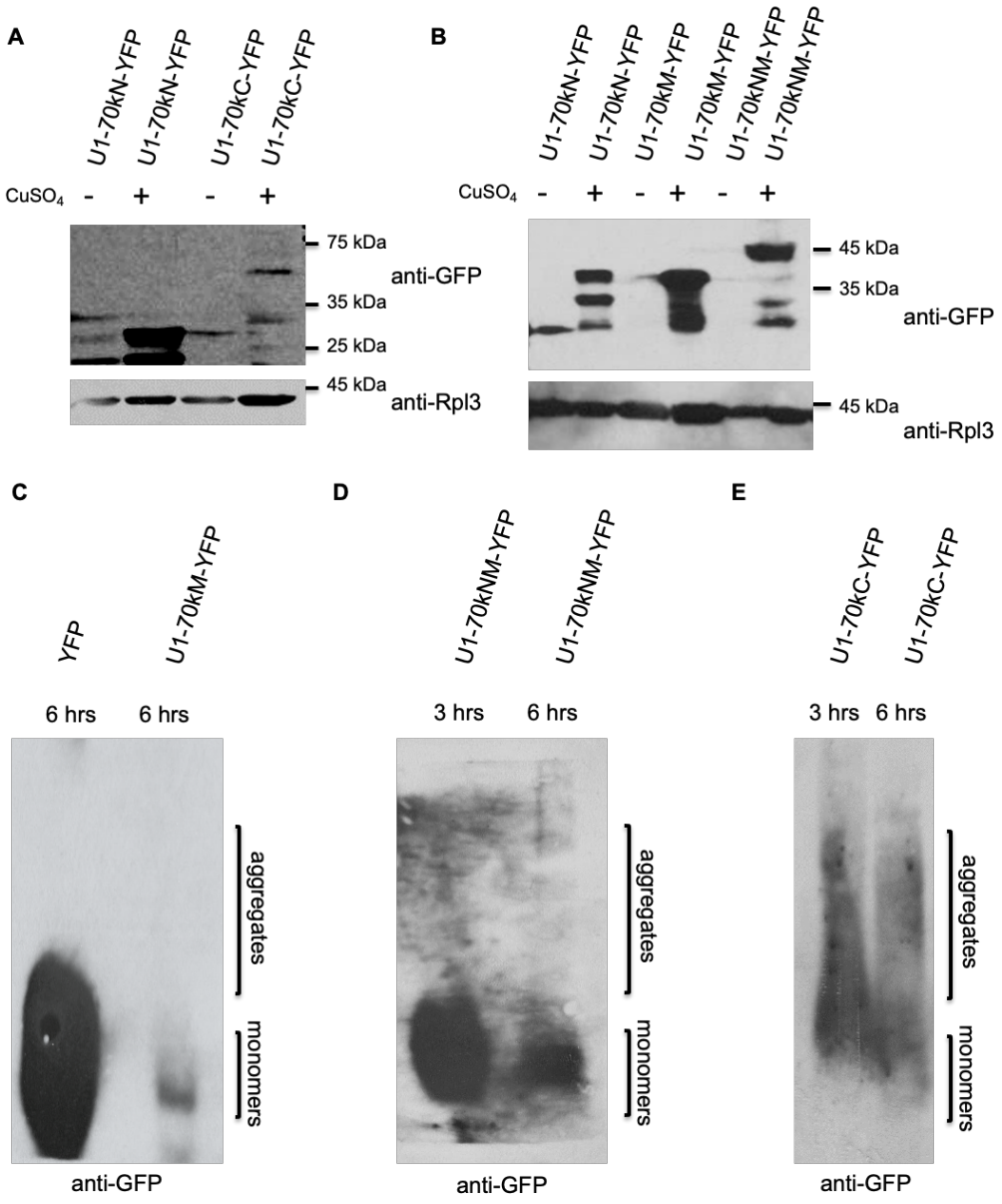

Figure 5.4 Biochemical characterization of aggregates formed by the U1-70K domains in yeast. (A) Overexpression of the constructs U1-70kN and U1-70kC and (B) U1-70kM and U1-70kNM fused to YFP in a [*psi*$^-$][*pin*$^-$] strain. Protein extracts were ran on a 10% acrylamide gel and detected using the anti-GFP antibody. The membranes were stripped and reprobed with the anti-Rpl3 antibody as a loading control. (C) Checking for detergent resistance by U1-70kM domain following overexpression, as detected by semi-denaturing detergent agarose gel electrophoresis, followed by Western blotting and reaction to anti-GFP antibody. Cell lysates were treated with sarkosyl and run on the agarose gel. (D and E) Same treatment as in Figure B, but for the U1-70kNM and U1-70kC constructs respectively.

(does not aggregate) and TauRDpro (does aggregate). There does appear to be a pattern on total protein levels between fusion proteins that do and do not aggregate. We also checked expression levels for the other domains, U1-70kM and U1-70kNM, to U1-70kN (Figure 5.4B). These domains all appear to be expressed at similar levels. The ribosomal protein Rpl3 was used as a loading control for comparison.

Next, we wanted to determine if the aggregates seen as fluorescent foci were amyloid in nature or another type of protein aggregate. Previous data has shown that U1-70k is a part of the sarkosyl-insoluble fraction in the AD brain proteome, and that its aggregation is dependent upon the LC1 domain located within the C-terminus [32]. To determine if our aggregates seen by fluorescent microscopy are amyloid in nature, we employed the technique of semi-denaturing detergent agarose gel electrophoresis (SDD-AGE) as described in Chapter 2. Detergent resistance is a characteristic of amyloid aggregates, but not those of other types (*e.g* stress granules). While multiple domains appeared to aggregate in our fluorescent microscopy assay, different domains had different results when analyzed by SDD-AGE. The RNA recognition motif U1-70kM ran as a monomer band, the same as compared to the YFP control as seen in Figure 5.4C. This same result was also seen by the U1-70kNM domain in Figure 5.4D. However, U1-70kC, which also formed fluorescent foci ran as an elongated smear on the gel, indicative of an amyloid aggregate (Figure 5.4E). While multiple domains of U1-70k are able to form fluorescent foci, there does appear to be a difference in the types of aggregates between these different domains.

Analysis of U1-70k aggregates by hexanediol

To further characterize the aggregates formed by both U1-70kNM and U1-70kC, we again employed the use of 1,6-hexanediol. As previously discussed in Chapter 4, 1,6-hexanediol is an aliphatic alcohol that weakens hydrophobic interactions and can inhibit LLPS. We studied both U1-70kNM (Figure 5.5A) and

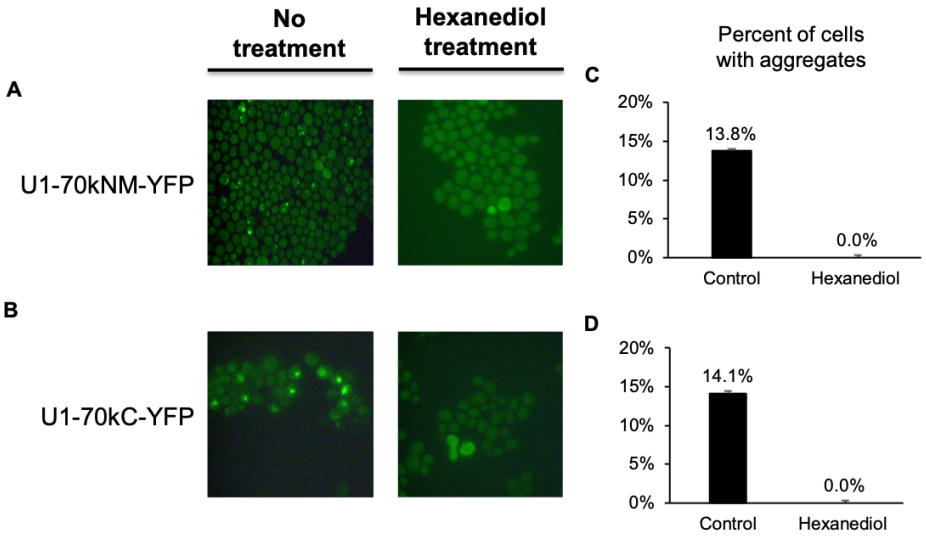

Figure 5.5 Hexanediol experiment with U1-70k plasmids. (A) Cells transformed with U1-70kNM-YFP or (B) U1-70kC-YFP were visualized by fluorescence microscopy following either 10 minutes of no treatment (control) or with hexanediol. (C) Quantitative analysis of aggregates by fluorescence microscopy by U1-70kNM and (D) U1-70kC following either no treatment or hexanediol treatment. Graphs depict pairwise comparisons within one experiment; however, three cultures were analyzed, showing a difference in the same direction. Error bars depict standard error.

U1-70kC (Figure 5.5B), both of which we previously showed formed fluorescent aggregates, however only U1-70kC was determined to be detergent resistant. As previously shown for both TauRDpro and MAPT, both domains of U1-70k were dissolved 10 minutes post-treatment with hexanediol. Numbers for the quantitative

analysis of U1-70kNM are shown in Figure 5.5C and U1-70kC in Figure 5.5D and are summarized in Table 5.2.

Table 5.2 Hexanediol treatment with U1-70k plasmids.

Strain	Transformed plasmid	Treatment	Cells with aggregates relative to all cells with fluorescence**		
			Average %	SE Range	Number
[*psi*$^-$][*pin*$^-$] GT409	U1-70kNM-YFP	Control	13.8	13.79 – 13.81	43
		Hexanediol	0	0 – 0.01	34
	U1-70kC-YFP	Control	14.1	14.09 – 14.11	92
		Hexanediol	0	0 – 0.01	80

Data for Figure 5.5

** Experiment shows pairwise comparison of one colony. Three colonies were examined showing a difference in the same direction.

Colocalization of U1-70k with other mammalian amyloidogenic proteins

We also performed colocalization studies between aggregating domains of U1-70k and Aβ_{42} and also MAPT. Colocalization of the aggregates could imply an interaction between these proteins; namely, that the aggregation of one could lead to the aggregation of another as discussed in the amyloid cascade hypothesis in Chapter 1. Here we show that both U1-70kNM (Figure 5.6A) and U1-70kC (Figure 5.6B) are both found colocalized with Aβ_{42} when co-expressed. Numbers for the quantitative analysis is shown in Figure 5.6C and summarized in Table 5.3. However, we did see a difference in colocalization between the U1-70kNM and U1-70kC domains when co-expressed with MAPT. Here we show that the U1-70kNM domain (Figure 5.7A) is less likely to be found colocalized with MAPT as compared to the U1-70kC domain (Figure 5.7B). Numbers for the quantitative analysis is shown in Figure 5.7C and summarized in Table 5.4.

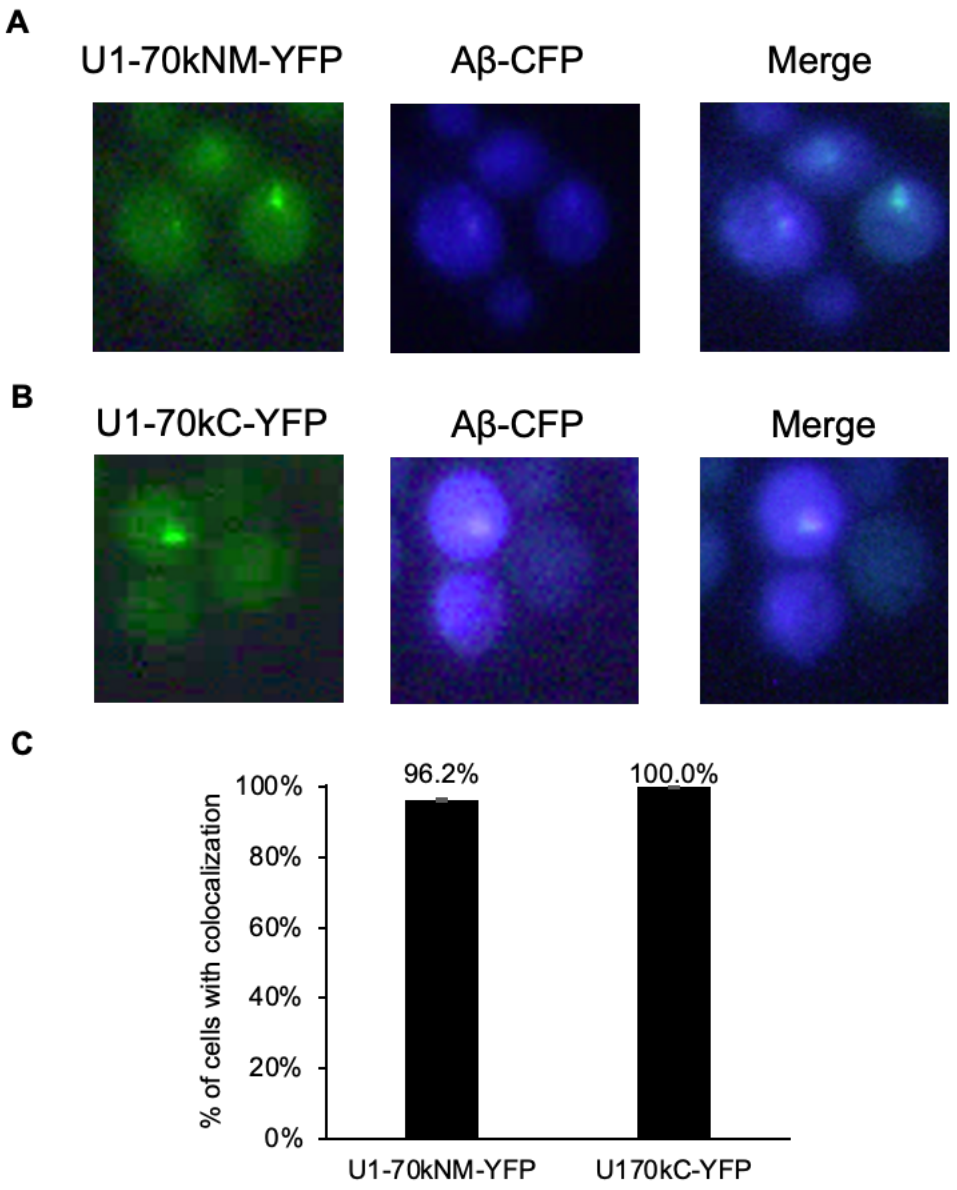

Figure 5.6 Colocalization of U1-70k-derived aggregates with Aβ in yeast cells. Fluorescent microscopy of (A) U1-70kNM and (B) U1-70kC along with $A\beta_{42}$ expressed under the P_{CUP1} promoter in a [*psi*$^-$][*pin*$^-$] strain. Overnight pre-cultures of cells expressing both plasmids were diluted to on OD_{600} of 0.5 and supplemented with 300 μM $CuSO_4$. Cells were harvested after 6 hours of incubation, washed with water, and the plated onto microscopy slides for imaging. (C) Quantitation of YFP (either U1-70kNM or U1-70kC) and $A\beta_{42}$-CFP colocalization. Percentages of colocalized dots detected in cells containing both types of aggregates are shown. Error bars depict standard error.

Table 5.3 Colocalization of U1-70k domains with Aβ$_{42}$.

Strain	Transformed plasmid	% of cells with aggregates colocalized out of total cells with both aggregates**		
		% Colocalization	SE range	Total cells with both plasmids
[*psi*$^-$][*pin*$^-$] GT409	U1-70kNM-YFP and Aβ$_{42}$-CFP	96.2	96.16 – 96.2	26
	U1-70kC-YFP and Aβ$_{42}$-CFP	100 ± 0.01	99.9 – 100	24

Data for Figure 5.6

**Standard error is calculated by binomial distribution.

5.4 Discussion

Our data demonstrates that the same sequence elements that drive amyloid formation in humans for U1-70k also drives protein aggregation in yeast, demonstrating the value of yeast models for studying protein aggregation.

The high expression of U1-70kN in our model results in the appearance of diffuse fluorescence, similar to that of the YFP control. While the N-domain contains an unstructured domain, a common element in many prion-like domains, it does not lead to the formation of cytoplasmic detectable aggregates in our assay. These results match findings by Diner *et al.* 2014, in which they showed the 1-99 amino acid region, the same as our U1-70kN construct, was unable to aggregate when seeded by AD brain homogenate [32]. In their experiments they also demonstrated a similar result for the U1-70kNM domain. Here, we are able to detect cytoplasmic aggregates formed by the high expression of U1-70kNM,

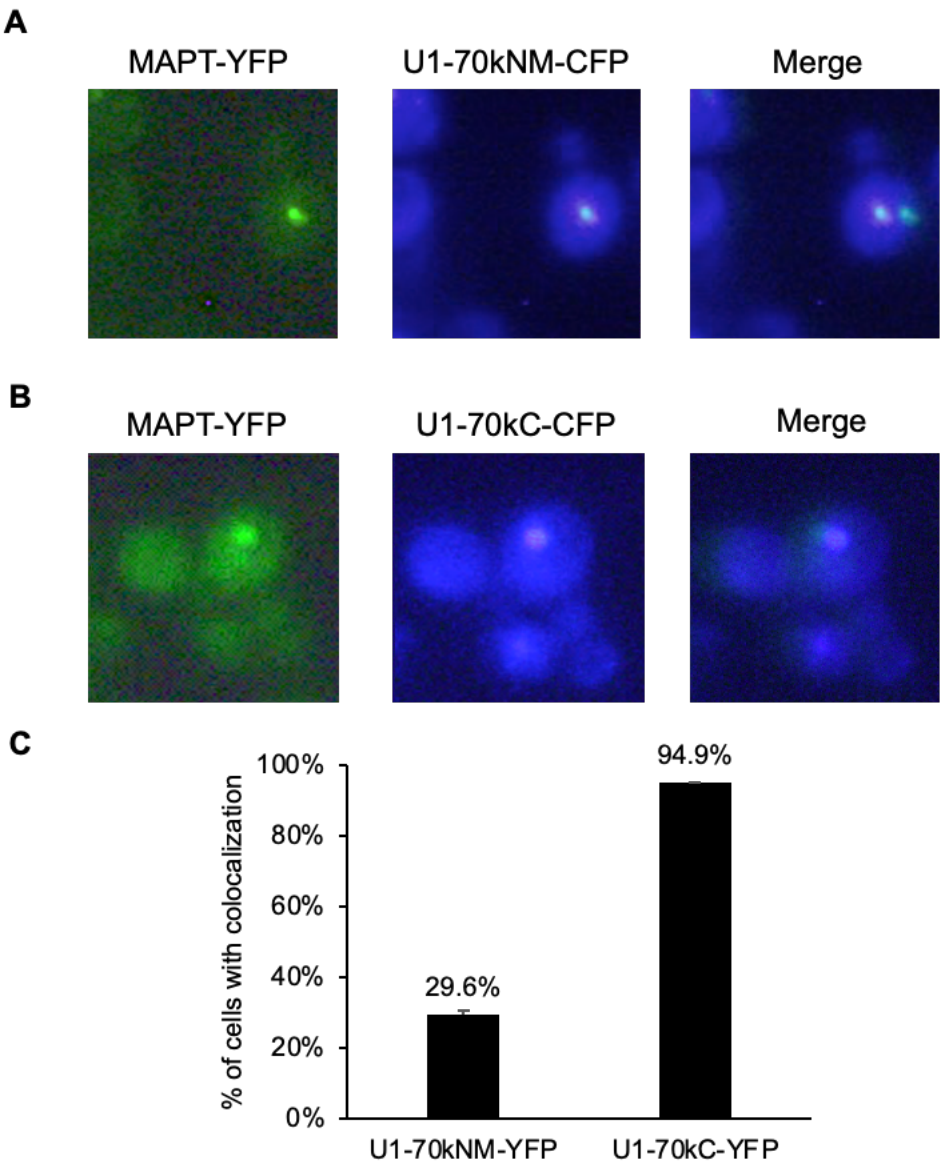

Figure 5.7 Colocalization of U1-70k-derived aggregates with MAPT in yeast cells. Fluorescent microscopy of (A) U1-70kNM and (B) U1-70kC along with MAPT expressed under the P_{CUP1} promoter in a [*psi*$^-$][*pin*$^-$] strain. Overnight pre-cultures of cells expressing both plasmids were diluted to on OD_{600} of 0.5 and supplemented with 300 μM $CuSO_4$. Cells were harvested after 6 hours of incubation, washed with water, and the plated onto microscopy slides for imaging. (C) Quantitation of CFP (either U1-70kNM or U1-70kC) and MAPT-YFP colocalization. Percentages of colocalized dots detected in cells containing both types of aggregates are shown. Error bars depict standard error.

Table 5.4 Colocalization of U1-70k domains with MAPT.

Strain	Transformed plasmid	% of cells with aggregates colocalized out of total cells with both aggregates**	
		(% Colocalization) ± SE	Total cells with both plasmids
[*psi*$^-$][*pin*$^-$] GT409	U1-70kNM-CFP and MAPT-YFP	29.6 ± 0.7	59
	U1-70kC-CFP and MAPT-YFP	94.9 ± 0.01	27

Data for Figure 5.7

**Standard error is calculated by binomial distribution.

however, analysis by SDD-AGE and sensitivity to hexanediol. These results taken together indicate that the U1-70kNM aggregates may be non-amyloidogenic in nature, which matches their previous result in which AD brain homogenate was unable to seed its conversion. In our model, we also tested the RNA recognition motif, U1-70kM, alone and showed a similar result to that of the U1-70kNM construct. While our data currently points to the idea that the aggregates formed by both U1-70kM and U1-70kNM may be a type of LLPS, it cannot be overlooked that these protein domains may have amyloidogenic properties as well. Recent data has shown that the RRM domains of other proteins associated with neurodegenerative diseases including TDP-43, FUS, and RBM45 are capable of forming amyloids *in vitro[101]*. Here, they show that the RRM domains of disease-associated proteins have different properties as compared to those from non-diseases-associated proteins, including reversable thermal folding and unfolding. While it is still unclear the exact role that RRM's play in protein aggregation, the

concept that they can play a role in the phase transition due to RRM domains unique properties remains a possibility, and could explain the results shown here for U1-70kM and U1-70kNM in our yeast model.

Our findings also show the detection of cytoplasmic aggregates for the U1-70kC domains as well. However, in the case of this domain, the aggregates do appear to by detergent-resistant. This result is again supported by existing findings indicating the aggregation-inducing abilities of that domain. Again, in Diner *et. al.* 2014, they show that the C-domain is required for aggregation, which they show by recombinant protein being seeded by AD brain homogenate and that it is located in the sarkosyl-insoluble fraction [32].

Just as MAPT has been demonstrated to be able to undergo LLPS, so has U1-70k [102]. In the study by Xue *et. al.* 2019, they are able to show that both the LC1 and LC2 domains of U1-70k are able to undergo LLPS, however, only the LC1 domain was able to also undergo aggregation, as they define as solid-like aggregates [102]. They use the method of fluorescence recovery after photobleaching (FRAP) to identify LLPS. They contribute this to the LC1 domain containing a high number of ampholytic residues. They were also able to show this both *in vitro* and *in vivo* in Neuro2a cells. Furthermore, they were also able to detect both LLPS and solid aggregates for both LC1 domain and full-length U1-70k simultaneously in N2a cells. They contribute that both types being found together as support for a hypothesis in the field of LLPS research, that aggregation may be a result of LLPS. As for our results, our fusion plasmid of U1-70kC-fused to YFP, which harbors both the LC1 and LC2 domains, was not resistant to treatment by

hexanediol, indicating that the cytoplasmic aggregates are LLPS. However, we were also able to show that the expressed protein of U1-70k was also able to form detergent-resistant aggregates in cells, indicating that there is a diversity of aggregates formed by U1-70kC in our yeast model. To our knowledge, no one to date has studied whether the region containing the first 181 amino acids (U1-70kNM) is capable of undergoing LLPS. Here, we show that aggregates formed by U1-70kNM are not detergent resistant and are sensitive to hexanediol indicating that they may be an aggregate that is non-amyloid in nature. One type of aggregate that is thought to form through LLPS are stress granules. Stress granules are membrane-less cytosolic bodies composed of mRNAs and proteins that assemble when translation initiation is limiting, and are thought to represent a pool of mRNPs stalled in the process of translation initiation [103, 104]. Genetic evidence has emerged implicating stress granules as a subcellular compartment that is central to the pathogenesis of a closely related set of degenerative diseases, including amyotrophic lateral sclerosis (ALS), frontotemporal dementia (FTD) and inclusion body myopathy (IBM) [86, 105]. While stress granule formation has not been shown for U1-70k, it has been shown for other RNA-binding proteins, including hnRNPA1. Previous studies have shown that the RNA-recognition motif contributes to LLPS, but only in the presence of RNA, and that fibrilization can occur in these protein rich droplets [89]. While most *in vivo* evidence points to the significance of the LC1 domain located in the C-terminus of U1-70k as the domain responsible for protein-protein interaction and driving aggregation, there is some *in vitro* evidence to suggest that the N-terminal domain of U1-70k can form high-

molecular weight oligomers [106]. Also, it is important to note that located within the N-terminus not only are there regions of disorder, but there is also a region of disorder containing a stretch of both acidic and basic amino acid residues, although shorter in comparison to both the LC1 and LC2 domains. While are current data cannot definitely confirm LLPS driven by the M-domain of U1-70k, current data does support that this is a theoretical possibility, and through other experiments are model is primed to be able to address these types of questions.

The aggregation of U1-70k has been shown to be exclusive to AD [99]. As such, we examined co-localization of U1-70k domains with both $A\beta_{42}$ and MAPT, both of which are also found aggregated in AD, and are reviewed in Chapters 3 and 4 respectively. Here, we show that aggregates formed by both U1-70kNM and U1-70kC are found colocalized with $A\beta_{42}$. This is somewhat a surprising result as previous reports do not show a direct connection between U1-70k and $A\beta_{42}$. However, it has been reported that the aggregation of U1-70k is correlated to the amount of $A\beta$ deposition, and this occurs in the absence of MAPT aggregates [107]. One explanation for this is that Aβ is secreted and predominantly aggregates in the extracellular space [108], so while an interaction may be possible, it may not have been previously shown in screens studying AD brain pathology due to spatial separation. We also investigated the colocalization of both U1-70kNM and U1-70kC with MAPT. Here, we show that aggregates composed of U1-70kC are able to interact with MAPT, while those of U1-70kNM. This matches what has been previously described for U1-70k, in which the LC1 domain located in the C-terminal

domain was found to interact more with MAPT in AD brain homogenate as compared to the N-domain alone[106].

Overall, our data strongly supports a yeast-based model that can be used for studying the amyloidogenic properties of U1-70k. Here, we show that in yeast it maintains its ability to form aggregates, with indication that specific domains are capable of forming different types of aggregates. We are also able to demonstrate that specific domains are also able to colocalize with other proteins associated with AD, matching what has been previously demonstrated. Our model could be used in future studies in unraveling the properties and conditions that control not only U1-70k's amyloidogenic nature, but other RNA-binding proteins associated with disease.

5.5 Conclusions

- The M, NM, and C-domains of U1-70k form fluorescent aggregates when expressed in yeast cells.
- Only aggregates formed by U1-70kC are detergent-insoluble, as typical of amyloids.
- Aggregates formed by both U1-70kNM and U1-70kC are dissolved following 10-minute treatment with hexanediol.
- Aggregates formed by the NM, and C-domains colocalize with $A\beta_{42}$, however only aggregates of the C-domain colocalize with MAPT.

CHAPTER 6. DETECTION OF NOVEL AMYLOIDOGENIC PROTEINS AND ANTI-AMYLOIDOGENIC COMPOUNDS BY AMYLOID NUECLATION ASSAY IN YEAST

This chapter includes data published in *Future Medicinal Chemistry*.

Hamulakova, S., Kudlickova, Z., Janovec, L., Mezencev, R., **Deckner, Z**., Chernoff, Y.O., Janockova, J., Ihnatova, V., Bzonek, P., Novalkova, N., Hepnarova, V., Hrabinova, M., Jun, D., Korabecn, J., Soukup, O., Kuca, K. (2021). Design and synthesis of novel tacrine-indole hybrids as potential multitarget-directed ligands for the treatment of Alzherimer's disease. Future Medicinal Chemistry

6.1 Summary

Amyloid formation occurs via a two-step process. First is nucleation, in which a normal soluble protein is converted into an aggregate or "nuclei" of the prion isoform. This nucleation event can be driven by mutations, but most often this is a sporadic phenomenon. Our lab has previously published a yeast assay in which we can detect the nucleation step of many amyloidogenic proteins/sequences that are associated with diseases in humans. This includes proteins such as PrP (associated with mammalian prion diseases), Aβ (AD), and α-synuclein (Parkinson's disease) just to name a few. We have also shown that the same sequence elements (protein domains/ mutations) in humans control protein aggregation in yeast. In this work, we attempted to expand our nucleation assay to study proteins that have been shown to have amyloid-like properties, whether experimentally or computationally, but are not classically associated with disease to determine if they also can nucleate [*PSI*$^{+}$] when fused to the prion domain of

Sup35 in the absence of a preexisting prion. This will provide further credence to our assay as a tool to determine whether proteins or protein sequences have amyloidogenic properties.

6.2 Specific materials and methods

Materials

Strains, plasmids, and oligonucleotide primers used in this study are described in Appendix tables A, B, and C respectively. The antibodies to Sup35C and HA are described in Chapter 2.

6.2.1.1 Strains

The haploid [*PSI*$^+$][*PIN*$^+$] strain GT81-1C is a meiotic spore of the homozygous autodiploid GT81. The [*psi*$^-$][*pin*$^-$] strain GT409 was obtained from GT81-1C via curing by guanidinium hydrochloride (GuHCl) and was previously described in Chernoff *et al.* 2000 [61], while the [*psi*$^-$][*PIN*$^+$] strain GT159 was obtained via curing GT81-1C of [*PSI*$^+$] using excess Hsp104. The [*psi*$^-$][*pin*$^-$] strain GT17 of the 74-D694 genotype was also employed in this study and is described in Bailleul *et. al.* 1999 [109].

6.2.1.2 Plasmids and primers

The overall scheme of construction of the mammalian genes of interest fused to prion forming domain of Sup35 (Sup35N or NM) (Figure 6.1) is described in detail as follows.

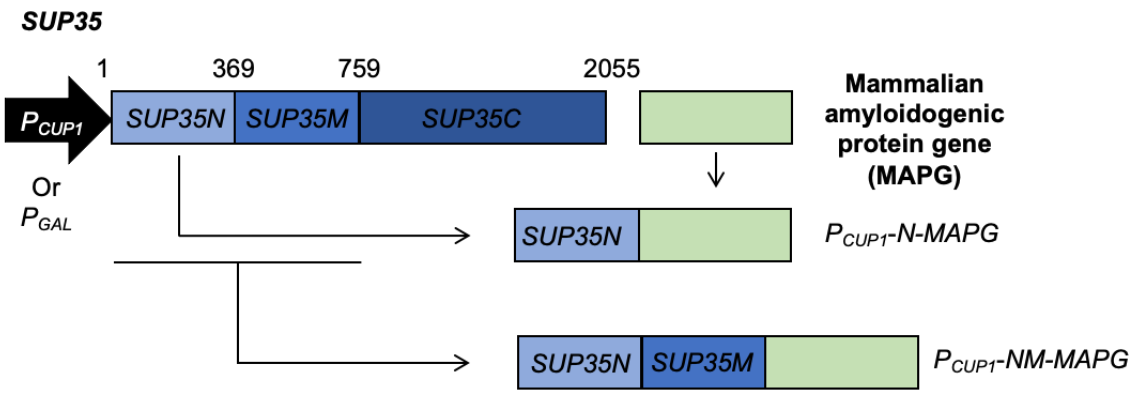

Figure 6.1 Scheme of construction of Su35N(NM) fused to amyloidogenic protein of interest. Any amyloidogenic protein (MAPG) of interest (small peptide or full protein) is attached to the C-terminal region of either the coding region of Sup35N or Sup35M to form chimeric genes. These fusions are under the copper inducible promoter.

6.2.1.2.1 Construction of P_{CUP1} expression vector

In order to generate the initial backbone vector, a centromeric shuttle vector containing the P_{CUP1} promoter with Sup35N with a *URA3* marker initially described in Chandramowlishwaran *et al.* 2018 [110] was digested with the restriction endonuclease *Eco*RI. This product was then subsequently digested using the Mung Bean nuclease to create blunt ends and then re-ligated together. This resulted in a vector containing a single *Eco*RI restriction site in the multi-cloning site that could be used for constructing chimeric genes. No other restriction sites in the multi-cloning sites were disrupted.

6.2.1.2.2 Construction of TauRD expressing plasmids

The gene coding for TauRD was PCR-amplified from the plasmid pcDNA-RD(WT) (kindly provided by Dr. Marc Diamond, Washington University) using primers containing *Eco*RI and *Sac*I restriction sites. The resulting *Eco*RI-*Sac*I

TauRD fragment was inserted into the previously described vector using the same enzyme sites to generate a plasmid expressing Sup35N-TauRD.

6.2.1.2.3 Construction of U1-70k expressing plasmids

The *SUP35N(NM)-U1-70kN*, *SUP35N(NM)-U1-70kNM*, and *SUP35N(NM)-U1-70kC* genes were made by using the plasmid containing the full coding region of U1-70k with a Myc tag in the pcDNA3.1 vector (provided by Dr. Nicholas Seyfried, Emory University). U1-70kN confers to the N-terminal domain of the protein containing amino acids 1-99. The NM domain describes the N-terminal domain along the DNA-binding domain of the protein encompassing the 1-181 amino acids. U1-70kC is the C-terminal portion of the protein containing the 182-437 amino acids. The chimeric fusions were generated by using PCR to amplify the corresponding regions of U1-70k with the addition of *Eco*RI and *Xba*I enzyme sites. These PCR products were then digested with these same enzymes and ligated into the P_{CUP1}-Sup35N vector digested by the same enzymes. The corresponding Sup35NM chimeric constructs containing these U1-70k domains were generated by digesting the Sup35N chimeric fusions with *Eco*RI-*Xba*I enzymes and ligating them into the P_{CUP1}-Sup35NM shuttle vector.

6.2.1.2.4 Construction of CREST and CBP expressing plasmids

The *SUP35N-CREST(C)*, *SUP35N-CREST*, and *SUP35N-CREST(Cmut)* were generated using the plasmid (provided by provided by Dr. Mike Sherman, Boston University) containing the full-length version of rat calcium responsive transactivator (CREST) protein. CREST(C) refers to the C-terminal domain of

CREST from amino acid 273 to 401. The CREST(Cmut) refers to the nonsense mutation at position 393 (position 388 in humans) which leads to a truncation of the protein by 9 amino acids and has been implicated in ALS [111, 112]. The CREST domains as well as full-length rat CREST were PCR-amplified using primers that included an *Eco*RI site along with an *Xba*I site that included an HA tag. The resulting fragments were then ligated into the P_{CUP1}-Sup35N vector using the same sites. The pYES2-CBP-GFP plasmid (also provided by Dr. Mike Sherman) containing the 5812 to 7290 bp coding sequence of mouse *CBP* was PCR-amplified using primers to encode *Eco*RI and *Xba*I restriction sites along with an HA tag in the reverse primer. The subsequent PCR product was digested using the same restriction enzymes and ligated into the P_{CUP1}-Sup35N shuttle vector to generate the chimeric gene containing the 2193-2360 amino acid region of CBP.

6.2.1.2.5 Construction of p53 expressing plasmids

To express genes of *SUP35N(NM)-p53N* and *SUP35N(NM)-p53M*, we used the plasmid pc53-SN3 containing wild-type human p53 (provided by Dr. Muxiang Zhou, Emory University). The domain p53N refers to the N-terminal domain of the protein containing the 1-63 amino acids, while p53M refers to the portion of the middle domain of p53, the 94-312 amino acids. The pc53-SN3 plasmid was used to PCR-amplify the respective p53 domains while encoding *Eco*RI and *Xba*I restriction sites. The PCR products were subsequently digested using the same enzymes and placed in the P_{CUP1}-Sup35N shuttle vector. To generate the *SUP35NM-p53N-HA* and *SUP35NM-p53M-HA* genes, the p53 domain coding regions were removed from the Sup35N chimeric genes using the

*Eco*RI and *Xba*I enzymes and placed into the P_{CUP1}-Sup35NM shuttle vector. It has been previously described that mutations within the p53 gene can confer amyloidogenic properties in cancer [113, 114]. One such mutation is the R248Q mutation, which confers a mutation that prevents target DNA interaction [115]. In order to generate this mutation in our *SUP35N-p53M* gene, we used the QuikChange Site-Directed Mutagenesis protocol as described in Chapter 6. To generate the *SUP35NM-p53M(R248Q)* gene, the *p53M(R248Q)* gene was removed from the Sup35N fusion by the *Eco*RI and *Xba*I enzyme and subsequently placed in the P_{CUP1}-Sup35NM shuttle vector.

6.2.1.2.6 Construction of PCH3 expressing plasmids

The Sup35N fusion plasmids containing the various isoforms of PHC3 were provided by the Amyloid Biology Lab at St. Petersburg University, Russia, and were generated by Dr. Nina Romanova. These cassettes containing the isoforms of PHC3 were amplified from a human cDNA library. One of these isoforms that was generated does not match the currently recognized list in UNIPROT. It has similarities to both the currently recognized isoform 5 and 6 of the protein and in this work, we list it as isoform 5-2. This protein was also studied using the Curli-amyloid generator (C-DAG) assay [116]. The plasmids *pVS72* (P_{BAD}-csgA$_{ss}$-Sup35NM-His$_6$) and *pVS105* (P_{BAD}-csgA$_{ss}$-Sup35M-His$_6$) were provided along with the required strain VS which contains the ∆(*csg*BAC). The C-DAG constructs containing the isoforms PHC3is5-1 and PHC3is6 were made by amplifying the PHC3 isoforms from the Sup35N plasmids using primers that contain *Not*I and *Xba*I restriction sites. These PCR sequences were digested and ligated into the

P_{BAD}-csgA$_{ss}$-Sup35M-His$_6$ vector digested by the same enzymes. This removed the Sup35M insert and generated the P_{BAD}-csgA$_{ss}$-PHC3is5-1-His$_6$ and P_{BAD}-csgA$_{ss}$-PHC3is6-His$_6$ plasmids.

6.2.1.2.7 Control plasmids

The plasmids used as both positive and negative controls in the nucleation assay including: P_{CUP1}-Sup35N-PrP(90-230), P_{CUP1}-Sup35N-Aβ_{42}, P_{CUP1}-Sup35N-IAPP, P_{CUP1}-Sup35N-Myo(WT), P_{CUP1}-Sup35N-Ade2, along with the plasmids used in the chemical curing experiments: P_{GAL}-Sup35N and P_{GAL}-Sup35N-Aβ_{42} were created by previous members of the lab either here at Georgia Tech or at St. Petersburg University and are described in Chandramowlishwaran *et al.* 2018 [1].

Methods

Standard protocols for plasmid construction including: DNA isolation, gel electrophoresis, restriction digestion, gel extraction, ligation, and bacterial transformation are described in Chapter 2. Procedures for inserting Standard procedures for yeast cultivation and transformation are also described in Chapter 2. Standard yeast and bacterial media, except for the media used in the C-DAG system, were used and are provided in Chapter 2. The C-DAG systems procedures and media are provided below.

6.2.2.1 Plate assay for [*PSI*$^+$] nucleation

To check for [*PSI*$^+$] nucleation by our protein sequences of interest, the chimeric fusion proteins containing MAPG's were transformed into a [*psi*$^-$][*pin*$^-$]

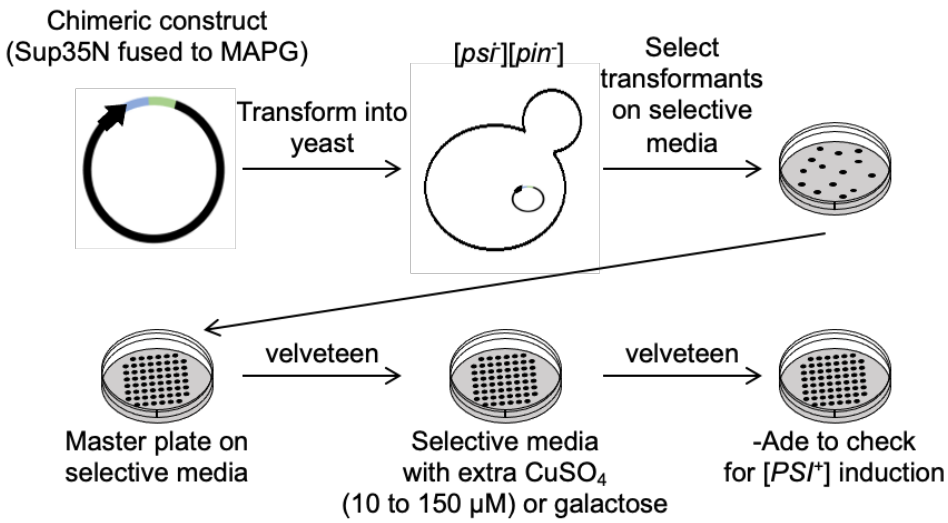

Figure 6.2 Schematic of nucleation assay of [*PSI*$^+$] by chimeric protein containing mammalian amyloidogenic proteins.

yeast strain. Tranformants were grown on media that was selective for the plasmid (e.g. -Ura). Transformants were selected and patched onto a master plate, again selective for the plasmid, and then subsequently velveteen replica plated onto the media containing the addition of either 0, 10, 50, 100, or 150 μM $CuSO_4$ (note that yeast media contains a background concentration of 3μM $CuSO_4$) to induce expression. After 3 days of growth, to allow for induction, the plates were replica plated onto -Ade media to check for [*PSI*$^+$] formation (Figure 6.2). [*PSI*$^+$] formation was scored by papillation on -Ade media after approximately 7-10 days of incubation. At least 8 independent transformants were checked for each plasmid to assure reproducibility, however for simplicity only one representative colony for each plasmid is shown in all figures. Strains carrying the control and experimental plasmids were always examined on the plates.

6.2.2.2 Site-directed mutagenesis of DNA

For site-directed mutagenesis to generate the R248Q mutation in the RRM domain of p53. Oligonucleotide primers that incorporate the desired point mutation were generated using the Primer X program. The site-directed mutagenesis procedure was carried out using the material and procedures provided in the Quickchange SiteDirected Mutagenesis kit (Agilent Technologies). Incorporation of the mutation into the plasmid was confirmed using Sanger sequencing provided by Eurofins MWG Operon Sequencing.

6.2.2.3 Curli-dependent amyloid generator (C-DAG) system

We also employed another assay developed by Anne Hochschild at Harvard University [116]. This assay uses another prion Curli (caused by the CsgA protein and is a part of the csgBA operon) in *E. coli* as a readout to determine if target proteins or protein sequences have amyloidogenic properties. It is also takes advantage of the phenotypic characteristics of Curli, in which it is able to stain red in medium supplemented with the dye Congo red (CR), a dye that is specific to amyloid binding [117].

For the colony color phenotype assay (Figure 6.7A) the plasmids containing these isoforms fused to the *csgA* exportation signal were transformed into the *E. coli* strain *VS39 (*an *E. coli* strain that is competent in Curli production and has a deletion in the genes of *csgA*, *csgB*, and *csgC* *)* and selected on LB media containing 100 μg/ml ampicillin, 25 μg/ml chloramphenicol, and 0.5% (wt/vol) glucose. A single transformant was then

inoculated into LB supplemented with 100 μg/ml ampicillin and 25 μg/ml chloramphenicol and grown overnight at 37°C as a preculture. The overnight preculture was then diluted to an OD_{600} of 0.1 and shacked at c for 30 minutes. The culture was then spotted (5 μM) onto multiple plates. Each culture was then spotted onto a LB media supplemented with ampicillin and chloramphenicol, a Congo-Red inducing plate (LB supplemented with 100 μg/ml ampicillin, 25 μg/ml chloramphenicol, 0.2% (wt/vol) L-arabinose, 1 mM IPTG, and 10 μg/ml Congo Red), and a Congo-Red non-inducing plate (LB supplemented with 100 μg/ml ampicillin, 25 μg/ml chloramphenicol, and 10μg/ml Congo Red). Once the spot has been absorbed into the media, the plates are grown upside down at 22°C for 5 days. Plates were examined for the formation of a red ring as indication of amyloid formation in the presence of Congo Red. The plasmids *pVS72* and *pVS105* were used as controls and examined on the same plates as colonies containing the experimental plasmids. Multiple colonies were analyzed for reproducibility. For the Congo Red birefringence analysis, colonies were selected from the Congo Red Inducing plate from the color-phenotype assay and spotted with 1 mL PBS to resuspend them and transferred into a 1.7 mL microcentrifuge tube. 5 μL of each sample to be tested were spotted onto a microscope slide and allowed to air-dry for 2 minutes. A coverslip was placed on top of each sample on the slide and examined under a light microscope with polarizing light for birefringence (note this assay was done both at Georgia Tech using the microscopy core facility located in EBB and at St. Petersburg University, Russia. Results shown are from the experiment completed in Russia by Konstantin Kulichikhin).

6.2.2.4 Inhibition of Aβ-dependent amyloid nucleation assay

The [*psi*$^-$][*pin*$^-$] strain GT17 were transformed with the *HIS3* marker plasmid expressing the chimeric construct *SUP35N- Aβ_{42}* under the P_{GAL} promoter. Nucleation was detected using the readthough assay as previously discussed in Chapter 1 section 1.3.1. Yeast cultures were grown overnight in -His liquid medium supplemented with glucose, washed and inoculated into -His medium containing 2% galactose instead of glucose for induction of the P_{GAL} promoter. The tested compound (140 μM) or solvent control (70% EtOH:DMSO in a 1:2.18 v/v ratio) was added at a starting cell density of OD_{600} of 0.1. After a period of 16-36 hours, as indicated, dilutions were either spotted or plated onto the following solid medium: -His for the detection of plasmid containing cells, or -His-Ade for the detection of cells with [*PSI*$^+$]; in some cases, spotting or plating onto YPD was performed in parallel. Concentrations of plasmid-containing cells were determined form numbers of colonies grown on -His medium (detected after 3-4 days of incubation), whereas concentrations of plasmid-containing cells with the [*PSI*$^+$] prion were determined from numbers of colonies grown on -His-Ade medium (as detected after 10-14 days of incubation). The frequency of prion nucleation was determined as a ratio between the concentration of [*PSI*$^+$] cells and the concentration of plasmid-containing cells (amyloid, nucleation frequency [ANF]).

6.3 Results

Protein or protein domains with [PSI$^+$] nucleating abilities

Here, we wanted to continue to check if certain domains of proteins that have been previously reported to be associated with mammalian amyloidogenic diseases, or were reported to have amyloid-like characteristics could also nucleate [*PSI*$^+$] when fused in tandem to the prion domain (PrD) of Sup35 (Sup35N). As has been previously published, we know that the overexpression of only the PrD of Sup35 is inefficient to induce [*PSI*$^+$] (only after high treatment of $CuSO_4$ and extended incubation can this be seen in plate assays)[51]. Another prion (e.g Rnq1 or [*PIN*$^+$]) is required as shown in Figure 6.3A. It has been previously published that the fusion of a PrD of previously known and well characterized mammalian amyloidogenic proteins are able to nucleate [*PSI*$^+$] *de novo* [110]. Here, the mammalian amyloidogenic protein is able to oligomerize and promote the PrD of Sup35 to convert into its prion state. The amyloid seed containing the chimeric fusion of both the PrD of the mammalian amyloidogenic proteins and the PrD of Sup35 is able to recruit the endogenous Sup35. The PrD of Sup35 in the oligomer of the chimeric seed is able to convert the endogenous Sup35 into [*PSI*$^+$] as shown in Figure 6.3B. The propagation of [*PSI*$^+$] can then be determined phenotypically by growth on -Ade medium (caused by the nonsense suppression by the readthrough of the *ade1-14* allele).

We wanted to expand our nucleation assay to proteins that are not classically thought of as being associated with disease, but have been suggested

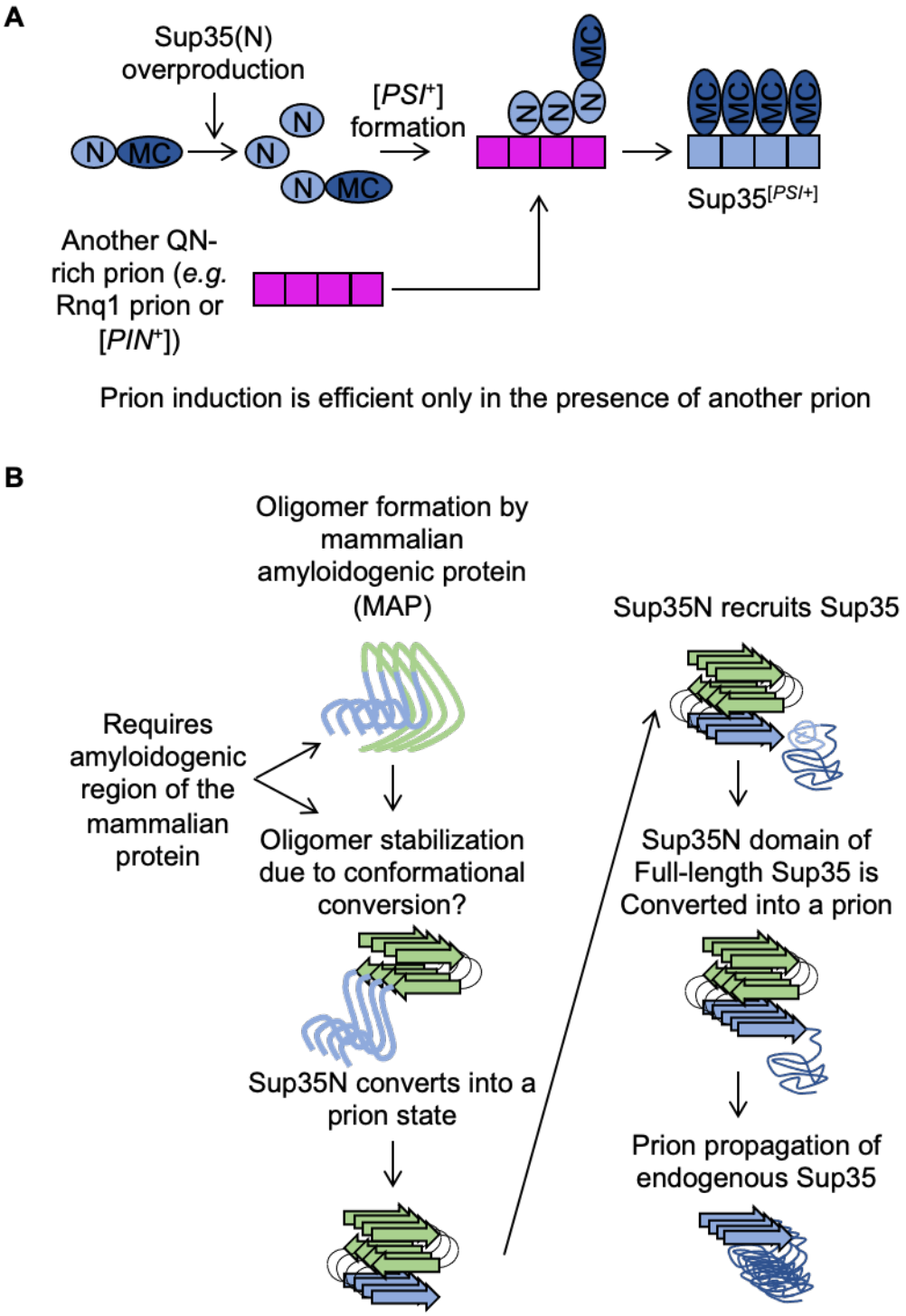

Figure 6.3 Principle of the yeast prion nucleation assay. (A) *De nono* [*PSI*$^+$] nucleation by overproduction of Sup35 (or N or NM) is rare, but can be facilitated by the presence of another yeast prion, e.g. [*PIN*$^+$], the prion isoform of Rnq1. (B) A model for [*PSI*$^+$] nucleation by mammalian amyloidogenic proteins (MAP). Non-prion isoforms are designated as lines, prion isoforms - as connected arrows.

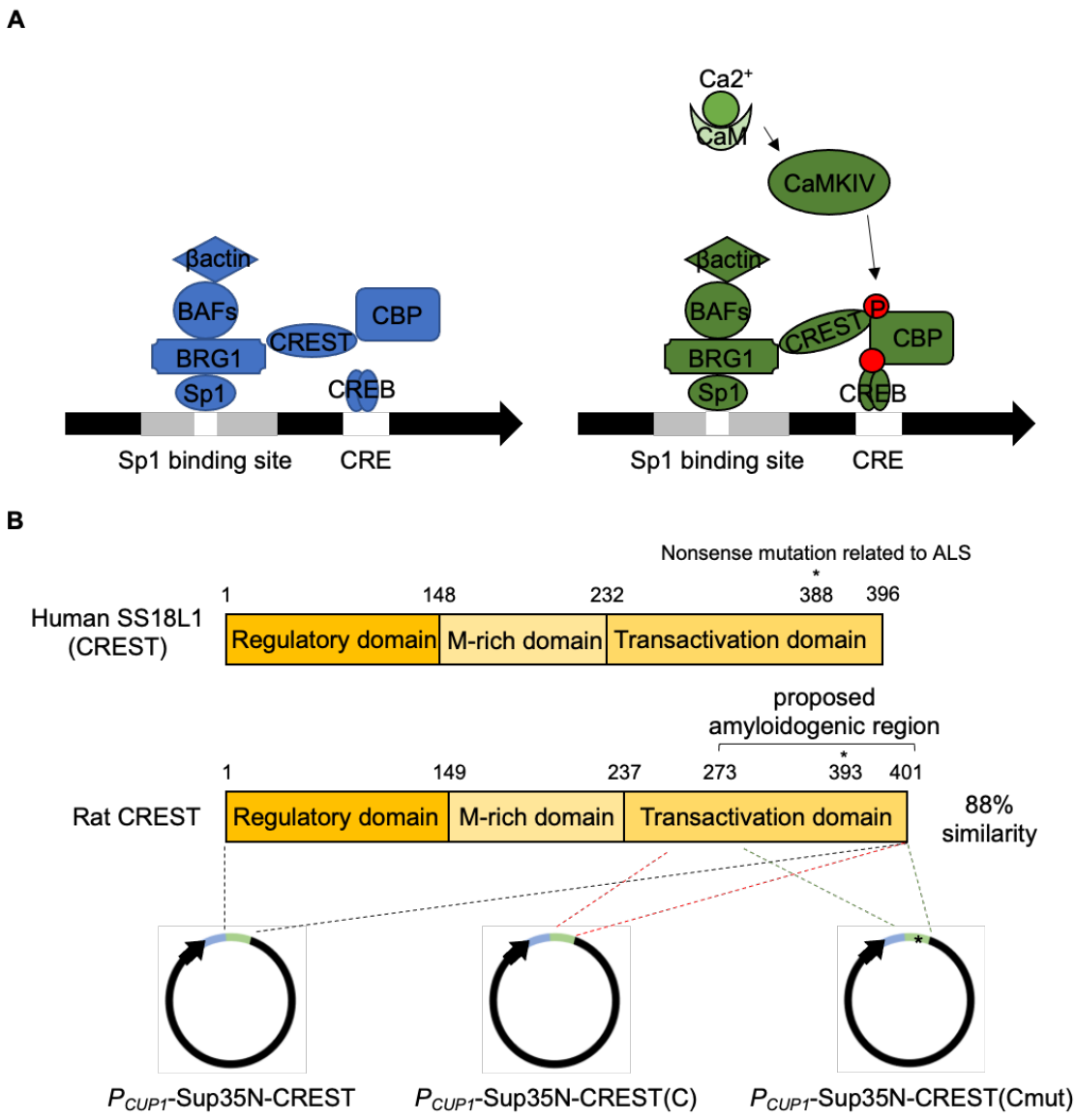

Figure 6.4 Functions and amyloidogenic domains of CREST. (A) Cartoon diagram highlighting the normal functions of CREST as a member of the BRG1 complex. (B) Schematic diagram of the protein domains of SS181L (CREST) and highlights certain features as it is related to specific amyloid diseases. The difference between Rat CREST and Human CREST are also highlighted as Rat CREST was used for experiments.

to have amyloidogenic properties. For this we chose to looked at both the CREST protein (also known as SS18L1) and polyhomeotic like protein 3 (PHC3). The CREST protein is a component of the CREST-BRG1 complex (Figure 6.4A), which

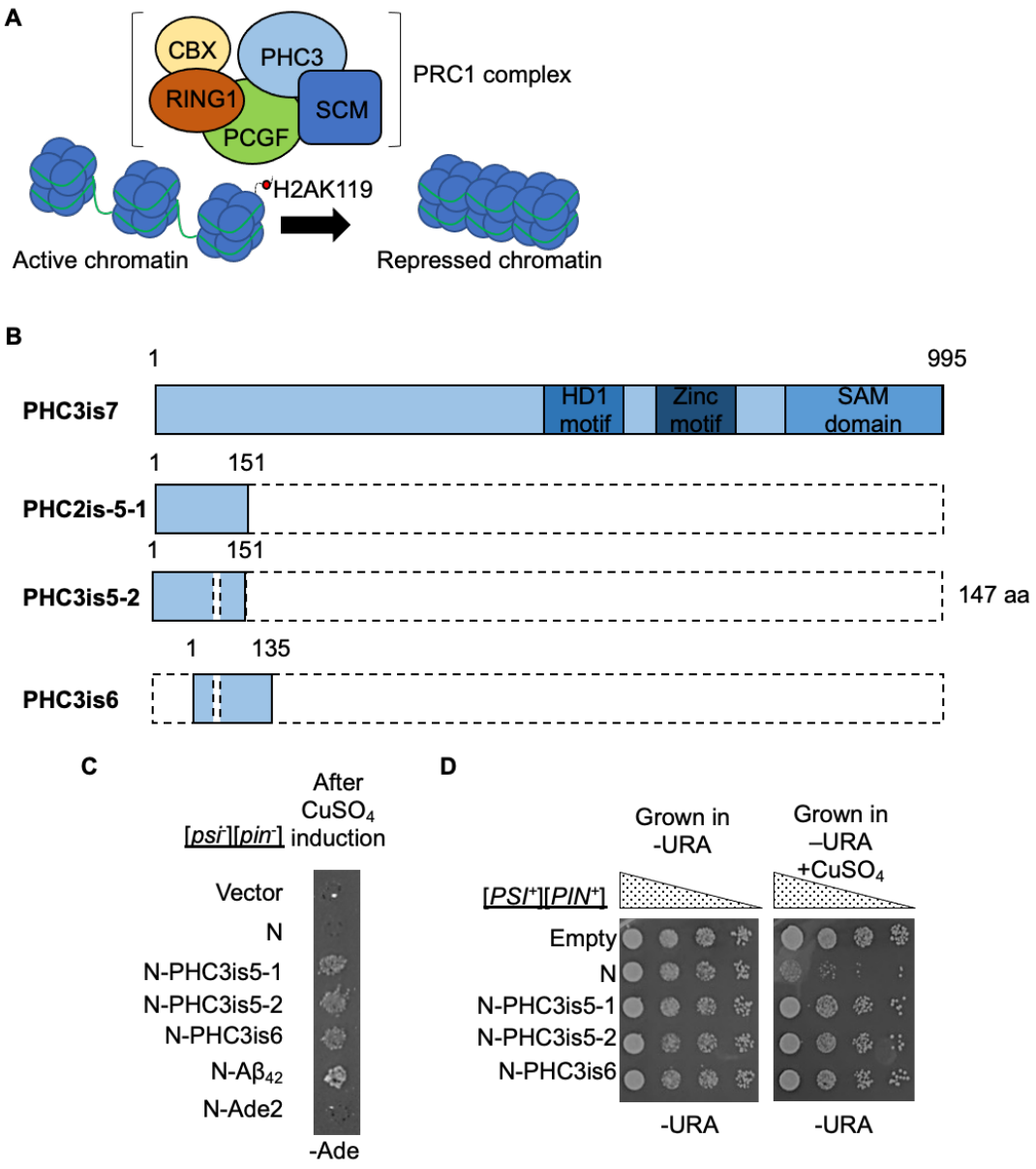

Figure 6.5 Functions and amyloidogenic isoforms of PHC3. (A) Cartoon highlight the normal functions of PHC3 as a member of the PRC1 complex. (B) Schematic diagram of the protein domains of Polyhomeotic-like protein 3 (PHC3) and highlights certain features as it is related to specific amyloid diseases. The misalignment of the protein isoforms is to show the overlapping of amino acids. (C) Copper induced overproduction of the chimeric proteins containing Sup35N fused to isoforms of PHC3 and $A\beta_{42}$ promote the *de novo* formation of [*PSI*$^+$] in a [*psi*$^-$][*pin*$^-$] strain. (D) Serial dilutions of cultures showing the toxicity of the chimeric constructs fused to Sup35N as expressed in a [*PSI*$^+$][*PIN*$^+$] strain. None of the isoforms show toxicity as compared to Sup35N control.

is a transcriptional activator required for calcium dependent dendritic growth in cortical neurons. There have been some recent publications indicating that specific domains of CREST have amyloidogenic properties and has been associated with ALS. PHC3 plays a key role in the polycomb-repressive complex. The PRC1 complex is responsible for maintaining a transcriptionally inactive state. It does this through chromatin remodeling via the modification of histones. Specifically, this complex monoubiquitinates the histone tail (Lys119) of the histone H2A (Figure 6.5A). While there are multiple isoforms of this protein that arise due to alternative splicing, previous computational work has shown that several short isoforms of the protein contain sequences that have the potential to produce amyloids (Figure 6.5B).

In our assay, we used rat CREST, which has 88% similarity to the human version. To study its properties, we fused the full-length version of CREST, as well as just a portion of the C-terminal domain which is proposed to be the PrD of CREST (referred to as CREST(C)) as shown in Figure 6.4B. We also introduced a mutation into the C-terminal construct (Q393Stop), which corresponds to the Q338Stop mutation in humans that has been associated with ALS. This construct is referred to as N-CREST(Cmut). The overexpression of N-CREST(C) in a [*psi*$^-$][*pin*$^-$] strain is able to induce [*PSI*$^+$] *de novo (*Figure 6.6A) as seen by growth on -Ade medium and biochemically by SDD-AGE (Figure 6.6C and D). This new data indicates for the first time (to our knowledge) that the C-terminal portion of rat CREST has amyloidogenic properties. The chimeric construct containing CREST

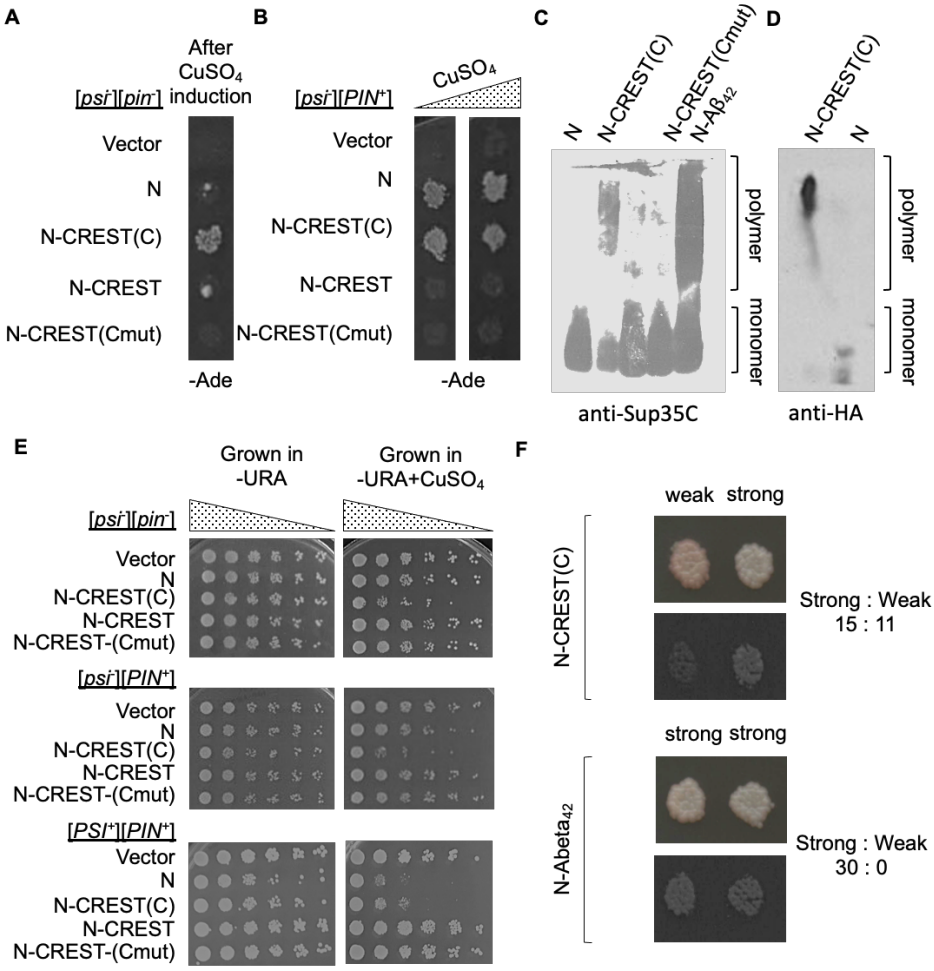

Figure 6.6 Phenotypic and biochemical characterization of aggregates formed by Sup35N fused to CREST. (A) Copper induced overproduction of the chimeric proteins containing Sup35N fused to Rat CREST(C) and Aβ$_{42}$ continue to promote the *de novo* formation of [*PSI*$^+$] in a [*psi*$^-$][*pin*-] strain. (B) Overproduction of the chimeric protein containing Sup35N fused to Rat CREST(C) induce [*PSI*$^+$] as expected in a [*PIN*$^+$] strain, however the chimeric proteins containing full-length CREST and the nonsense mutation mimic do not indicating an anti-amyloid effect. (C) Formation of [*PSI*$^+$] by the endogenous Sup35 following overexpression of the CREST(C) and Aβ$_{42,}$ as detected by semi-denaturing detergent agarose gel electrophoresis, followed by Western blotting and reaction to anti-Sup35C antibody. Cell lysates were treated with SDS and run on the agarose gel. (D) Overexpression of the chimeric constructs of Sup35N-CREST(C) in a [*psi*$^-$][*pin*$^-$] strain. Protein extracts were ran on a agarose gel and detected using the anti-HA antibody. (D) Serial dilutions of cultures showing the toxicity of the chimeric constructs as expressed in a [*psi*$^-$][*pin*$^-$] strain (top panel), [*psi*$^-$][*PIN*$^+$] (middle), and a [*PSI*$^+$][*PIN*$^+$] strain (bottom). CREST(C) fusions are slightly toxic in both the [*psi*$^-$][*pin*$^-$] and [*psi*$^-$][*PIN*$^+$] strain, however the CREST and CREST nonsense mimic are not toxic. (E) Spectra of [*PSI*$^+$] strains formed by N-CREST(C) chimeric constructs. [*PSI*$^+$] strains were distinguished by color on YPD and amount of growth on –Ade. Strong [*PSI*$^+$] white or white-pink on YPD, and weak [*PSI*$^+$] appeared red-pink on YPD and grew after longer incubation on –Ade. Previously published strain expressing Sup35N-Aβ$_{42}$ were used as comparison for classification of strains.

and CREST(Cmut) did not nucleate [*PSI*$^{+}$], however they also did not nucleate [*PSI*$^{+}$] in a [*psi*$^{-}$][*PIN*$^{+}$] strain either (Figure 6.6B). Fusion of the short isoforms of PHC3, isoform 5 (both 5-1 and 5-2) and 6, that had been identified to have amyloidogenic properties computationally, to the PrD of Sup35 results in the nucleation of [*PSI*$^{+}$] *de novo* (Figure 6.5B), and is also capable of nucleating in a [*psi*$^{-}$][*PIN*$^{+}$] strain (Figure S6.1). This is for the first time, evidence that an epigenetic factor in humans has amyloidogenic properties.

Analysis of [PSI^{+}] strains induced by SUP35N-CREST(C)

It has been shown that a single protein has the ability to misfold into various amyloid structures, which are referred to as prion strains (or “variants” in yeast). This includes the yeast prion protein Sup35 [55, 71]. Strains of Sup35 can be easily differentiated from each other based on phenotypic manifestations and biochemical characteristics. For Sup35, strains are typically classified between classes of “stronger” and “weaker” variants. Stronger [*PSI*$^{+}$] variants are created by amyloid fibrils that are shorter cores, which can be more easily fragmented by the chaperone machinery. This leads to the production of more “seeds”, which in turn can proliferate the prion [*PSI*$^{+}$] state more efficiently. Strains that contain strong variants of [*PSI*$^{+}$], usually have phenotypes associated with stronger growth on -Ade media (caused by higher levels of nonsense suppression associated with the readthrough of the *ade1-14* reporter system) and high mitotic stability. Weaker variants are associated with lower mitotic stability, and the [*PSI*$^{+}$] state can be lost in colonies through multiple generations.

Since the C-terminal fusion of CREST was able to nucleate [*PSI*$^+$], we also wanted to determine if it could generate different prion variants (or “strains) as has been reported for other mammalian amyloidogenic proteins [110]. In order to determine this, [*PSI*$^+$] colonies were streaked out from the -Ade plate, and colonies were divided into “variant/strain” categories based on growth on -Ade medium and color on YPD. The colonies were scored after loss of the chimeric plasmid, in order to exclude that the variant of [*PSI*$^+$] was determined by its continuous presence. As shown in Figure 6.6F, Sup35N-CREST(C) is able to nucleate both strong and weak variants of [*PSI*$^+$], while the control of Sup35N-Aβ_{42} induced only strong variants as previously published [110].

Analysis of PHC3 isoforms using the C-DAG assay

To expand our understanding on the isoforms of PHC3 and its amyloidogenic properties, we also employed another assay developed by Anne Hochschild at Harvard University. Here, we show that the overexpression of both these isoforms are able to lead to biofilm production that is able to be stained by the Congo red supplemented in the medium that also contains IPTG and arabinose. This staining is seen as a red ring around the colony in which the protein is being expressed (Figure 6.7B). This was done in comparison to the published controls of Sup35NM (positive control) and Sup35M (negative control) [116].

Because these proteins are exported from the cell, this assay also makes it possible to study these proteins of interest using *in vitro* assays as well. Another one of these assays takes advantage of another characteristic of amyloids,

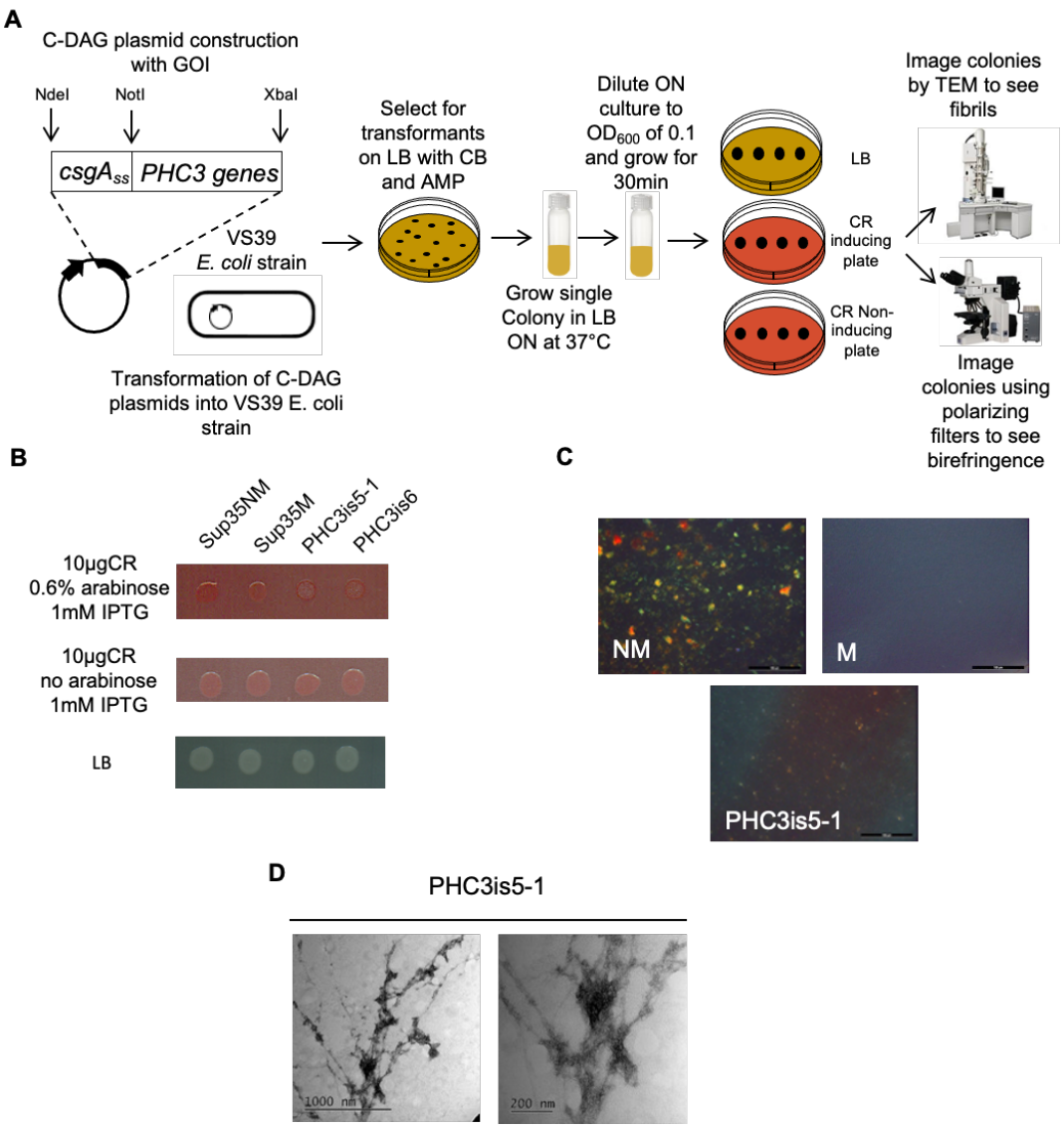

Figure 6.7 Aggregation of isoforms of PHC3 in the C-DAG assay. (A) Schematic of colony-color phenotype assay and birefringence. Highlights construction strategy of the plasmids used in the C-DAG system for the genes producing different isoforms of PHC3 and steps for the colony-color phenotype assay and birefringence assay. (B) Colony-color phenotype assay. Colonies that are expressing an amyloidogenic protein will form a red ring around the colony on the 10µgCR with 0.6% arabinose and 1mM IPTG plate. The 10µgCR, no arabinose, and 1mM IPTG and LB are growth control plates. Plasmids expressing the prion-domain of Sup35 (Sup35NM) is used as a positive control, and a non-prion forming domain (Sup35M) are used as a positive and negative control respectively. (C) Birefringence assay. Proteins that are able to form an amyloid will be able to bind to the congo red pigment in the media and will be cause a birefringence property to be observed for that protein under polarized light. (D) TEM showing the fibrils formed by PHC3is5-1.

birefringent properties when bound with congo red. Birefringence is an optical property of material caused by double refraction (a phenomenon in which a ray of light is split by polarization into taking different paths). Here, we show that PHC3is5-1 produce the goldish birefringence when visualized under polarized light (Figure 6.7C). This again is in comparison to the published controls of Sup35NM and Sup35M. As expected Sup35NM also had birefringence capabilities due to its ability to form an amyloid, while Sup35M did not. PHC3is6 also had birefringence properties, but data is not shown. We were also able to visualize the specific fibers formed by the proteins using transmission electron microscopy (Figure 6.7D). This analysis was completed by Konstantin Kulichinkin using the facilities at St. Petersburg University, Russia.

Protein domains that nucleate [PSI$^+$] only when fused to Sup35NM

It has also been reported that the tumor suppressor protein 53 (p53) also has amyloidogenic properties [113]. p53 is known for its role as a regulator of the cell cycle through its ability to activate DNA repair mechanisms. Because of this, it has been deemed the “guardian of the genome” for its ability to prevent genome mutations (Figure 6.8A). Cancer, as its own group of associated disease, is known to cause serious illness and death, but is not classically associated with amyloidogenic proteins. However, there is increasing evidence indicating a link between cancer and amyloidogenic proteins. An example of this can be seen with PrP, the human prion protein, associated with human spongiform encephalotomy (human mad cow disease) [118]. Furthermore, 50% of cancers are associated with a loss of function in p53, giving further credence to the suggestion of the role of

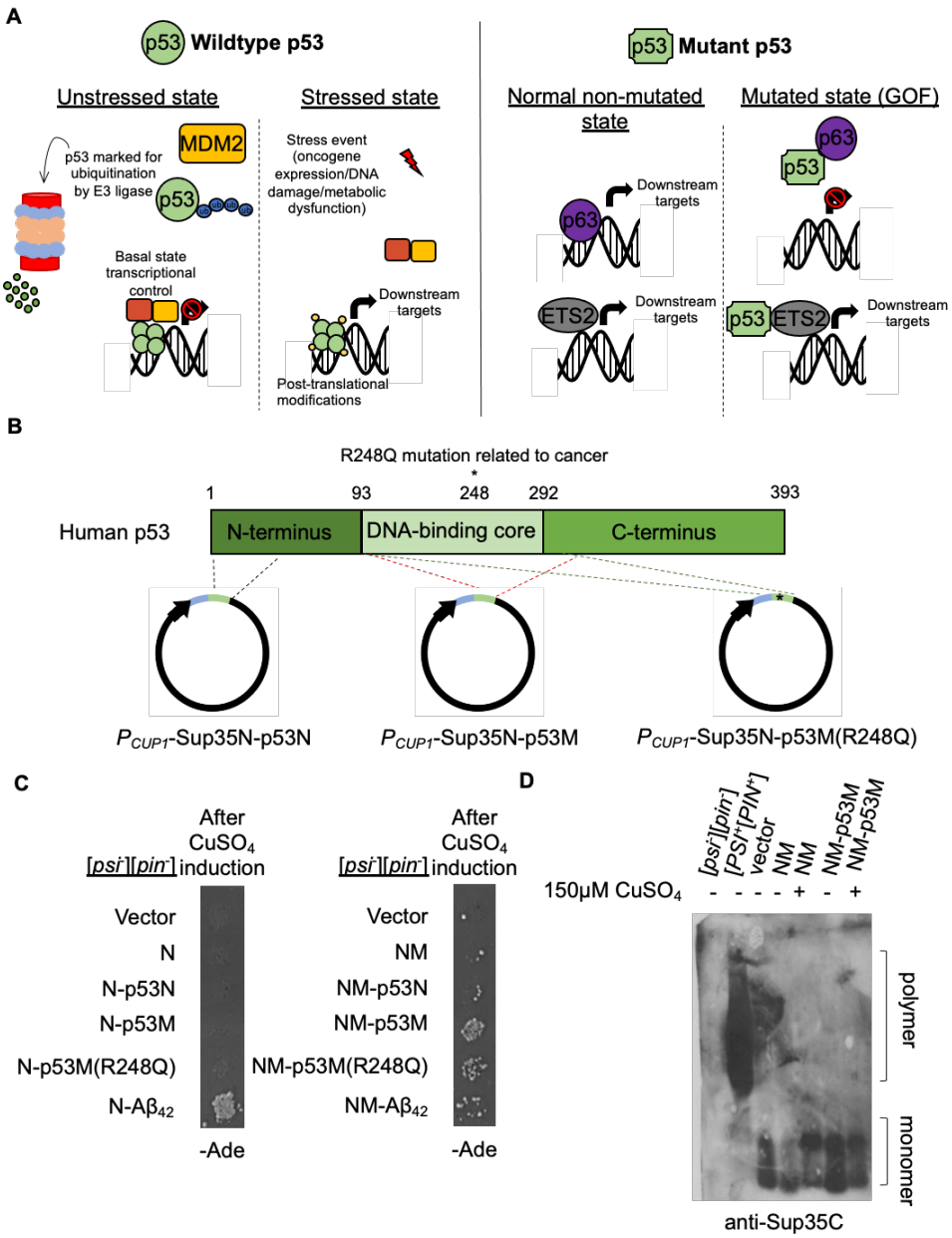

Figure 6.8 Prion nucleation by p53 in yeast. (A) Cartoon diagram highlighting the normal functions of p53 as a transcription factor. (B) Schematic diagram of the protein domains of p53 and highlights certain features as it is related to specific amyloid properties. (C) Copper induced overproduction of the chimeric proteins containing Sup35NM fused to p53M and the chimeric construct containing the R248Q mutant promotes the *de novo* formation of [*PSI*$^+$] in a [*psi*$^-$][*pin*$^-$] strain, however the Sup35N fusion does not. (D) No formation of [*PSI*$^+$] by the endogenous Sup35 following overexpression of the NM-p53M, as detected by semi-denaturing detergent agarose gel electrophoresis, followed by Western blotting and reaction to anti-Sup35C antibody. Cell lysates were treated with SDS and run on the agarose gel. The second SDD-AGE gel is probed with the anti-HA antibody detecting the chimeric construct of NM-p53M.

amyloids in tumor formation. For our study we chose to study specific domains that had been implicated to have amyloidogenic properties that had been reported in mammalian cell models. This included the N-terminal portion of the protein which included the 1-93 amino acids (referred to as p53N) and the region of the 94-312 amino acids, which includes the DNA-binding domain (referred to as p53M). There are also several mutations known to occur in reference to p53 and its ability to adopt and amyloid fold[119]. One of these mutations, R248Q, was studied in our yeast model and referred to as p53M(R248Q) as shown in Figure 6.8B.

Upon over-expression of the p53 domains fused to Sup35N, there is no induction of [*PSI*$^{+}$] as seen by no growth on -Ade medium. However, upon overexpression when fused to the Sup35NM domain, the Sup35NM-p53M and Sup35NM-p53M(R248Q) are able to cause nonsense suppression leading to papillation of -Ade medium (Figure 6.8C*)*. This is interesting as other mammalian amyloidogenic proteins show decreased ability to induce [*PSI*$^{+}$] when fused to Sup35N as compared to Sup35NM. The M domain of Sup35 contains a large number of charged amino acids and is thought in helping to keep Sup35 in a soluble state. Also, interestingly, upon biochemical characterization of the endogenous Sup35 after overexpression of Sup35NM-p53M the endogenous Sup35 remains monomeric as seen on the SDD-AGE gel in Figure 6.8D and Figure S6.2. This indicates that the growth on -Ade medium shown in Figure 6.8C is not caused by the formation of [*PSI*$^{+}$] by the endogenous Sup35.

Protein or protein domains that nucleate [PSI$^+$] only in a [PIN$^+$] background

Also associated with the Brg1 complex, the transcription factor CREB-binding protein (CBP), has also been implicated to have amyloidogenic properties [15]. It should also be noted that CBP also has functions outside of this complex, but all are involved in transcriptional coactivation and acetyltransferase activity. For this protein, we studied the mouse version and chose the domain of amino acids of 2193-2360 which contains the PolyQ portion of the protein (Figure 6.9A), which has been implicated as its prion forming domain. The polyQ portion is of significance as many PrD's have been known to be glutamine/asparagine rich in numerous eukaryotes [120].

We also examined the amyloidogenic properties of microtubule associated protein Tau (MAPT). As previously discussed in Chapter 4, it is thought that the amyloidogenic properties of Tau are associated with the microtube binding domain (TauRD). For this assay we fused TauRD containing the amino acids 244-372 (also known to be the region containing 4 repeat domains) to the PrD of Sup35 (Figure 6.10A).

Here we show that fusion of either CBP (Figure 6.9B) or TauRD (Figure 6.10B) to the PrD of Sup35 is unable to nucleate [*PSI*$^+$] *de novo* as determined phenotypically. For TauRD this matches the data presented in Chapter 4, in which overexpression of TauRD fused to YFP is seen as diffuse fluorescence (Figure 4.3 and 4.4). However, overexpression of the same constructs in a [*psi*$^-$][*PIN*$^+$] strain is able to nucleate [*PSI*$^+$] indicating that the chimeric construct containing Sup35N

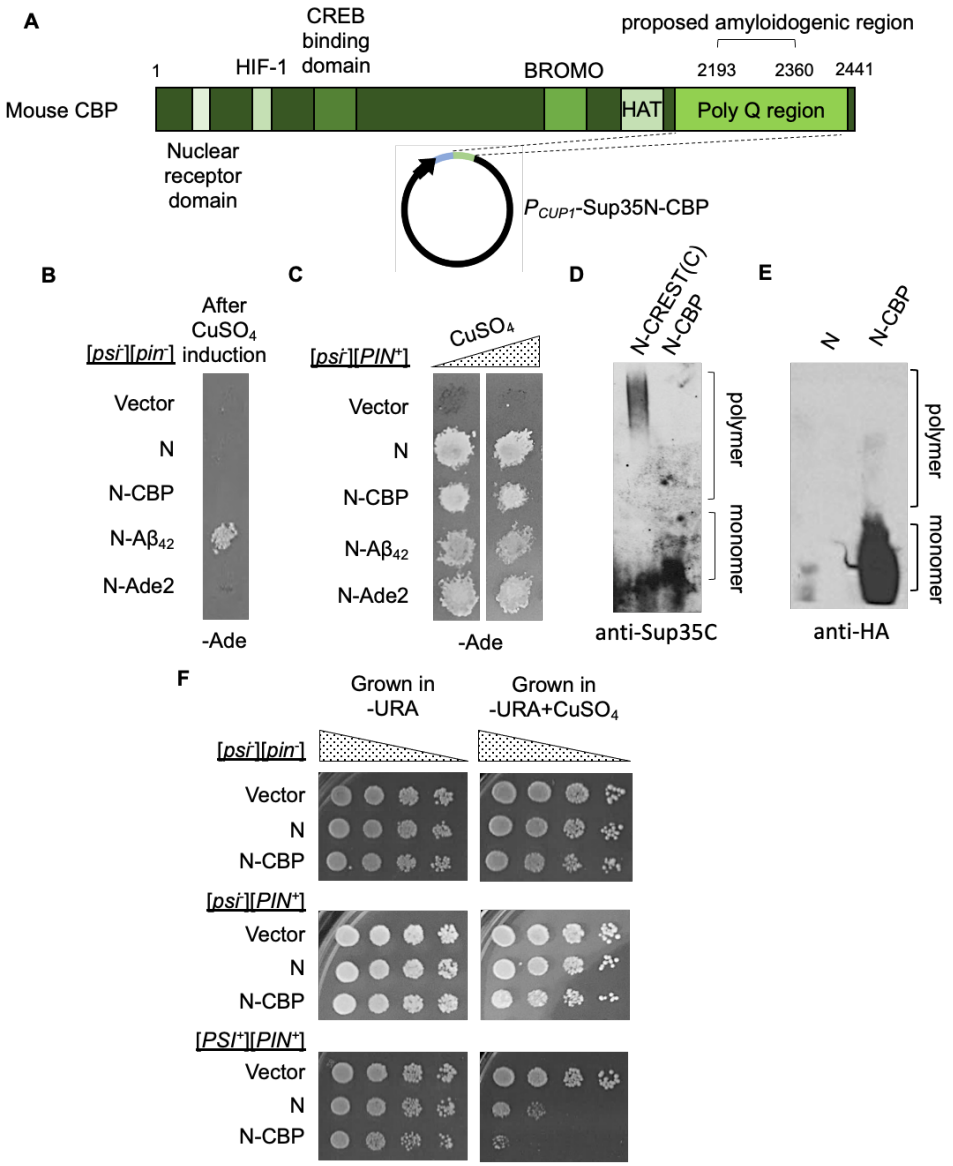

Figure 6.9 Phenotypic and biochemical characterization of Sup35N fused to CBP. (A) Schematic of nucleation assay of [*PSI*$^+$] by chimeric protein containing CBP. Schematic diagram of the protein domains of mouse CBP. The polyQ rich region perceived to be amyloidogenic used in the experiment is highlighted. (B) Copper induced overproduction of the chimeric protein containing Sup35N fused to mouse CBP does not induce [*PSI*$^+$] in comparison to the Aβ$_{42}$ control. CBP shows a similar result to that of CREST(C) and Aβ$_{42}$ and promotes the *de novo* formation of [*PSI*$^+$] in a [*psi*$^-$][*PIN*$^+$] strain as expected, and matches SDD-AGE data in which the endogeonus Sup35 remains monomeric. (D) as detected by the Sup35C antibody, and the chimeric fusion runs as a monomer (E) as detected by the HA antibody. (F) However, overexpression of the chimeric constructs is toxic in the presence of [*PSI*$^+$] as seen by serial dilution after overexpression (bottom panel).

(also containing both CBP and TauRD) is still able to be nucleated by other PrD's (e.g [*PIN*$^+$]) and nucleate the endogenous Sup35 into [*PSI*$^+$] (Figure 6.9C and Figure 6.10C). Lack of nucleation by CBP was also confirmed biochemically using SDD-AGE. The chimeric protein containing CBP is unable to form a detergent resistant aggregate as indicated by the monomeric band on the SDD-AGE gel (Figure 6.9D and E).

Protein or protein domains that do not nucleate [PSI$^+$]

Next, we looked at the amyloidogenic properties of specific domains of the U1 ribonucleoprotein 70k (U1-70k) that was also previously examined by fluorescence microscopy in Chapter 5. Here we fused the following domains of U1-70k to the PrD of Sup35: the N-domain (amino acids 1-99), the NM-domain (amino acids 1-181), the C-domain (amino acids 182-437), and the full-length protein (referred to as U1-70k). We also examined the yeast homolog of U1-70k, SNP1, however it was not expected to produce an amyloid as it only has 30% similarity to U1-70k, and there is no evidence to suggest a PrD as seen in other proteins (e.g QN rich domains) (Figure 6.11A) [121]. After over-expression of all of the domains of U1-70k, as well as SNP1, and then replica plating onto -Ade medium, none of the colonies tested showed [*PSI*$^+$] induction (Figure 6.11B). This is especially interesting, since the U1-70kNM and U1-70kC domains were able to form their own aggregates in yeast when over-expressed, as shown in Figure 5.2. We confirmed this biochemically using the technique of semi-denaturing detergent gel electrophoresis in which the endogenous Sup35 runs as a monomer on the gel after over-expression of U1-70k (Figure 6.11C). Interestingly however, when

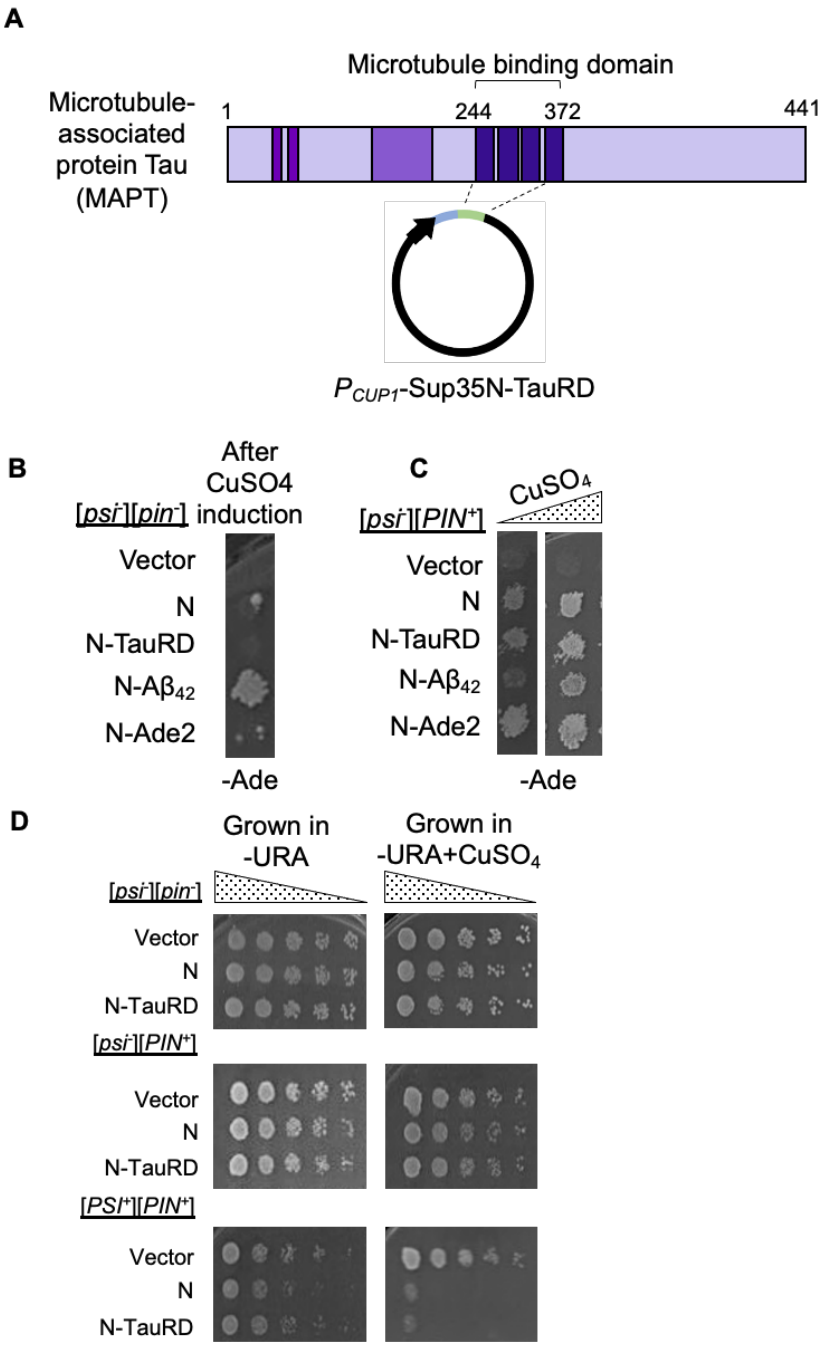

Figure 6.10 Effects of Tau on yeast prions. (A) Schematic diagram of the protein domains of MAPT and highlights certain features as it is related to specific amyloid properties. (B). Copper induced overproduction of the chimeric proteins fused to Sup35N containing the repeat domain of MAPT does not promote the *de novo* formation of [*PSI*$^+$] in a [*psi*$^-$][*pin*$^-$] strain. (C) Copper induced overproduction of the chimeric proteins containing Sup35N(NM) fused to TauRD to promote the de novo formation of [*PSI*$^+$] in a [*psi*$^-$][*PIN*$^+$]. (D) Toxicity of TauRD after overproduction in the presence of [*PSI*$^+$].

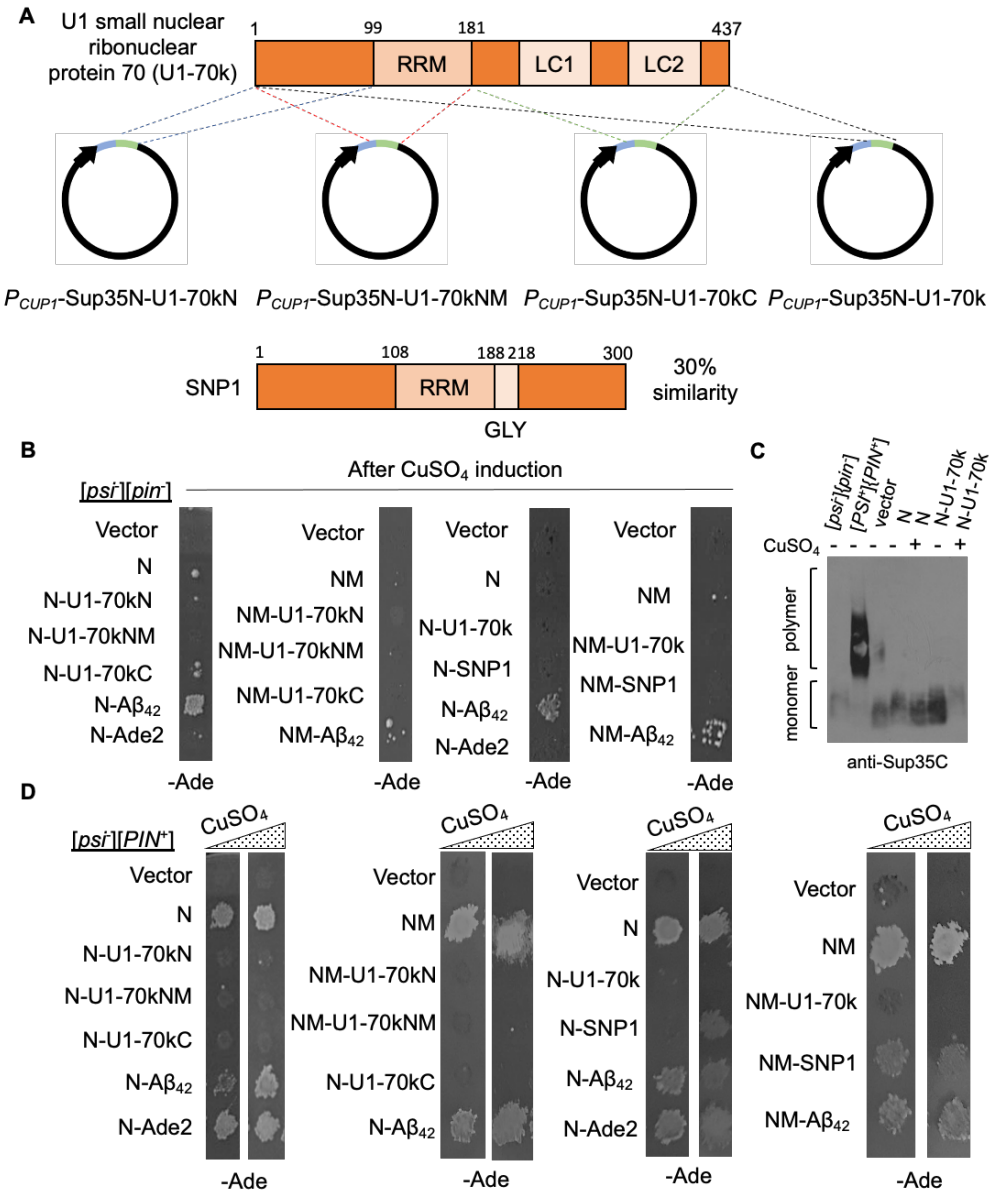

Figure 6.11 Effects of U1-70k on yeast prions. (A) Schematic diagram of the protein domains of U1-70k and highlights certain features as it is related to specific amyloid properties. (B). Copper induced overproduction of the chimeric proteins fused to Sup35N(NM) containing domains of U1-70k do not promote the *de novo* formation of [*PSI*$^+$] in a [*psi*$^-$][*pin*$^-$] strain. (C) Biochemical characterization and toxicity of chimeric fusion containing domains of U1-70k. No formation of [*PSI*$^+$] by the endogenous Sup35 following overexpression of the NM-U1-70k, as detected by semi-denaturing detergent agarose gel electrophoresis, followed by Western blotting and reaction to anti-Sup35C antibody. Cell lysates were treated with SDS and run on the agarose gel. (D) Copper induced overproduction of the chimeric proteins containing Sup35N(NM) fused to domains of U1-70k do not promote the formation of [*PSI*$^+$] in a [*psi*$^-$][*PIN*$^+$].

overexpressing these same chimeric constructs in a [*psi*$^-$][*PIN*$^+$] strain, none of the chimeric constructs containing domains of U1-70k were able to nucleate [*PSI*$^+$] indicating some sort of anti-amyloid effect as seen as Figure 6.11D. However, it should be noted that SNP1 was able to nucleate [*PSI*$^+$] in this strain indicating that there is something different going on between those chimeric constructs expected to have amyloidogenic properties as compared to those that do not.

Toxic effects upon overexpression in the presence of [PSI$^+$]

One possible explanation for the inability of some protein domains to not induce the formation of [*PSI*$^+$] is due to toxicity upon overexpression. It was previously known that the overexpression of Sup35N in a [*PSI*$^+$] strain is toxic [51]. To test for toxicity in the presence of [*PSI*$^+$] the chimeric plasmids were transformed into the [*PSI*$^+$] strain GT81-1C. Single colonies were inoculated into 10 mL of -Ura medium and grown overnight at 30°C. Cultures were then diluted into new tubes to an OD_{600} of 0.1 containing only -Ura medium or -Ura medium supplemented with an additional 150 μM $CuSO_4$. Cultures were again incubated for 18 hours, followed by serial dilutions and plating onto -Ura plates. Plates were examined following 2-3 days of growth for toxicity.

The overexpression of the Sup35N-TauRD (Figure 6.10D) and Sup35N-CBP (Figure 6.9F) leads to high toxicity in the presence of [*PSI*$^+$], as compared to the Sup35N control. Both of these protein domains were unable to nucleate [*PSI*$^+$] in a [*psi*$^-$][*pin*$^-$] strain. The high toxic nature of these plasmids in the presence of [*PSI*$^+$] could be a possible explanation for the why these domains are unable to

Table 6.1 Summary of nucleation and toxicity data for each chimeric construct.

	Plasmids	Nucleation of [*PSI*$^+$] in a [*psi*$^-$][*pin*$^-$] strain	Nucleation of [*PSI*$^+$] in a [*psi*$^-$][*PIN*$^+$] strain	Toxicity			Aggregates in fluorescent assay in a [*psi*$^-$][*pin*$^-$] strain not fused to Sup35N
				[*psi*$^-$] [*pin*$^-$]	[*psi*$^-$] [*PIN*$^+$]	[*PSI*$^+$] [*PIN*$^+$]	
Controls	Vector	No	No	No	No	No	N/A
	Sup35N	No	Yes	No	No	Yes	Yes (non-prion aggregates)
	N-Aβ_{42}	Yes	Yes	No	No	No	Yes (Rubel *et.al.* 2013/This study)
	N-IAPP	Yes	Yes	No	No	No	Not checked
	N-Myo(WT)	Yes	Yes	No	No	No	Not checked
	N-PrP(90-230)	Yes	Yes	No	No	No	Yes (Rubel *et.al.* 2013)
Tau domain	N-TauRD	No	Yes	No	No	Yes	Yes (This Study)
U1-70k domains	N(M)-U1-70kN	No	No	No	No	No	No (This study)
	N(M)-U1-70kM	No	No	No	No	No	Yes (This Study)
	N(M)-U1-70kC	No	No	No	No	No	Yes (This Study)
	N(M)-U1-70k	No	No	No	No	No	Not checked
	N(M)-SNP1	No	Yes	No	No	No	Not checked
CREST domains	N-CREST(C)	Yes	Yes	No	No	Yes	Not checked
	N-CREST	No	No	No	No	No	Not checked
	N-CREST(Cmut)	No	No	No	No	No	Not checked
CBP domain	N-CBP	No	Yes	No	No	Yes	Not checked
p53 domains	N(M)-p53N	No	Yes	No	No	Yes	Not checked
	N-p53M	No	Yes	No	No	No	Not checked
	N-p53M(R248Q)	No	Yes	No	No	No	Not checked
	NM-p53M	Yes	Yes	No	No	No	Not checked
	NM-p53M(R248Q)	Yes	Yes	No	No	No	Not checked
PHC3 isoforms	N-PHC3is5-1	Yes	Yes	No	No	No	Not checked
	N-PHC3is5-2	Yes	Yes	No	No	No	Not checked
	N-PHC3is6	Yes	Yes	No	No	No	Not checked

nucleate in our system. However, toxicity may not completely abolish the capabilities of protein domains form being able to nucleate [*PSI*$^+$] in our system.

The CREST(C) chimeric construct is slightly toxic as compared to the Sup35N control, indicating that protein domains with at least slight toxicity are still able to nucleate [*PSI*$^{+}$] (Figure 6.6E). The chimeric constructs containing Sup35N-CREST and Sup35N-CREST(Cmut) showed no toxicity (Figure 6.6E) and were also unable to nucleate [*PSI*$^{+}$] *de novo* (Figure 6.8A).

We also examined the chimeric constructs expressing the domains of U1-70k for toxicity. Interestingly, these chimeric constructs showed no toxicity ruling out the possibility that the lack of nucleating potential is due to toxicity (Figure S6.3).

We also observed in Figure S6.4, that the control plasmid Sup35N-Aβ_{42} when overexpressed is not toxic in the presence of [*PSI*$^{+}$]. This matches other characteristics of other proteins, either here or in *Chandramolwishwaran et. al.* 2018 that proteins or amyloidogenic domains capable of inducing [*PSI*$^{+}$], are not toxic in yeast and can also induce [*PSI*$^{+}$] in a [*psi*$^{-}$][*PIN*$^{+}$] strain when fused to the PrD of Sup35. Table 6.1 summarizes both the toxicity and nucleation data seen for each chimeric construct tested.

[redacted]*Nucleation reduction by chemical 3C by Sup35N-Aβ42*

Initial prion nucleation is postulated to be an early step in the formation of amyloidogenic fibrils associated with numerous amyloid/prion diseases. In previous sections we have demonstrated that our nucleation assay can be used to identify proteins or protein domains that contain amyloidogenic sequences. Here we show that it can also be employed to investigate potential therapeutic

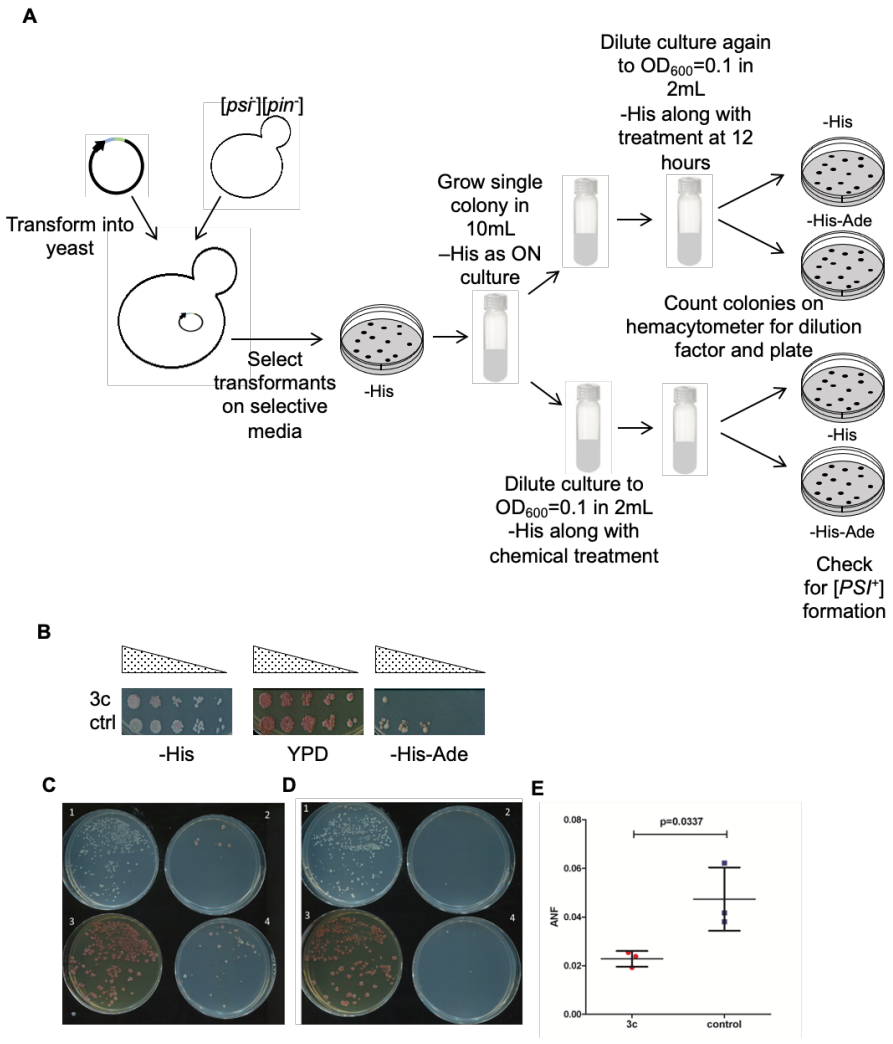

Figure 6.12 Semi-quantitative detection of the inhibition of amyloid nucleation by 3c in the yeast assay. (A) Scheme of curing assay for studying effects of chemicals on prion nucleation by Sup35N-Aβ$_{3-42}$ in yeast. [*psi*-][*pin*-] strain GT17 expressing the chimeric Sup35N-Aβ42 construct from the galactose-inducible P_{GAL} promoter were grown in the galactose medium in the presence of either compound 3c or solvent control for 36 hours. (B) Serial dilutions of 3c-treated (upper line) and solvent-treated control (lower line) cultures were spotted on the plasmid-selective medium (-His), compete organic medium (YPD) or plasmid-selective medium lacking adenine (-His-Ade), that allows for the detection of [*PSI*$^+$] colonies originated from cells in which nucleation of an amyloid has occurred. Equal dilutions of cultures treated with solvent (C) or 3c (D) were plated onto -His medium (1); -His/-Ade medium (2); and YPD medium (3); or velveteen replica-plated from -His medium to -His/-Ade medium. (E) Quantitative detection of the inhibition of amyloid nucleation by 3c in the yeast assay. Cells of the [*psi*$^-$][*pin*$^-$] strain GT17 expressing the chimeric Sup35N-Aβ42 construct from the galactose-inducible P_{GAL} promoter were grown in the galactose medium in the presence of either compound 3c or solvent control for 16 hours, followed by plating cells onto the -His and -His-Ade media (as shown on Figure 6.20B and C). Amyloid nucleation frequency (ANF) was determined as the ratio between the concentrations of His$^+$ Ade$^+$ and total His$^+$ cells as described in Experimental section. Means and standard deviations are shown for 3 biological replicates (p-value as per two-tailed t-test).

compounds and conditions specifically modulating the process of initial amyloid nucleation in both a general and a protein-specific manner. For this study we investigated the compound 3C, a newly synthesized compound whose structure combines both tacrine and indole moieties that have been shown to have effects in the treatment of AD [122]. To do this we used the chimeric plasmid containing the *SUP35N-Aβ_{42}* under the P_{GAL} promoter, that has already been shown to be able to nucleate [*PSI*$^{+}$] in the absence of any preexisting prions [110].

To do this we transformed the *PGAL*-SUP35N-Aβ_{42} construct into both the [*psi*$^{-}$][*pin*$^{-}$] strain GT17. Plasmid-containing cells were grown in galactose medium for protein expression, in either the presence or absence of 3c (140 μM), and plated onto glucose medium, where the *PGAL* promoter was repressed, lacking either only histidine (–His), for determining the concentration of plasmid containing cells, or both histidine and adenine (–His/–Ade), allowing for the detection of Ade+ colonies resulting from the nucleation of the amyloid form of Sup35 protein, [*PSI*$^{+}$] (Figure 6.12A).

The culture treated with 3c displayed reduced formation of His^{+} Ade^{+} colonies in comparison with the solvent control-treated culture (Figures 6.12B–E). This decrease indicated inhibition of Aβ-dependent amyloid nucleation. The result was confirmed two different periods of time, 36 h (Figure 6.12B-D) and 16 h (Figure 6.12E), respectively. Statistical significance of the differences shown in Figure 6.12B-D was confirmed by the t-test (two-tailed $p = 0.0337$). Thus, 3c is likely to inhibit an early triggering step in the Aβ cascade. Further experiments are needed to determine if 3c physically interferes with amyloid nucleation and whether or not

this effect is specific to Aβ. However, even if 3c possesses a general anti-nucleation effect applicable to various amyloids, it does not invalidate its potential anti-Alzheimer's properties.

6.4 Discussion

Our lab has previously demonstrated that the fusion of the Sup35 PrD to a mammalian protein or protein domain with proven amyloidogenic properties is sufficient for nucleating the formation of Sup35-based prions in yeast cells lacking known pre-existing prions [47, 110]. Here we are able to demonstrate that our experimental system can also be used to demonstrate *in vivo* (inside a living organism) protein misfolding of proteins or protein domains that have only been implicated in having amyloidogenic properties. This is demonstrated by our data showing that the overexpression of our chimeric fusions with both the rat CREST(C) domain (Figure 6.6C) and our data with the protein isoforms of PHC3 (Figure 6.5C) To our knowledge, no one has demonstrated that the CREST protein in rats had amyloidogenic properties, only that the human version is implicated in ALS. Interestingly, only the C-terminal portion of CREST in our assay was able to nucleate [*PSI*$^{+}$], not the full protein. One explanation for this is that the protein sequence in the proposed PrD of CREST is more similar in sequence between rat and humans and that the full-length protein is capable of overriding this feature. Only certain isoforms of PHC3 were predicted to have amyloidogenic properties. This was done using the computational ArchCandy 1.0 program, developed by Dr. Andry Kajava (Montpellier University, France) which can predict proteins sequence that are able to adopt β-arcade structures [123].

In our model certain chimeric constructs containing fusions to proteins that were predicted to have amyloidogenic properties were unable to induce [*PSI*$^+$]. This includes both TauRD (Figure 6.10B) and CBP (Figure 6.9B). In both cases the overexpression of these chimeric fusions was either more or had similar toxicity to the overexpression of the control of Sup35N alone. As previously discussed, the overexpression of Sup35 in a [*PSI*$^+$] strain inhibits growth. This is due to the sequestration of Sup45, the polypeptide release factor (eRF1). Sup35 in its non-prion form is able to associate with Sup45 via its C-terminal domain, and both work together to terminate translation of newly formed polypeptide chains [124].

One possible explanation for both TauRD and CBP's inability to nucleate [*PSI*$^+$] is that their expression is so toxic that the formation of [*PSI*$^+$] is lethal in these strains, which would result in their inability to be detected by growth on -Ade medium. However, in the case of the chimeric fusion Sup35N-CREST(C) which showed mild toxic behavior (Figure 6.6E) was still able to nucleate [*PSI*$^+$]. This could be due its ability to partly counteract sequestration of Sup45 into amyloids, because Sup45 interacts with the C region of Sup35, and these proteins, when included into the heterogenous structure, may shield Sup35 C-regions from interaction with Sup45.

With our model we have also previously demonstrated that the ability of these chimeric constructs to induce [*PSI*$^+$] is based on the fusion proteins amyloidogenicity [47, 110]. Multimerization alone was not sufficient to trigger the formation of [*PSI*$^+$]. This was specifically demonstrated by both the non-amyloidogenic multimeric proteins Ade2 and LacZ [110]. Interestingly, here we

show that the p53M domain was able to nucleate [*PSI*$^{+}$], but only when fused to the Sup35NM domain (Figure 6.8C) In most cases, we previously demonstrated (such as in the case of PrP) that the M-domain when present in these chimeric constructs takes on an anti-nucleation effect, which could be due to the presence of potentially repulsive charged residues. In the case of p53M, which is a protein domain capable of oligomerizing in its normal cellular function. Here the addition of the M-domain of Sup35 to the chimeric fusion could allow for enough distance in which to allow the domains of p53M to interact leading to the ability to grow on -Ade medium giving the false impression of [*PSI*$^{+}$] formation (Figure 6.13).

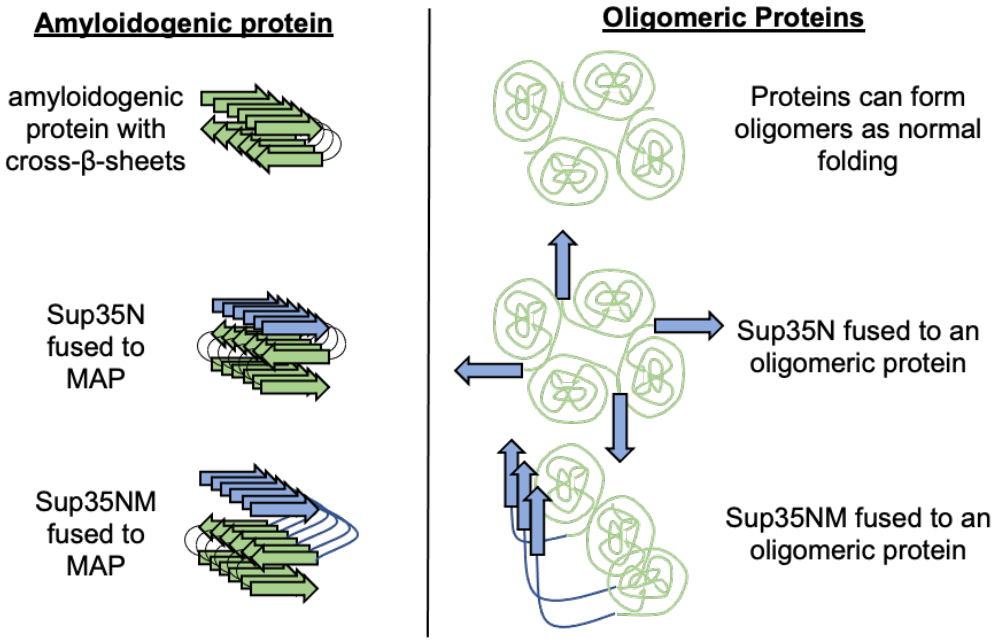

Figure 6.13 Model for [*PSI*$^{+}$] induction by oligomeric prone proteins.

We were also unable to detect [*PSI*$^{+}$] formation of by the protein domain U1-70kC using this assay. This is interesting as we previously demonstrated that the overexpression of this protein domain led to the formation of cytoplasmic aggregates that were detectable in yeast (Figure 5.2E) and that these aggregates were detergent resistant (Figure 5.4E). One possible explanation for this includes that fusion of protein sequences could lead to folding conformations in which the PrD's are not accessible or in conditions that are undesirable.

This data and those previously published (Chandramowlishwaran *et. al* 2018) demonstrated that our assay can be used to identify amino acid residues specifically important for polymer nucleation, a crucial step triggering the subsequent amyloid formation and pathogenicity of disease-related amyloidogenic proteins. The rapid and easy phenotypic detection of prion nucleation in yeast makes our assay amenable to high- throughput approaches. Moreover, this assay can be employed to search for chemical factors and conditions specifically modulating the process of initial amyloid nucleation.

6.5 Conclusions

- The QN-rich C-terminal domain of CREST and PHC3 isofoms5-1, 5-2, and 6 can nucleate [*PSI*$^{+}$]. CREST(C) produced detergent-resistant prion polymers as detected by SDD-AGE.
- Sup35N-CREST(C) can form nucleate different spectra of prion variants.

- Amyloidogenic potential of PHC3 isoforms 5 and 6 was confirmed in the C-DAG assay in *E. coli.*
- Proteins TauRD and PolyQ domain of CBP are unable to nucleate [*PSI*$^{+}$], however they have been shown to be toxic when overexpressed in the presence of [*PSI*$^{+}$].
- The RNA-binding domain of p53 (p53M) shows growth on -Ade medium when fused to Sup35NM. However, SDD-AGE analysis indicates that it remains monomeric indicating growth on -Ade is due not due to sequestration of endogenous Sup35.
- U1-70k domains are unable to nucleate [*PSI*$^{+}$], and also does not show toxicity in the presence of [*PSI*$^{+}$].
- Yeast nucleation assay based on Sup35N-Aβ_{42} can be used to detect anti-amyloidogenic activity of 3C, a newly synthesized drug compound.

OVERALL THESIS CONCLUSIONS

- Amyloids of human Aβ peptide, that is associated with Alzheimer's disease (AD) can generate self-propagating strains of the chimeric protein, in which the aggregation-prone region of yeast release factor Sup35 is substituted by $A\beta_{42}$ ($A\beta_{42}$-Sup35NR-MC).
- The spectrum of strains derived from AD patients is different from those from *in vitro* produced $A\beta_{42}$.
- $A\beta_{42}$-region is required for the maintenance of prion state by the chimeric Aβ-NR-MC protein. This confirms that our system provides an adequate experimental assay for the phenotypic detection of amyloid formation and propagation by Aβ.
- Human wild-type microtubule-associated protein Tau (MAPT) and its repeat domain (TauRD) with tauopathy-associated mutations (but not wild-type TauRD) are able to form aggregates, detectable by fluorescence microscopy upon high expression in yeast, and these aggregates are detergent resistant, a characteristic of amyloids. This establishes a yeast assay for amyloid formation by Tau.
- The C-terminal region of human RNA-binding protein U1-70k, containing low-complexity domains is able to form detergent resistant aggregates following high-expression in yeast cells. The same sequence elements control U1-70k aggregation in human and yeast cells.

- Yeast prion nucleation assay, based on chimeric prion domains, can be applied for the identification of new mammalian amyloidogenic proteins and detection of new anti-amyloidogenic compounds.

APPENDIX

A. LIST OF YEAST STRAINS USED AND CONSTRUCTED IN THIS WORK

Strain	Prion Background	Genotype
GT409	[*psi*$^-$][*pin*$^-$]	*MAT***a** *ade1-14 his3-Δ200 or 11,15 leu2-3,112 lys2 trp1-Δ ura3-52*
GT81-1C	[*PSI*$^+$][*PIN*$^+$]	*MAT***a** ade1-14 his3-Δ200 or 11,15 leu2-3,112 lys2 trp1-Δ ura3-52
GT159	[*psi*$^-$] [*PIN*$^+$]	*MAT***a** ade1-14 his3-Δ200 or 11,15 leu2-3,112 lys2 trp1-Δ ura3-52
GT17	[*psi*$^-$][*pin*$^-$]	*MAT***a** *ade1-14 his3-Δ200 leu2-3, 112 trp1-289 ura3-52*
GT2126 [*abe*$^-$]	[*psi*$^-$][*pin*$^-$] [*abe*$^-$]	*MATα ade1-14 his3Δ (or 11,15) lys2 leu2-3,112 trp1 sup35::HIS3* [*URA3* P_{SUP35}-$Aβ_{42}$-*SUP35NR-MC*]
GT2306 [*ABE*$^+$*-25*]	[*psi*$^-$][*pin*$^-$] [*ABE*$^+$]	*MATα ade1-14 his3Δ (or 11,15) lys2 leu2-3,112 trp1 sup35::HIS3* [*URA3* P_{SUP35}-$Aβ_{42}$-*SUP35NR-MC*]
GT2217 [*ABE*$^+$*-10*]	[*psi*$^-$][*pin*$^-$] [*ABE*$^+$]	*MATα ade1-14 his3Δ (or 11,15) lys2 leu2-3,112 trp1 sup35::HIS3* [*URA3* P_{SUP35}-$Aβ_{42}$-*SUP35NR-MC*]
GT2216 [*ABE*$^+$*-9*]	[*psi*$^-$][*pin*$^-$] [*ABE*$^+$]	*MATα ade1-14 his3Δ (or 11,15) lys2 leu2-3,112 trp1 sup35::HIS3* [*URA3* P_{SUP35}-$Aβ_{42}$-*SUP35NR-MC*]
GT680	[*psi*$^-$][*pin*$^-$]	*MATα ade1-14 his3Δ (or 11,15) lys2 ura3-52 leu2-3,112 trp1 sup35::HIS3* [*URA3 SUP35*]
GT2387* [*ABE*$^+$*-37*]	[*psi*$^-$][*pin*$^-$] [*ABE*$^+$]	*MATα ade1-14 his3Δ (or 11,15) lys2 leu2-3,112 trp1 sup35::HIS3* [*URA3* P_{SUP35}-$Aβ_{42}$-*SUP35NR-MC*]
GT2380* [*ABE*$^+$*-30*]	[*psi*$^-$][*pin*$^-$] [*ABE*$^+$]	*MATα ade1-14 his3Δ (or 11,15) lys2 leu2-3,112 trp1 sup35::HIS3* [*URA3* P_{SUP35}-$Aβ_{42}$-*SUP35NR-MC*]
GT2376* [*ABE*$^+$*-26*]	[*psi*$^-$][*pin*$^-$] [*ABE*$^+$]	*MATα ade1-14 his3Δ (or 11,15) lys2 leu2-3,112 trp1 sup35::HIS3* [*URA3* P_{SUP35}-$Aβ_{42}$-*SUP35NR-MC*]
GT2381* [*ABE*$^+$-31]	[*psi*$^-$][*pin*$^-$] [*ABE*$^+$]	*MATα ade1-14 his3Δ (or 11,15) lys2 leu2-3,112 trp1 sup35::HIS3* [*URA3* P_{SUP35}-$Aβ_{42}$-*SUP35NR-MC*]

GT2384* [*ABE*$^+$-34]	[*psi*$^-$][*pin*$^-$] [*ABE*$^+$]	*MATα ade1-14 his3Δ (or 11,15) lys2 leu2-3,112 trp1 sup35::HIS3* [*URA3* P_{SUP35}-$Aβ_{42}$-*SUP35NR-MC*]
GT2386* [*ABE*$^+$-36]	[*psi*$^-$][*pin*$^-$] [*ABE*$^+$]	*MATα ade1-14 his3Δ (or 11,15) lys2 leu2-3,112 trp1 sup35::HIS3* [*URA3* P_{SUP35}-$Aβ_{42}$-*SUP35NR-MC*]
GT2378* [*ABE*$^+$-28]	[*psi*$^-$][*pin*$^-$] [*ABE*$^+$]	*MATα ade1-14 his3Δ (or 11,15) lys2 leu2-3,112 trp1 sup35::HIS3* [*URA3* P_{SUP35}-$Aβ_{42}$-*SUP35NR-MC*]
GT2379* [*ABE*$^+$-29]	[*psi*$^-$][*pin*$^-$] [*ABE*$^+$]	*MATα ade1-14 his3Δ (or 11,15) lys2 leu2-3,112 trp1 sup35::HIS3* [*URA3* P_{SUP35}-$Aβ_{42}$-*SUP35NR-MC*]
GT2127 [*ABE*$^+$-1]	[*psi*$^-$][*pin*$^-$] [*ABE*$^+$]	*MATα ade1-14 his3Δ (or 11,15) lys2 leu2-3,112 trp1 sup35::HIS3* [*URA3* P_{SUP35}-$Aβ_{42}$-*SUP35NR-MC*]
GT2147 [*ABE*$^+$-2]	[*psi*$^-$][*pin*$^-$] [*ABE*$^+$]	*MATα ade1-14 his3Δ (or 11,15) lys2 leu2-3,112 trp1 sup35::HIS3* [*URA3* P_{SUP35}-$Aβ_{42}$-*SUP35NR-MC*]
GT2382* [*ABE*$^+$-32]	[*psi*$^-$][*pin*$^-$] [*ABE*$^+$]	*MATα ade1-14 his3Δ (or 11,15) lys2 leu2-3,112 trp1 sup35::HIS3* [*URA3* P_{SUP35}-$Aβ_{42}$-*SUP35NR-MC*]
GT2383* [*ABE*$^+$-33]	[*psi*$^-$][*pin*$^-$] [*ABE*$^+$]	*MATα ade1-14 his3Δ (or 11,15) lys2 leu2-3,112 trp1 sup35::HIS3* [*URA3* P_{SUP35}-$Aβ_{42}$-*SUP35NR-MC*]
GT2385* [*ABE*$^+$-35]	[*psi*$^-$][*pin*$^-$] [*ABE*$^+$]	*MATα ade1-14 his3Δ (or 11,15) lys2 leu2-3,112 trp1 sup35::HIS3* [*URA3* P_{SUP35}-$Aβ_{42}$-*SUP35NR-MC*]
GT671	[*psi*$^-$][*pin*$^-$]	*MATα ade1-14 his3Δ (or 11,15) lys2 ura3-52 leu2-3,112 trp1 sup35::HIS3* [*LEU2 SUP35*]
OT224 (BY4741)	[*psi*$^+$] [*PIN*$^+$]	*MAT***a** *his3-1 leu2-0 met15-0 ura3-0*
Deletion collection BY4741 *mds1Δ*	[*psi*$^+$] [*PIN*$^+$]	*MAT***a** *leu2-0 met15-0 ura3-0 mds1Δ:: kanMX4*
Deletion collection BY4741 *pho85Δ*	[*psi*$^+$] [*PIN*$^+$]	*MAT***a** *leu2-0 met15-0 ura3-0 pho85Δ:: kanMX4*
GT2365*	[*psi*$^+$] [*PIN*$^+$]	*MAT***a** *leu2-0 met15-0 ura3-0 mds1Δ:: kanMX4 pho85::HIS5*

* Denotes strains constructed in this work.

B. LIST OF SHUTTLE PLASMIDS USED AND CONSTRUCTED IN THIS WORK

Collection Number	Plasmid Name	Plasmid Type	Yeast Marker	Promoter	Expression cassette under promoter
1480	P_{SUP35}-Aβ42-Sup35NR-Sup35MC	CEN	*URA3*	P_{SUP35}	*Aβ42-SUP35NR-SUP35MC*
1524	P_{SUP35}-Aβ42-Sup35NR-Sup35MC	CEN	*LEU2*	P_{SUP35}	*Aβ42-SUP35NR-SUP35MC*
1723*	P_{CUP1}-Sup35NR-Sup35MC	CEN	*LEU2*	P_{CUP1}	*SUP35NR-SUP35MC*
1745*	P_{CUP1}- Aβ42-Sup35NR-Sup35MC	CEN	*LEU2*	P_{CUP1}	*Aβ42-SUP35NR-SUP35MC*
1738*	P_{CUP1}- Aβ42-Sup35NR-Sup35MC	CEN	*URA3*	P_{CUP1}	*Aβ42-SUP35NR-SUP35MC*
1585	P_{CUP1}-*YFP*	CEN	*LEU2*	P_{CUP1}	*YFP*
1586	P_{CUP1}-*CFP*	CEN	*URA3*	P_{CUP1}	*CFP*
1588	P_{GPD}-*YFP*	2μ	*URA3*	P_{GPD}	*YFP*
1603*	P_{CUP1}-*TauRD-YFP*	CEN	*LEU2*	P_{CUP1}	*TAURD-YFP*
1695*	P_{GPD}-*TauRDpro-YFP*	2μ	*URA3*	P_{GPD}	*TAURDPRO-YFP*
1685*	P_{GPD}-*TauRD-YFP*	2μ	*URA3*	P_{GPD}	*TAURD-YFP*

1696*	*P_{CUP1}-MAPT-YFP*	CEN	*LEU2*	*P_{CUP1}*	*MAPT-YFP*
1651	*P_{CUP1}-Sup35N-GFP*	CEN	*URA3*	*P_{CUP1}*	*SUP35N-GFP*
1680*	*P_{GPD}*- Aβ$_{42}$-CFP	*2μ*	*LEU2*	*P_{GPD}*	*Aβ$_{42}$-CFP*
1607	*P_{CUP1}*- Aβ$_{42}$-CFP	CEN	*URA3*	*P_{CUP1}*	*Aβ$_{42}$-CFP*
1599*	*P_{CUP1}*- U1-70kN-YFP	CEN	*LEU2*	*P_{CUP1}*	*U1-70KN-YFP*
1600*	*P_{CUP1}*- U1-70kNM-YFP	CEN	*LEU2*	*P_{CUP1}*	*U1-70KNM-YFP*
1664*	*P_{CUP1}*- U1-70kM-YFP	CEN	*LEU2*	*P_{CUP1}*	*U1-70KM-YFP*
1647*	*P_{CUP1}*- U1-70kC-YFP	CEN	*LEU2*	*P_{CUP1}*	*U1-70KC-YFP*
1602*	*P_{CUP1}*- U1-70kNM-CFP	CEN	*URA3*	*P_{CUP1}*	*U1-70KNM-CFP*
1717*	*P_{CUP1}*- U1-70kC-CFP	CEN	*URA3*	*P_{CUP1}*	*U1-70KC -CFP*
186	pYCH-U2	CEN	*URA3*	*P_{SUP35}*	*SUP35*
171	pRS415	CEN	*LEU2*	*P_{GAL}*	*EMPTY*
407	pMCUP1	CEN	*URA3*	*P_{CUP1}*	*EMPTY*
1258	*P_{CUP1}*-Sup35N-HA	CEN	*URA3*	*P_{CUP1}*	*SUP35N-HA*
1344*	*P_{CUP1}*-Sup35N-CREST(C)-HA	CEN	*URA3*	*P_{CUP1}*	*SUP35N-CREST(C)-HA*

1690*	P_{CUP1}-Sup35N-CREST-HA	CEN	*URA3*	P_{CUP1}	*SUP35N-CREST-HA*
1691*	P_{CUP1}-Sup35N-CREST(Q394Stop)-HA	CEN	*URA3*	P_{CUP1}	*SUP35N-CREST(Q394STOP)-HA*
1345*	P_{CUP1}-Sup35N-CBP-HA	CEN	*URA3*	P_{CUP1}	*SUP35N-CBP-HA*
1433	P_{CUP1}-nERI-Sup35N-Aβ(mE1-42)	CEN	*URA3*	P_{CUP1}	*SUP35N-Aβ(me1-42)*
1496	P_{CUP1}-Sup35N-Ade2	CEN	*URA3*	P_{CUP1}	*SUP35N-ADE2*
1134	P_{CUP1}-NM-HA	CEN	*URA3*	P_{CUP1}	*SUP35NM-HA*
1491	P_{CUP1}-Sup35N-PCH3is5-1	CEN	*URA3*	P_{CUP1}	*SUP35N-PCH3IS5-1*
1492	P_{CUP1}-Sup35N-PCH3is5-2	CEN	*URA3*	P_{CUP1}	*SUP35N-PCH3IS5-2*
1495	P_{CUP1}-Sup35N-PCH3is6	CEN	*URA3*	P_{CUP1}	*SUP35N-PCH3IS6*
1631*	P_{CsgA}-PHC3is5-1		N/A	P_{CsgA}	*CSGASS-PHC3is5-1*
1642*	P_{CsgA}-PHC3is6		N/A	P_{CsgA}	*CSGASS-PHC3is6*

1511	*pVS72*		N/A	P_{CsgA}	*CSGASS-SUP35NM*
1512	*pV105*		N/A	P_{CsgA}	*CSGASS-SUP35M*
1320	pc53-SN3		N/A	P_{p53}	*P53*
1335*	P_{CUP1}-Sup35NM-p53N-HA	CEN	*URA3*	P_{CUP1}	*SUP35NM-P53N-HA*
1336*	P_{CUP1}-Sup35NM-p53M-HA	CEN	*URA3*	P_{CUP1}	*SUP35NM-P53M-HA*
1339*	P_{CUP1}-Sup35N-p53N-HA	CEN	*URA3*	P_{CUP1}	*SUP35N-P53N-HA*
1340*	P_{CUP1}-Sup35N-p53M-HA	CEN	*URA3*	P_{CUP1}	*SUP35N-P53M-HA*
1479*	P_{CUP1}-Sup35N-p53M(R248Q)-HA	CEN	*URA3*	P_{CUP1}	*SUP35N-P53M(R248Q)-HA*
1484*	P_{CUP1}-Sup35NM-p53M(R248Q)	CEN	*URA3*	P_{CUP1}	*SUP35NM-P53M(R248Q)*
1322*	P_{CUP1}-nERI-Sup35NM-PrP	CEN	*URA3*	P_{CUP1}	*NERI-SUP35NM-PRP*
1324*	P_{CUP1}-nERI-Sup35N-Aβ3-42	CEN	*URA3*	P_{CUP1}	*NERI-SUP35N-AB3-42*
1321*	P_{CUP1}-nERI	CEN	*URA3*	P_{CUP1}	*EMPTY*

1145					*NM-PRP90-230*
1222	*P_{CUP1}*-Sup35N-$A\beta_{3-42}$	CEN	*URA3*	*P_{CUP1}*	*SUP35N-AB_{3-42}*
1387			N/A		*U1-70K*
1525*	*P_{CUP1}*-Sup35N-U1-70kN	CEN	URA3	*P_{CUP1}*	*SUP35N-U1-70KN*
1526*	*P_{CUP1}*-Sup35N-U1-70kNM	CEN	URA3	*P_{CUP1}*	*SUP35N-U1-70KNM*
1487*	*P_{CUP1}*-Sup35N-U1-70kC	CEN	URA3	*P_{CUP1}*	*SUP35N-U1-70KC*
1498*	*P_{CUP1}*-Sup35N-U1-70k	CEN	URA3	*P_{CUP1}*	*SUP35N-U1-70K*
1527*	*P_{CUP1}*-Sup35N-SNP1-HA	CEN	URA3	*P_{CUP1}*	*SUP35N-SNP1-HA*
1548*	*P_{CUP1}*-Sup35NM-U1-70kN	CEN	URA3	*P_{CUP1}*	*SUP35NM-U1-70KN*
1549*	*P_{CUP1}*-Sup35N-U1-70kNM	CEN	URA3	*P_{CUP1}*	*SUP35N-U1-70KNM*

1485*	P_{CUP1}-Sup35NM-U1-70kC	CEN	URA3	P_{CUP1}	*SUP35NM-U1-70KC*
1486*	P_{CUP1}-Sup35NM-U1-70k	CEN	URA3	P_{CUP1}	*SUP35NM-U1-70K*
1550*	P_{CUP1}-Sup35NM-SNP1-HA	CEN	URA3	P_{CUP1}	*SUP35NM-SNP1-HA*
1633*	P_{CUP1}-Sup35N-TauRD-HA	CEN	URA3	P_{CUP1}	*SUP35N-TAURD-HA*
1472	pcDNA-RD WT-HA		N/A		
1264	pLA1-Sup35N	CEN	*HIS3*	P_{GAL}	*SUP35N*
1268	pLA1-Sup35N-$A\beta_{3-42}$	CEN	*HIS3*	P_{GAL}	*SUP35N-$A\beta_{3-42}$*
1423	P_{CUP1}-Sup35N-IAPP	CEN	*URA3*	P_{CUP1}	*SUP35N-IAPP*
1328	P_{CUP1}-nER1-Sup35N-MyoWT	CEN	*URA3*	P_{CUP1}	*SUP35N-MYOWT*

* Denotes plasmid constructed in this work.

C. LIST OF PRIMERS USED IN THIS WORK

Collection Number	Name	Sequence 5'-3'	Direction
1080	CREST 0.4For	CAGAATTCATGAGTCAACAGTACTAC	Forward
1081	CREST 0.4 Rev HA	CCTCTAGATTTAGCGTAATCTGGTACGTCGTATGGGTATTGCTGGTAATTTCCA	Reverse
1322	CREST(Full) EcoRI For	CAGAATTCATGTCCGTGGCCTTCGCGTCG	Forward
1323	CREST(Full) XbaI HA Rev	CCTCTAGATTAAGCGTAATCTGGTACGTCGTATGGGTATTGCTGGTAATTTCCACATTG	Reverse
1324	CREST Q338Stop XbaI Rev	CCTCTAGATTAAGCGTAATCTGGTACGTCGTATGGGTACTCATAGCCGTAAGGCCGCTGCTG	Reverse
1078	CBP 0.5For	AAGAATTCATGTTACGGAGGCAGCTG	Forward
1079	CBP 0.5Rev HA	CCTCTAGATTTAGCGTATCTGGTACGTCGTATGGGTAGGAATGTGGAGGCTGGGACTG	Reverse
1287	PHC3is5-1 NotI For	TATAGCGGCCGCAATGGCGGAA	Forward
1288	PHC3is5-1 Rev	TATATCTAGATTAGTGATGATGGTGATGGTAAAATTT	Reverse
1289	PHC3is6 Not For	TATAGCGGCCGCAATGGATACT	Forward
1088	p53M For	GGGAATTCTCATCTTCTGTCCCTTCCC	Forward
1089	p53M Rev	CCTCTAGATTAAGCGTAATCTGGTACGTCGTATGGGTAGGTGTTGTTGGGCAGTGC	Reverse

1090	p53N For	CCGAATTCATGGAGGAGCCGCAGTCAG	Forward
1091	p53N Rev	GCTCTAGATTAAGCGTAATCTGGTACGTCGTATGGGTAAGCTTCATCTGGACCTGGG	Reverse
1170	p53M mut. Foward	GCATGGGCGGCATGAACCAGAGGCCCATCCTCA CCATC	Forward
1171	p53M mut. Reverse	GATGGTGAGGATGGGCCTCTGGTTCATGCCGCC CATCG	Reverse
1138	U1-70KN For	CGCCGAATTCATGACCCAGTTCCTGCCGC	Forward
1165	U1-70KC For	GGGCGAATTCCGAACCGTCAAGGGCTGGA	Forward
1167	U1-70KC XbaI Rev	GTTCTAGATTACTCCGGCGCAGCCTCCAT	Reverse
1244	U1-70kN XbaI Rev	TCTCTAGATTACCCCTGAGCATTGGGATCATTGTG	Reverse
1245	U1-70kRRM XbaI Rev	CGTCTAGATTAGCCCCTCTCCACGTCCA	Reverse
1246	SNP1 EcoRI Forward	CGCCGAATTCATGAATTATAATCTATCCAAGTATCCAGACGACGTGTC	Forward
1259	SNP1-HA Not1 Reverse	AAGCGGCTTAAGCGTAATCTGGTACGTCGTATGGGTAATAGTAGTCGGGCGCTTC	Reverse
1131	ECORI Tau (244) For	GCGTGAATTCCAGACAGCCCCCGTGCCCATGCCA	Forward
1298	Tau RD SacI Rev	AGTCGAGCTCTCAAGCGTAATCTGGAACATCGTATGGGTATTCAACTTTTTTATT	Reverse
1136	Tau (244-372) BamHI For	GCGTGGATCCGTCGCCACCATGCAGACAGCC CCCGTG	Forward

1329	Tau FL XbaI Rev	GCTCTAGACAAACCCTGCTTGGCCAGGGAGGC	Reverse
1263	U1-70kN BamHI For	CGCCGGATCCATGACCCAGTTCCTGCC	Forward
1264	U1-70kN XbaI Rev	TCTCTAGACCCCTGAGCATTGGGATCATTGTG	Reverse
1265	U1-70k RRM XbaI Reverse	GCTCTAGAGCCCCTCTCCACGTCCA	Reverse
1266	U1-70kC BamHI For	CGGGATCCATGCGAACCGTGAAGGGCTGG	Forward
1267	U1-70k Full Rev	TCTCTAGACTCCGGCGCAGCCTCCATCAAATA	Reverse

D. SUPPLEMENTAL FIGURES AND TABLES

Table S3.1 Summary of weak subtypes generated after transfection from samples derived from AD brain extracts and *in vitro* seeded by brain extracts.

Origin of $A\beta_{42}$ sample	Brain region or patient ID	Strains of Ade^+ transfectants			Total Ade^+
		Subtype 1	Subtype 2	Subtype3	
In vitro seeded by AD brain extracts	Frontal Lobe	3	8	7	18
	Occipital Lobe	2	5	14	21
	Temporal Lobe	1	1	4	6
	Parietal Lobe	0	1	0	1
	Total	6	15	25	46
AD brain extracts	OSO-159	1	7	3	11
	OSO-163	2	4	4	10
	OSO-300	1	2	5	8
	E14-14	0	1	0	1
	Total	4	14	12	30

Table S4.1 Statistical comparison by t-test for the experiments shown on Figure 4.9.

Transformed plasmid	Compared Strains	*p value**
MAPT-YFP	WT and *mds1Δ*	0.020
	WT and *pho85Δ*	0.117
	WT and *mds1Δ pho85Δ*	0.036
$A\beta_{42}$-CFP	WT and *mds1Δ*	0.014
	WT and *pho85Δ*	0.926
	WT and *mds1Δ pho85Δ*	0.006

Table S4.2 Comparison of normalized MAPT level in deletion strains vs. wild-type.

strain	Mean ratio of protein level in the deletion versus wild-type stain after high expression of MAPT-YFP (with standardized error)
mds1Δ	5.2 ± 0.9
pho85Δ	0 ± 0.2
mds1Δ pho85Δ	6.5 ± 2.8

MAPT protein was detected by GFP antibody. Band intensities were measured to densitometry and normalized by loading control (Coomassie or Ponceau S). Ratios between the normalized protein levels in the deletion strain and control wild-type were always determined for the pairs run on the one and the same gel. Mean ratios and errors were calculated based on results from 3 independent cultures.

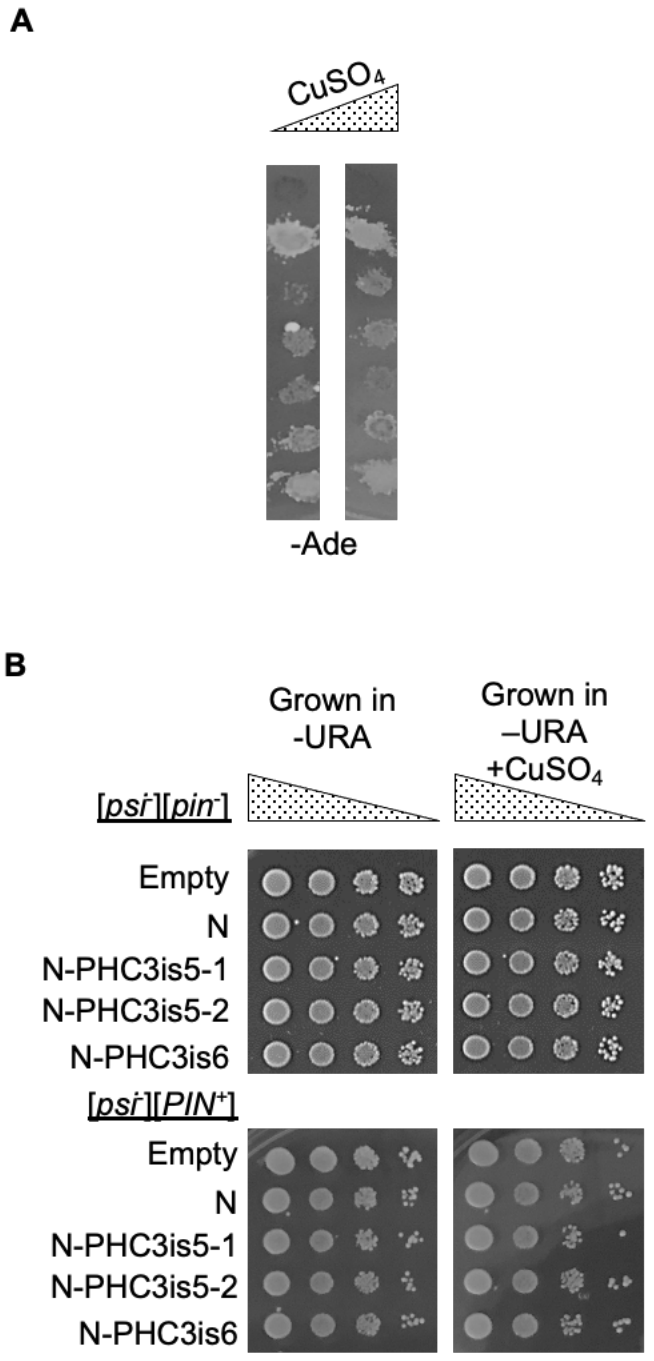

Figure S6.1 Phenotypic detection of nucleation by isoforms of PHC3 in a [*psi*$^-$][*PIN*$^+$] strain and toxicity data. (A) Copper induced overproduction of the chimeric proteins containing Sup35N fused to the isofoms of PHC3 and $A\beta_{42}$ continue to promote the de novo formation of [*PSI*$^+$] in a [*psi*$^-$][*PIN*$^+$] strain. (B) Serial dilutions of cultures showing the toxicity of the chimeric constructs fused to Sup35N as expressed in a [*psi*$^-$][*pin*$^-$] strain (top panel) and [*psi*$^-$][*PIN*$^+$] (bottom).

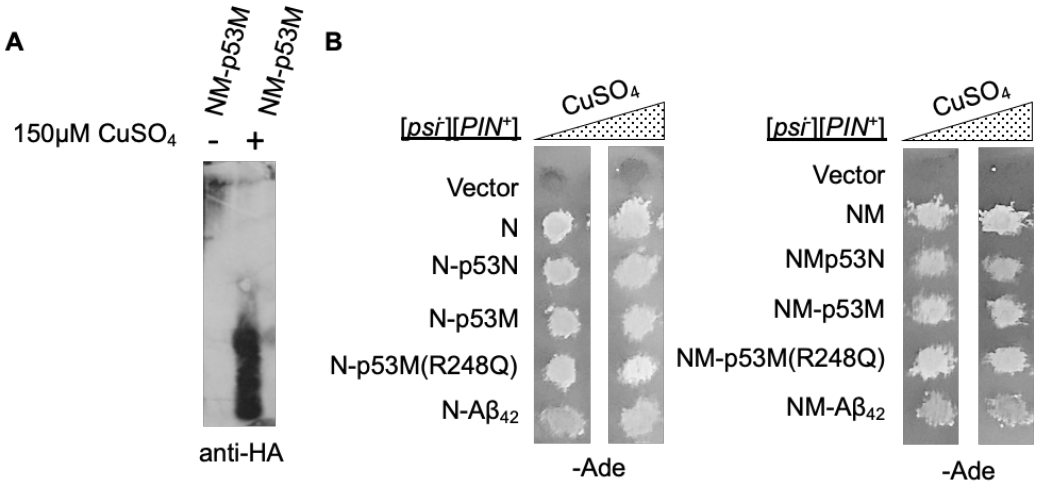

Figure S6.2 Biochemical characterization and nucleation by p53 in a [*psi*-][*PIN*$^+$] strain. (A) SDD-AGE gel is probed with the anti-HA antibody detecting the chimeric construct of NM-p53M. (B) Overexpression of all of the domains of p53 fused to either Sup35N and Sup35NM are able to induce [*PSI*$^+$] when overexpressed in a [*PIN*$^+$] strain.

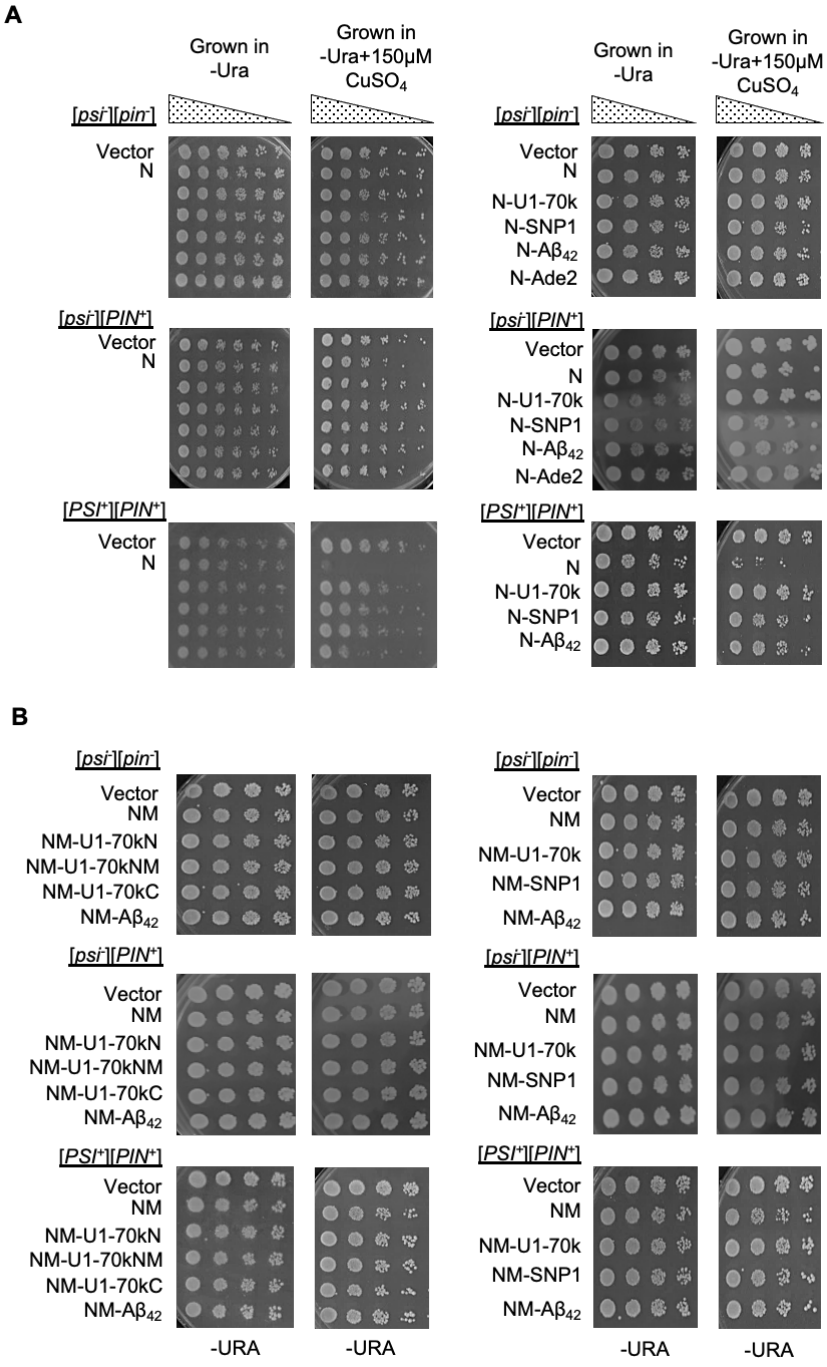

Figure S6.3 Toxicity of chimeric fusion containing domains of U1-70k. (A) Serial dilutions of cultures showing the toxicity of the chimeric constructs as expressed in a [*psi*$^-$][*pin*$^-$] strain (top panel), [*psi*$^-$][*PIN*$^+$] (middle), and a [*PSI*$^+$][*PIN*$^+$] strain (bottom) of Sup35N fusion constructs. (B) Toxicity by Sup35NM fusion constructs.

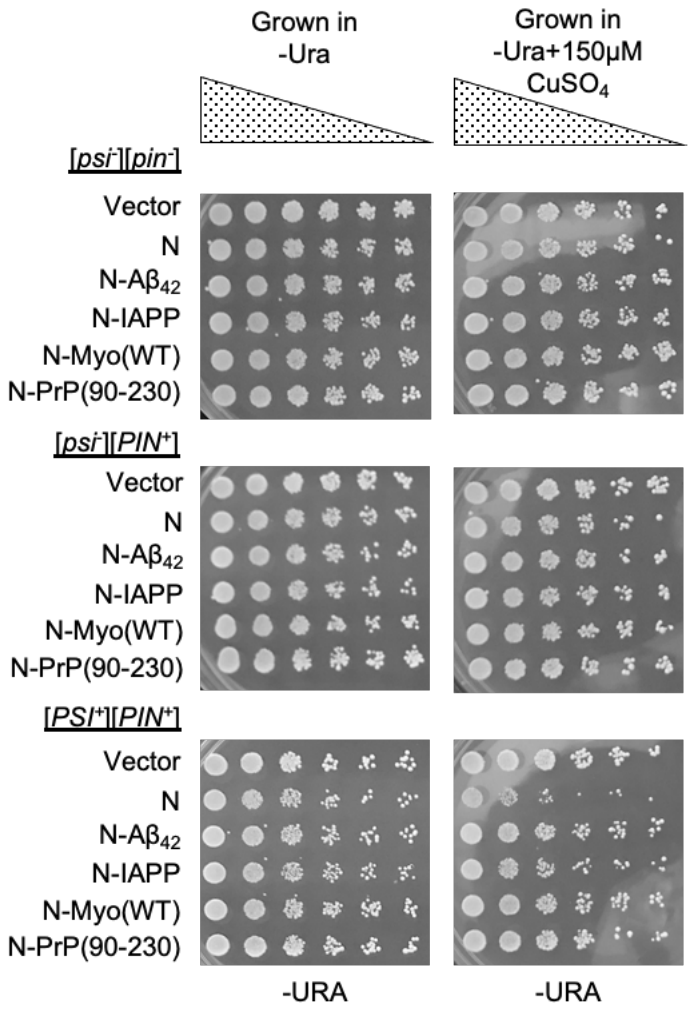

Figure S6.4 Toxicity of previously published control plasmids. Serial dilutions of cultures showing the toxicity of the chimeric constructs as expressed in a [*psi*$^-$][*pin*$^-$] strain (top panel), [*psi*$^-$][*PIN*$^+$] (middle), and a [*PSI*$^+$][*PIN*$^+$] strain (bottom).

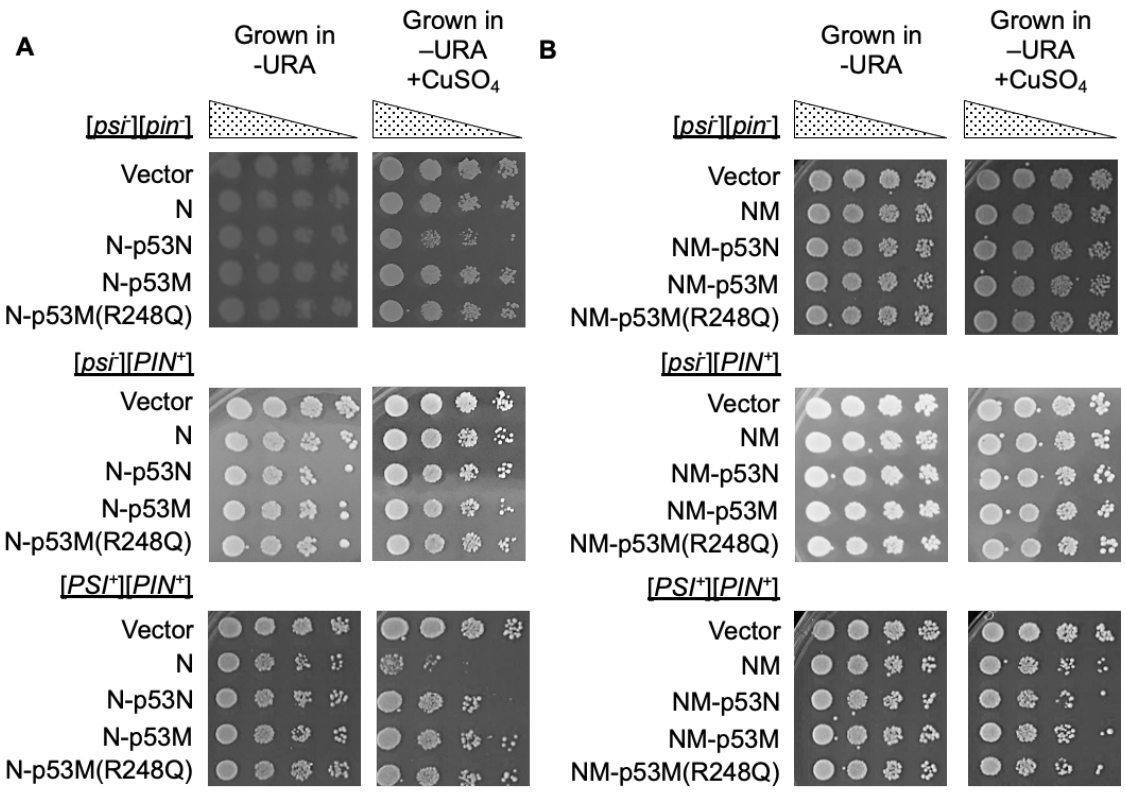

Figure S6.5 Toxicity caused by domains of p53. (A) Serial dilutions of cultures showing the toxicity of the chimeric constructs fused to Sup35N as expressed in a [*psi*$^-$][*pin*$^-$] strain (top panel), [*psi*$^-$][*PIN*$^+$] (middle), and a [*PSI*$^+$][*PIN*$^+$] strain (bottom). p53N shows slight toxicity as compared to Sup35N control. (B) Toxicity data continued for Sup35NM constructs.

REFERENCES

1. Knowles, T.P., M. Vendruscolo, and C.M. Dobson, *The amyloid state and its association with protein misfolding diseases.* Nat Rev Mol Cell Biol, 2014. **15**(6): p. 384-96.

2. Westermark, P., A. Andersson, and G.T. Westermark, *Islet amyloid polypeptide, islet amyloid, and diabetes mellitus.* Physiol Rev, 2011. **91**(3): p. 795-826.

3. Prusiner, S.B., *Prions.* Proc Natl Acad Sci U S A, 1998. **95**(23): p. 13363-83.

4. Kushnirov, V.V., et al., *Prion and nonprion amyloids: a comparison inspired by the yeast Sup35 protein.* Prion, 2007. **1**(3): p. 179-84.

5. Chiti, F. and C.M. Dobson, *Protein Misfolding, Amyloid Formation, and Human Disease: A Summary of Progress Over the Last Decade.* Annu Rev Biochem, 2017. **86**: p. 27-68.

6. Uptain, S.M. and S. Lindquist, *Prions as protein-based genetic elements.* Annu Rev Microbiol, 2002. **56**: p. 703-41.

7. Morel, B. and F. Conejero-Lara, *Early mechanisms of amyloid fibril nucleation in model and disease-related proteins.* Biochim Biophys Acta Proteins Proteom, 2019. **1867**(11): p. 140264.

8. Jarrett, J.T. and P.T. Lansbury, Jr., *Seeding "one-dimensional crystallization" of amyloid: a pathogenic mechanism in Alzheimer's disease and scrapie?* Cell, 1993. **73**(6): p. 1055-8.

9. Fowler, D.M., et al., *Functional amyloid formation within mammalian tissue.* PLoS Biol, 2006. **4**(1): p. e6.

10. Maji, S.K., et al., *Structure-activity relationship of amyloid fibrils.* FEBS Lett, 2009. **583**(16): p. 2610-7.

11. Si, K., S. Lindquist, and E.R. Kandel, *A neuronal isoform of the aplysia CPEB has prion-like properties.* Cell, 2003. **115**(7): p. 879-91.

12. *Alzheimer's Association, 2009 Alzheimer's disease facts and figures.* Alzhermer's and Dementia, 2009. **5**(3): p. 234-270.

13. James, B.D., et al., *Contribution of Alzheimer disease to mortality in the United States.* Neurology, 2014. **82**(12): p. 1045-50.

14. Salawu, F.K., J.T. Umar, and A.B. Olokoba, *Alzheimer's disease: a review of recent developments.* Ann Afr Med, 2011. **10**(2): p. 73-9.

15. Olzscha, H., et al., *CBP/p300 Bromodomains Regulate Amyloid-like Protein Aggregation upon Aberrant Lysine Acetylation.* Cell Chem Biol, 2017. **24**(1): p. 9-23.

16. LaFerla, F.M., K.N. Green, and S. Oddo, *Intracellular amyloid-beta in Alzheimer's disease.* Nat Rev Neurosci, 2007. **8**(7): p. 499-509.

17. Barage, S.H. and K.D. Sonawane, *Amyloid cascade hypothesis: Pathogenesis and therapeutic strategies in Alzheimer's disease.* Neuropeptides, 2015. **52**: p. 1-18.

18. Karran, E., M. Mercken, and B. De Strooper, *The amyloid cascade hypothesis for Alzheimer's disease: an appraisal for the development of therapeutics.* Nat Rev Drug Discov, 2011. **10**(9): p. 698-712.

19. Huang, H.C. and Z.F. Jiang, *Accumulated amyloid-beta peptide and hyperphosphorylated tau protein: relationship and links in Alzheimer's disease.* J Alzheimers Dis, 2009. **16**(1): p. 15-27.

20. Jucker, M. and L.C. Walker, *Pathogenic protein seeding in Alzheimer disease and other neurodegenerative disorders.* Ann Neurol, 2011. **70**(4): p. 532-40.

21. Iqbal, K., et al., *Tau in Alzheimer disease and related tauopathies.* Curr Alzheimer Res, 2010. **7**(8): p. 656-64.

22. Mietelska-Porowska, A., et al., *Tau protein modifications and interactions: their role in function and dysfunction.* Int J Mol Sci, 2014. **15**(3): p. 4671-713.

23. Schraen-Maschke, S., et al., *Tau as a biomarker of neurodegenerative diseases.* Biomark Med, 2008. **2**(4): p. 363-84.

24. Gendron, T.F. and L. Petrucelli, *The role of tau in neurodegeneration.* Mol Neurodegener, 2009. **4**: p. 13.

25. Will, C.L. and R. Lührmann, *Spliceosome structure and function.* Cold Spring Harb Perspect Biol, 2011. **3**(7).

26. Murphy, M.P. and H. LeVine, 3rd, *Alzheimer's disease and the amyloid-beta peptide.* J Alzheimers Dis, 2010. **19**(1): p. 311-23.

27. Korneta, I. and J.M. Bujnicki, *Intrinsic disorder in the human spliceosomal proteome.* PLoS Comput Biol, 2012. **8**(8): p. e1002641.

28. Kato, M., et al., *Cell-free formation of RNA granules: low complexity sequence domains form dynamic fibers within hydrogels.* Cell, 2012. **149**(4): p. 753-67.

29. Maziuk, B., H.I. Ballance, and B. Wolozin, *Dysregulation of RNA Binding Protein Aggregation in Neurodegenerative Disorders.* Front Mol Neurosci, 2017. **10**: p. 89.

30. Lagier-Tourenne, C., M. Polymenidou, and D.W. Cleveland, *TDP-43 and FUS/TLS: emerging roles in RNA processing and neurodegeneration.* Hum Mol Genet, 2010. **19**(R1): p. R46-64.

31. Harrison, A.F. and J. Shorter, *RNA-binding proteins with prion-like domains in health and disease.* Biochem J, 2017. **474**(8): p. 1417-1438.

32. Diner, I., et al., *Aggregation properties of the small nuclear ribonucleoprotein U1-70K in Alzheimer disease.* J Biol Chem, 2014. **289**(51): p. 35296-313.

33. Bai, B., et al., *Integrated approaches for analyzing U1-70K cleavage in Alzheimer's disease.* J Proteome Res, 2014. **13**(11): p. 4526-34.

34. Chernova, T.A., K.D. Wilkinson, and Y.O. Chernoff, *Physiological and environmental control of yeast prions.* FEMS Microbiol Rev, 2014. **38**(2): p. 326-44.

35. Nakayashiki, T., et al., *Yeast prions [URE3] and [PSI+] are diseases.* Proc Natl Acad Sci U S A, 2005. **102**(30): p. 10575-80.

36. Tuite, M.F. and B.S. Cox, *The genetic control of the formation and propagation of the [PSI+] prion of yeast.* Prion, 2007. **1**(2): p. 101-9.

37. Tanaka, M., et al., *Conformational variations in an infectious protein determine prion strain differences.* Nature, 2004. **428**(6980): p. 323-8.

38. Vasconcelos, B., et al., *Heterotypic seeding of Tau fibrillization by pre-aggregated Abeta provides potent seeds for prion-like seeding and propagation of Tau-pathology in vivo.* Acta Neuropathol, 2016. **131**(4): p. 549-69.

39. Morales, R., K. Abid, and C. Soto, *The prion strain phenomenon: molecular basis and unprecedented features.* Biochim Biophys Acta, 2007. **1772**(6): p. 681-91.

40. Gitler, A.D., *Disease models and mechanisms in the classroom.* Dis Model Mech, 2009. **2**(3-4): p. 103-6.

41. Smith, M.G. and M. Snyder, *Yeast as a model for human disease.* Curr Protoc Hum Genet, 2006. **Chapter 15**: p. Unit 15.6.

42. Sherman, F., *Getting started with yeast.* Methods Enzymol, 2002. **350**: p. 3-41.

43. Kaiser, C., Michaelis, S., Mitchel, A. , *Methods in Yeast Genetics: A Cold Spring Harbor Laboratory Course Manual*. 1994, Cold Spring Harbor, NY: Cold Spring Harbor Laboratory Press.

44. Gietz, R.D. and R.H. Schiestl, *High-efficiency yeast transformation using the LiAc/SS carrier DNA/PEG method.* Nat Protoc, 2007. **2**(1): p. 31-4.

45. Bagriantsev, S.N., V.V. Kushnirov, and S.W. Liebman, *Analysis of amyloid aggregates using agarose gel electrophoresis.* Methods Enzymol, 2006. **412**: p. 33-48.

46. McDonald, J.H., *Handbook of Biological Statistics.* . 2009, Baltimore: Sparky House Publishing.

47. Chandramowlishwaran, P., *Prion nucleation and propagation by mammalian amyloidogenic proteins in yeast*, in *Biological Sciences*. 2018, Georgia Institute of Technology: Georgia Tech Library. p. 1-141.

48. Tanaka, M. and J.S. Weissman, *An efficient protein transformation protocol for introducing prions into yeast.* Methods Enzymol, 2006. **412**: p. 185-200.

49. Safar, J., et al., *Eight prion strains have PrP(Sc) molecules with different conformations.* Nat Med, 1998. **4**(10): p. 1157-65.

50. Sondheimer, N. and S. Lindquist, *Rnq1: an epigenetic modifier of protein function in yeast.* Mol Cell, 2000. **5**(1): p. 163-72.

51. Derkatch, I.L., et al., *Genetic and environmental factors affecting the de novo appearance of the [PSI+] prion in Saccharomyces cerevisiae.* Genetics, 1997. **147**(2): p. 507-19.

52. Wickner, R.B., *[URE3] as an altered URE2 protein: evidence for a prion analog in Saccharomyces cerevisiae.* Science, 1994. **264**(5158): p. 566-9.

53. Byrne, L.J., et al., *Cell division is essential for elimination of the yeast [PSI+] prion by guanidine hydrochloride.* Proc Natl Acad Sci U S A, 2007. **104**(28): p. 11688-93.

54. Grimminger, V., et al., *The prion curing agent guanidinium chloride specifically inhibits ATP hydrolysis by Hsp104.* J Biol Chem, 2004. **279**(9): p. 7378-83.

55. Derkatch, I.L., et al., *Genesis and variability of [PSI] prion factors in Saccharomyces cerevisiae.* Genetics, 1996. **144**(4): p. 1375-86.

56. Liebman, S.W. and Y.O. Chernoff, *Prions in yeast.* Genetics, 2012. **191**(4): p. 1041-72.

57. King, C.Y. and R. Diaz-Avalos, *Protein-only transmission of three yeast prion strains.* Nature, 2004. **428**(6980): p. 319-23.

58. Zhou, P., et al., *The yeast non-Mendelian factor [ETA+] is a variant of [PSI+], a prion-like form of release factor eRF3.* Embo j, 1999. **18**(5): p. 1182-91.

59. Park, S.K., et al., *Development and validation of a yeast high-throughput screen for inhibitors of $A\beta_{42}$ oligomerization.* Dis Model Mech, 2011. **4**(6): p. 822-31.

60. Bolmont, T., et al., *Induction of tau pathology by intracerebral infusion of amyloid-beta -containing brain extract and by amyloid-beta deposition in APP x Tau transgenic mice.* Am J Pathol, 2007. **171**(6): p. 2012-20.

61. Chernoff, Y.O., et al., *Evolutionary conservation of prion-forming abilities of the yeast Sup35 protein.* Mol Microbiol, 2000. **35**(4): p. 865-76.

62. Longtine, M.S., et al., *Additional modules for versatile and economical PCR-based gene deletion and modification in Saccharomyces cerevisiae.* Yeast, 1998. **14**(10): p. 953-61.

63. Rubel, A.A., et al., *Identification of PrP sequences essential for the interaction between the PrP polymers and Aβ peptide in a yeast-based assay.* Prion, 2013. **7**(6): p. 469-76.

64. Rosen, R.F., et al., *Tauopathy with paired helical filaments in an aged chimpanzee.* J Comp Neurol, 2008. **509**(3): p. 259-70.

65. Jicha, G.A., et al., *Alz-50 and MC-1, a new monoclonal antibody raised to paired helical filaments, recognize conformational epitopes on recombinant tau.* J Neurosci Res, 1997. **48**(2): p. 128-32.

66. Larson, A.G., et al., *Liquid droplet formation by HP1α suggests a role for phase separation in heterochromatin.* Nature, 2017. **547**(7662): p. 236-240.

67. Strom, A.R., et al., *Phase separation drives heterochromatin domain formation.* Nature, 2017. **547**(7662): p. 241-245.

68. Schmidt, H.B. and D. Görlich, *Transport Selectivity of Nuclear Pores, Phase Separation, and Membraneless Organelles.* Trends Biochem Sci, 2016. **41**(1): p. 46-61.

69. Alberti, S. and S. Carra, *Quality Control of Membraneless Organelles.* J Mol Biol, 2018. **430**(23): p. 4711-4729.

70. Patino, M.M., et al., *Support for the prion hypothesis for inheritance of a phenotypic trait in yeast.* Science, 1996. **273**(5275): p. 622-6.

71. Zhou, P., I.L. Derkatch, and S.W. Liebman, *The relationship between visible intracellular aggregates that appear after overexpression of Sup35 and the yeast prion-like elements [PSI(+)] and [PIN(+)].* Mol Microbiol, 2001. **39**(1): p. 37-46.

72. Caine, J., et al., *Alzheimer's Abeta fused to green fluorescent protein induces growth stress and a heat shock response.* FEMS Yeast Res, 2007. **7**(8): p. 1230-6.

73. Hardy, J. and D. Allsop, *Amyloid deposition as the central event in the aetiology of Alzheimer's disease.* Trends Pharmacol Sci, 1991. **12**(10): p. 383-8.

74. Hardy, J.A. and G.A. Higgins, *Alzheimer's disease: the amyloid cascade hypothesis.* Science, 1992. **256**(5054): p. 184-5.

75. De Vos, A., et al., *Yeast as a model system to study tau biology.* Int J Alzheimers Dis, 2011. **2011**: p. 428970.

76. Vandebroek, T., et al., *Identification and isolation of a hyperphosphorylated, conformationally changed intermediate of human protein tau expressed in yeast.* Biochemistry, 2005. **44**(34): p. 11466-75.

77. Vandebroek, T., et al., *Microtubule binding and clustering of human Tau-4R and Tau-P301L proteins isolated from yeast deficient in orthologues of glycogen synthase kinase-3beta or cdk5.* J Biol Chem, 2006. **281**(35): p. 25388-97.

78. Vanhelmont, T., et al., *Serine-409 phosphorylation and oxidative damage define aggregation of human protein tau in yeast.* FEMS Yeast Res, 2010. **10**(8): p. 992-1005.

79. Lindwall, G. and R.D. Cole, *Phosphorylation affects the ability of tau protein to promote microtubule assembly.* J Biol Chem, 1984. **259**(8): p. 5301-5.

80. Drechsel, D.N., et al., *Modulation of the dynamic instability of tubulin assembly by the microtubule-associated protein tau.* Mol Biol Cell, 1992. **3**(10): p. 1141-54.

81. Jameson, L., et al., *Inhibition of microtubule assembly by phosphorylation of microtubule-associated proteins.* Biochemistry, 1980. **19**(11): p. 2472-9.

82. Ledesma, M.D., M. Medina, and J. Avila, *The in vitro formation of recombinant tau polymers: effect of phosphorylation and glycation.* Mol Chem Neuropathol, 1996. **27**(3): p. 249-58.

83. Ambadipudi, S., et al., *Liquid-liquid phase separation of the microtubule-binding repeats of the Alzheimer-related protein Tau.* Nat Commun, 2017. **8**(1): p. 275.

84. Wegmann, S., et al., *Tau protein liquid-liquid phase separation can initiate tau aggregation.* Embo j, 2018. **37**(7).

85. Toretsky, J.A. and P.E. Wright, *Assemblages: functional units formed by cellular phase separation.* J Cell Biol, 2014. **206**(5): p. 579-88.

86. Li, Y.R., et al., *Stress granules as crucibles of ALS pathogenesis.* J Cell Biol, 2013. **201**(3): p. 361-72.

87. Murakami, T., et al., *ALS/FTD Mutation-Induced Phase Transition of FUS Liquid Droplets and Reversible Hydrogels into Irreversible Hydrogels Impairs RNP Granule Function.* Neuron, 2015. **88**(4): p. 678-90.

88. Patel, A., et al., *A Liquid-to-Solid Phase Transition of the ALS Protein FUS Accelerated by Disease Mutation.* Cell, 2015. **162**(5): p. 1066-77.

89. Molliex, A., et al., *Phase separation by low complexity domains promotes stress granule assembly and drives pathological fibrillization.* Cell, 2015. **163**(1): p. 123-33.

90. Lin, Y., et al., *Electrostatically Driven Complex Coacervation and Amyloid Aggregation of Tau Are Independent Processes with Overlapping Conditions.* ACS Chem Neurosci, 2020. **11**(4): p. 615-627.

91. Lin, Y., et al., *Liquid-Liquid Phase Separation of Tau Driven by Hydrophobic Interaction Facilitates Fibrillization of Tau.* J Mol Biol, 2021. **433**(2): p. 166731.

92. Kroschwald, S., et al., *Promiscuous interactions and protein disaggregases determine the material state of stress-inducible RNP granules.* Elife, 2015. **4**: p. e06807.

93. Oddo, S., et al., *Triple-transgenic model of Alzheimer's disease with plaques and tangles: intracellular Abeta and synaptic dysfunction.* Neuron, 2003. **39**(3): p. 409-21.

94. Götz, J., et al., *Formation of neurofibrillary tangles in P301l tau transgenic mice induced by Abeta 42 fibrils.* Science, 2001. **293**(5534): p. 1491-5.

95. Morales, R., et al., *Titration of biologically active amyloid-β seeds in a transgenic mouse model of Alzheimer's disease.* Sci Rep, 2015. **5**: p. 9349.

96. Griner, S.L., et al., *Structure-based inhibitors of amyloid beta core suggest a common interface with tau.* Elife, 2019. **8**.

97. Fushimi, K., et al., *Expression of human FUS/TLS in yeast leads to protein aggregation and cytotoxicity, recapitulating key features of FUS proteinopathy.* Protein Cell, 2011. **2**(2): p. 141-9.

98. Johnson, B.S., et al., *A yeast TDP-43 proteinopathy model: Exploring the molecular determinants of TDP-43 aggregation and cellular toxicity.* Proc Natl Acad Sci U S A, 2008. **105**(17): p. 6439-44.

99. Bai, B., et al., *U1 small nuclear ribonucleoprotein complex and RNA splicing alterations in Alzheimer's disease.* Proc Natl Acad Sci U S A, 2013. **110**(41): p. 16562-7.

100. Bai, B., et al., *Integrated Approaches for Analyzing U1-70K Cleavage in Alzheimer's Disease.* Journal of Proteome Research, 2014. **13**(11): p. 4526-4534.

101. Agrawal, S., et al., *RNA recognition motifs of disease-linked RNA-binding proteins contribute to amyloid formation.* Sci Rep, 2019. **9**(1): p. 6171.

102. Xue, S., et al., *Low-complexity domain of U1-70K modulates phase separation and aggregation through distinctive basic-acidic motifs.* Sci Adv, 2019. **5**(11): p. eaax5349.

103. Anderson, P. and N. Kedersha, *Stress granules.* Curr Biol, 2009. **19**(10): p. R397-8.

104. Buchan, J.R. and R. Parker, *Eukaryotic stress granules: the ins and outs of translation.* Mol Cell, 2009. **36**(6): p. 932-41.

105. Ramaswami, M., J.P. Taylor, and R. Parker, *Altered ribostasis: RNA-protein granules in degenerative disorders.* Cell, 2013. **154**(4): p. 727-36.

106. Bishof, I., et al., *RNA-binding proteins with basic-acidic dipeptide (BAD) domains self-assemble and aggregate in Alzheimer's disease.* J Biol Chem, 2018. **293**(28): p. 11047-11066.

107. Hales, C.M., et al., *Changes in the detergent-insoluble brain proteome linked to amyloid and tau in Alzheimer's Disease progression.* Proteomics, 2016. **16**(23): p. 3042-3053.

108. Spillantini, M.G. and M. Goedert, *Tau pathology and neurodegeneration.* Lancet Neurol, 2013. **12**(6): p. 609-22.

109. Bailleul, P.A., et al., *Genetic study of interactions between the cytoskeletal assembly protein sla1 and prion-forming domain of the release factor Sup35 (eRF3) in Saccharomyces cerevisiae.* Genetics, 1999. **153**(1): p. 81-94.

110. Chandramowlishwaran, P., et al., *Mammalian amyloidogenic proteins promote prion nucleation in yeast.* J Biol Chem, 2018. **293**(9): p. 3436-3450.

111. Chesi, A., et al., *Exome sequencing to identify de novo mutations in sporadic ALS trios.* Nat Neurosci, 2013. **16**(7): p. 851-5.

112. Teyssou, E., et al., *Genetic analysis of SS18L1 in French amyotrophic lateral sclerosis.* Neurobiol Aging, 2014. **35**(5): p. 1213.e9-1213.e12.

113. Rangel, L.P., et al., *The aggregation of mutant p53 produces prion-like properties in cancer.* Prion, 2014. **8**(1): p. 75-84.

114. Silva, J.L., et al., *Expanding the prion concept to cancer biology: dominant-negative effect of aggregates of mutant p53 tumour suppressor.* Biosci Rep, 2013. **33**(4).

115. Petitjean, A., et al., *Impact of mutant p53 functional properties on TP53 mutation patterns and tumor phenotype: lessons from recent developments in the IARC TP53 database.* Hum Mutat, 2007. **28**(6): p. 622-9.

116. Sivanathan, V. and A. Hochschild, *A bacterial export system for generating extracellular amyloid aggregates.* Nat Protoc, 2013. **8**(7): p. 1381-90.

117. Collinson, S.K., et al., *Thin, aggregative fimbriae mediate binding of Salmonella enteritidis to fibronectin.* J Bacteriol, 1993. **175**(1): p. 12-8.

118. Antony, H., et al., *Potential roles for prions and protein-only inheritance in cancer.* Cancer Metastasis Rev, 2012. **31**(1-2): p. 1-19.

119. Gong, H., et al., *Amyloidogenicity of p53: a hidden link between protein misfolding and cancer.* Curr Protein Pept Sci, 2015. **16**(2): p. 135-46.

120. Michelitsch, M.D. and J.S. Weissman, *A census of glutamine/asparagine-rich regions: implications for their conserved function and the prediction of novel prions.* Proc Natl Acad Sci U S A, 2000. **97**(22): p. 11910-5.

121. Hilleren, P.J., H.Y. Kao, and P.G. Siliciano, *The amino-terminal domain of yeast U1-70K is necessary and sufficient for function.* Mol Cell Biol, 1995. **15**(11): p. 6341-50.

122. Muñoz-Ruiz, P., et al., *Design, synthesis, and biological evaluation of dual binding site acetylcholinesterase inhibitors: new disease-modifying agents for Alzheimer's disease.* J Med Chem, 2005. **48**(23): p. 7223-33.

123. Kajava, A.V., U. Baxa, and A.C. Steven, *Beta arcades: recurring motifs in naturally occurring and disease-related amyloid fibrils.* Faseb j, 2010. **24**(5): p. 1311-9.

124. Vishveshwara, N., M.E. Bradley, and S.W. Liebman, *Sequestration of essential proteins causes prion associated toxicity in yeast.* Mol Microbiol, 2009. **73**(6): p. 1101-14.